Aortic plasmacytoid dendritic cells protect aortas from atherosclerosis by regulatory T cells induction

Tae Jin Yun

Division of Experimental Medicine

Faculty of Medicine

McGill University, Montreal

Jun 2017

A thesis submitted to McGill University in partial fulfillment of the requirements of the degree of Doctor of Philosophy

TABLE OF CONTENTS

ABSTRACT

Atherosclerosis is one of the most prevalent diseases over the world and it becoming one of leading cause of death across nationals. Even though many studies on the immunological aspects of atherosclerosis have been focused on foam cells, which are derived from lipid containing macrophages, relatively fewer studies have investigated the role of dendritic cells in atherosclerosis. Plasmacytoid dendritic cells (pDCs) are one of the dendritic cells subsets. PDCs develop from the bone marrow and are found in lymphoid and non-lymphoid tissues through blood circulation. A unique function of pDCs is the secretion of large amounts of type I interferons during viral infection for inducing immune responses. On the other hand, pDCs are also known to induce tolerance in sterile-inflammation conditions. However, the immunomodulatory role of aortic pDCs in atherosclerosis remains poorly understood. In this study, we identified functional mouse and human pDCs in the aortic intima in steady state and in atherosclerosis. Also, using transgenic mouse models, we showed that selective and inducible pDCs depletion in mice exacerbates atherosclerosis. Also we showed that aortic pDCs expressed CCR9 and indoleamine 2,3-dioxygenase 1 (IDO-1), an enzyme involved in driving the generation of regulatory T cells (Tregs), which indicate that aortic pDCs in atherosclerosis are not matured or tolerogenic. In line with this, deletion of IDO-1 resulted in aggravated atherosclerosis and reduced number of regulatory T cells in aorta. Moreover, antibody-mediated antigen delivery to pDCs expanded antigen-specific Tregs in the atherosclerotic aorta. Notably, Tregs ablation affected pDCs homeostasis in diseased aorta. Accordingly, pDCs in human atherosclerotic aortas colocalized with

Tregs. Taken together, we describe a local mechanism of atheroprotection mediated by tolerogenic aortic pDCs through the induction of Tregs in aorta.

RÉSUMÉ

L'athérosclérose est l'une des maladies les plus répandues dans le monde et elle devient l'une des principales causes de décès chez les canadiens. Même si de nombreuses études sur les aspects immunologiques de l'athérosclérose ont été axées sur les foam cells, qui sont des dérivées de macrophages contenant des lipides, il y a relativement peu de recherches sur le rôle des cellules dendritiques dans l'athérosclérose. Cellules dendritiques plasmacytoides (pDC) sont une des sous-populations de cellules dendritiques. Les pDC se développent à partir de la moelle osseuse et se retrouvent dans les tissus lymphoïdes et non-lymphoïdes via la circulation sanguine. Une fonction unique des pDC est la sécrétion de grandes quantités d'interférons de type I pendant une infection virale pour induire des réponses immunitaires. D'autre part, les pDC sont également connues pour induire une tolérance dans des conditions d'inflammation stérile. Cependant, le rôle immunomodulateur des pDC aortiques dans l'athérosclérose est mal compris. Dans cette étude, nous avons identifié des pDC humaines et murines dans l'intima aortique à l'état normal et en athérosclérose. De plus, en utilisant des modèles de souris transgéniques, nous avons démontré que la déplétion sélective et inductible des pDC chez la souris aggravait l'athérosclérose. Nous avons également démontré que les pDC aortiques exprimaient le CCR9 et l'indolamine 2,3-dioxygenase 1 (IDO-1) une enzyme impliquée dans la production de cellules régulatrices T (Tregs) qui indiquent que les pDC aortiques dans l'athérosclérose ne sont pas matures ou tolérogéniques. Conformément à cette observation, la délétion d' IDO-1 aggrave athérosclérose et réduit le nombre de Tregs

dans l'aorte. De plus, la libération d'antigène médiée par des anticorps aux pDC induit une expansion des Tregs spécifiques de l'antigène dans l'aorte athérosclérotique. De plus, l'ablation de Tregs affecte l'homéostasie des pDC dans l'aorte malade. Finalement, les pDC dans les aortes athéroscléreuses humaines co-localisent avec les Tregs. Ces observations prises ensembles, nous décrivons un mécanisme local d'athéroprotection médiée par les pDC aortiques tolerogènes qui régulent l'expansion des Tregs dans l'aorte.

ACKNOWLEDGEMENTS

First and foremost, I would like to express my gratitude to one of my supervisors, Dr. Cheolho Cheong. I was fortunate to be the first student in his lab and able to learn many things such as from setting up and managing a laboratory to experimental techniques. Even though, Dr. Cheong, without question, pushed me to my limits in many ways more than anyone I have ever met, I believe that he gave me all the opportunities because he always believed in me. Recently I am involved in closing his laboratory and it gives me a lot to think about the last 4 years. For the last 4 years from the beginning of my study in his lab, Dr. Cheong was always a very enthusiastic and ambitious researcher with full of energy, and I have been influenced and accelerated in a positive way by him. I had the pleasure of studying and working on my graduate research with Dr. Cheong. Thank you for all the opportunities, discussions, challenges, and advice. Dr. Cheong. It has been a great pleasure to work with you and I sincerely thank you for all from the bottom of my heart.

I would like to thank all my colleagues who were in Dr. Cheong laboratory as graduate students, post-docs or summer students. Thank you Jun Seong Lee, Kawthar Machmach, Jin Sam Chang, Mohammad-Alam Miah, Bin Li, Youngwoong Kim, Jinyong Kim, Areej Al Rabea, Jeongyoon Moon and Kyungsu Lee. It has been always the great pleasure to work with all of you, and also I was able to balance my life in the lab and out of the lab with you guys. Without your help, support and contribution, it would not have been impossible to finish my graduate study. I am very grateful. Also I sincerely thank D.V.M. Ovidiu Jumanca, Ève-Lyne Thivierge, Caroline Dubé and Marie-Claude Lavallée

for all mouse facility, and Eric Massicotte for help and advice for flowcytometry service in IRCM. Also it is important to address my sincere gratitude to my supervisor, Dr. Javier Marcelo Di Noia, and advisors: Dr. Artur Kania, Dr. Woong-Kyung Suh, Dr. Maziar Divangahi, Dr. Eric A. Cohen, Dr. Martin G. Sirois, Dr. Jae-Hoon Choi, Dr. Goo Taeg Oh and Dr. Youngsun Kang. Your advices and discussion influenced my study and allowed me to reach to this far. Also I sincerely thank to Dr. Martin Guimond for his contribution of time and effort.

Finally I would like to thank my family who continuously supported me even though I am 10,000 km away. My father, mother, brother and sister-in-law have always understood and helped me to follow and strive for my dream. Also I especially need to thank to my baby nephew, Juho, who is about 300 days old. Your pictures and videos always give me big smiles. Je t'aime toute ma famille.

Sincerely,

Tae Jin Yun

PREFACE AND CONTRIBUTION OF AUTHORS

The study discussed in this thesis encompasses our research on aortic dendritic cells in atherosclerosis and contribution of bridging two different fields of the dendritic cell biology and the cardiovascular disease. Throughout the course of my graduate study and research in Dr. Cheolho Cheong laboratory, our collaborators and we have focused on the dendritic cells, specifically plasmacytoid dendritic cells, in aorta and their role in the development of atherosclerosis and published the result of the investigation of aortic plasmacytoid dendritic cells.

Tae Jin Yun participated in the study design, isolated cells from mouse and human organ samples, analyzed and interpreted FACS data, performed cell culture experiments and measured IFN-α, analyzed and participated in quantitative PCR for target genes from isolated aortic single cells, and drafted and revised the manuscript and figures. **Jun Seong Lee** prepared and analyzed mouse aorta and spleen samples for FACS analysis. **Kawthar Machmach** analyzed human aorta samples for FACS analysis, and performed cell culture experiments and measured IFN-α. **Dahee Shim, Junhee Choi, Young Jin Wi, Hyung Seok Jang, In-Hyuk Jung, and Kyeongdae Kim** performed the histopathological assessment of atherosclerosis, immunohistochemistry and immunofluorescence analysis of mouse and human aorta, and quantitative PCR for target genes of aorta samples. **Won Kee Yoon** profiled serum lipid levels of mice. **Mohammad Alam Miah, Bin Li, and Jinsam Chang** aided in isolation of mice aorta and spleen samples for FACS analysis. **Mariana G. Bego, Tram N.Q. Pham and Eric A. Cohen** designed and helped human IFN-α measurement. **Jakob Loschko and**

Jakob Loschko provided OVA-linked anti-Siglec-H antibody. **Tibor Keler** provided us human Flt3 ligands for expansion of dendritic cells. **Jean V. Guimond and Elie Haddad** provided hu-mice. **Eric A. Cohen, Seung-Pyo Lee, Martin G. Sirois, and Ismail El-Hamamsy** provided human patient samples. **Jorg Hermann Fritz and Marco Colonna** provided materials and resources such as mouse lines and antibodies. **Goo Taeg Oh, Jae-Hoon Choi, and Cheolho Cheong** conceived the study, participated in study design, supervised experimentation, interpreted and analyzed data, drafted and revised the manuscript. All authors actively reviewed and edited the manuscript.

LIST OF FIGURES

LIST OF TABLE

ABBRIVIATION

1-MT	1-methyltryptophan
AP3	adapter protein-3
ApoB100	apolipoprotein B100
APRIL	a proliferation-inducing ligand
BAFF	B cell-activating factor
BFA	brefeldin A
BST-2	bone marrow stromal cell antigen 2
CCR	C-C chemokine receptor
cDCs	conventional dendritic cells
CDPs	common DCs progenitors
CHOW	normal diet
CLPs	common lymphoid progenitors
CMPs	common myeloid precursors
CpG	cytosine-guanosine-dinucleotide-containing oligonucleotides
CXCL	CXC ligand
DAP12	DNAX-activation protein 12
DC-SIGN	DC-specific ICAM3-grabbing non-integrin
DCs	dendritic cells
DOTAP	1,2-dioleoyloxy-3-trimethylammonium-propane
EBI2	epstein-Barr virus induced receptor 2
ER	endoplasmic reticulum
ESAM	Endothelial cell-specific adhesion molecule
FACS	fluorescence-activated cell sorting
Flt3	FMS-related tyrosine kinase 3
Flt3L	FMS-like tyrosine kinase 3 ligand
HAV	hepatitis A virus
HCV	hepatitis C virus
hs-CRP	high-sensitivity C-reactive protein
HSCs	human stem cells
ICAM-1	intercellular adhesion molecule 1
ICOSL	inducible T cell co-stimulator ligand
ICS	intracellular staining
IDO-1	indoleamine 2,3-dioxygenase
IF	immunofluorescence
IFNAR	IFN α/β receptor
IFR	interfollicular region
IHC	immunohistochemistry
ILT7	immunoglobulin-like transcript 7
IRF	interferon regulatory factor
LAMP	lysosome-associated membrane protein
LAMP5	lysosome-associated membrane protein 5

LCMV	lymphocytic choriomeningitis virus
LDL	low-density lipoprotein
LNs	draining lymph nods
Ly6C	lymphocyte antigen 6 complex
MAVS	mitochondrial antiviral signaling protein
MCMV	murine cytomegalovirus
MDPs	monocytes and DCs committed precursors
MERTK	tyrosine protein kinase MER
MHC	major histocompatibility complex
MHV	mouse hepatitis virus
MIIC	MHC class II compartment
moDCs	monocyte-derived DCs
mTOR	mammalian target of rapamycin
MYD88	primary-response protein 88
MΦs	macrophages
NDV	newcastle disease virus
NK cells	natural killer cells
NSG	NOD/SCID/γc-null
OVA	ovalbumin
oxLDL	oxidized low-density lipoprotein
PAMPs	pathogen-associated molecular patterns
PDCA1	plasmacytoid dendritic cell antigen 1
pDCs	plasmacytoid dendritic cells
PHT1	peptide/histidine transporter 1
PI3K	phosphoinositide 3-kinase
PI3K	Phosphatidylinositol-3 kinase
PIR-B	paired immunoglobulin-like receptor B
PRRs	pattern-recognition receptors
PTPRS	protein tyrosine phosphatase sigma
RIG-I	retinoic acid-inducible gene I
RLR	retinoic acid-inducible gene I-like receptors
SED	subepithelial dome
SIV	simian immunodeficiency virus
SLE	systemic lupus erythematosus
SMCs	vascular smooth muscle cells
TAP	transporter associated with antigen processing
Th1	T-helper 1
TIM1	T cell immunoglobulin mucin family member 1
TIP DCs	TNF-α and iNOS-producing DCs
TLR	Toll-like receptor
TNBS	2,4,6-trinitrobenzenesulfonic acid
TRAIL	TNF-related apoptosis-inducing ligand
Tregs	regulatory T cells

VCAM-1	vascular cell adhesion molecule 1
VSV	vesicular stomatitis virus
WD	western-type diet
WT	wild-type
XCR1	X-C Motif Chemokine Receptor 1

1. INTRODUCTION

1.1. Role of dendritic cells

Dendritic cells (DCs) are a small subset of hematopoietic cells and reside in lymphoid and nonlymphoid tissues. DCs have a superior ability, compared to other immunes cells, to patrol tissue damages and infections, recognize and uptake several types of environmental or cell related antigens, and process and present the antigens to induce immune response or enforce tolerance. For instance, once DCs encounter pathogens, they undergo a complex development program known as maturation that changes their function profoundly. Maturation induces DCs to uptake antigens efficiently but transiently, for about 20 hours [1, 2, 3]. Also the expression of major histocompatibility complex (MHC) molecules and co-stimulatory molecules, CD40, CD80, and CD86, on DCs increases compared to steady state[4]. Furthermore, DCs start to produce cytokines and chemokines and migrate to nearby draining lymph nods (LNs) to present antigens[5, 6]. The key functions defining DCs from other hematopoietic cells are described below.

1.1.1. Antigen processing and presentation

DCs present peptide antigens produced by intracellular proteolysis to T cells to induce T cell response. Peptide antigens are produced and presented by two different

antigen presentation pathways; the endogenous pathway via major histocompatibility complex (MHC) class I and the exogenous pathway via MHC class II. Antigens presented in the context of MHC class I molecules are recognized by $CD8^+$ T cells, whereas antigens presented by MHC class II molecules are recognized by $CD4^+$ T cells.

Antigen-derived peptides are processed by two major proteolytic pathways, depending on the source of the antigens. Most proteolysis for endogenous proteins in the cytosolis are mediated by proteasomes. The short peptides generated are then translocated to the endoplasmic reticulum (ER). This translocation is mediated by transporter associated with antigen processing (TAP) proteins which allows the transport of peptides across the ER membranes. In the ER, MHC class I molecules lacking antigen-derived peptides bind to tapasins, which allow recruitment of TAP proteins, and TAP-tapasin-MHC class I complexes facilitate small antigen-derived peptides binding[7]. In contrast, exogenous proteins that are captured through endocytosis and phagocytosis are degraded in lysosomes and phagolysosomes, respectively. Antigens acquired by endocytosis enter a vesicular network through early endosomes, late endosomes and lysosomes, but antigens from phagocytosis are in phagosomes and fused with lysosomes to become phagolysosomes. Endogenous nuclear antigens in autophagosomes from autophagy are also fused with lysosomes. Lysosomes are acidic, with pH ranging between 4.5 and 5, and contain the proteases cathepsins to degrade the antigens. In the late endosomes, which is also known as MHC class II compartment (MIIC), peptides from lysosomes and phagosomes are

loaded onto MHC class II molecules that transited from trans-Golgi network or recycled from the cell surface.

Although MHC class I and II molecules generally bind to peptides derived from proteasomal proteolysis and lysosomal proteolysis, respectively, both MHC molecules can bind antigens from both of pathways. For example, MHC class II molecules can bind to antigens originated from endogenous source and degraded by lysosomal proteolysis. Also MHC class I molecules have access to antigens from exogenous origins and internalized by endocytosis and phagocytosis, that can be presented to $CD8^+$ T cells. This specific mechanism of MHC class I presentation of exogenous antigens is known as cross-presentation. Cross-presentation is mediated by specific subset of DCs; $CD8\alpha^+$ DCs and more recently $CD103^+$ DCs in peripheral tissues[8, 9, 10]. $CD8\alpha^+$ DCs express higher levels of the GTPase RAC2, which represses protease activity by inducing phagosomal alkalinization to favor cross-presentation[11]. Also $CD8\alpha^+$ DCs tend to destabilize phagosomes membrane for cross-presentation by GTPase IGTP[12]. Also a recent study reported that DC-specific ICAM3-grabbing non-integrin (DC-SIGN) expressing monocyte-derived DCs (moDCs) are potent cross-presenting cells[13], in addition to $CD8\alpha^+$ DCs and $CD103^+$ DCs.

1.1.2. Migration to lymph nodes

DCs act as sentinels in various body barriers, such as the skin and mucosal

surface, where they encounter numerous antigens. To initiate the stimulation of T cells upon DCs maturation, DCs acquire mobility to migrate to tissue-draining LNs through lymphatic vessels or to the T cell zones within their respective lymphoid organ of residence.

Peripheral tissue-resident DCs migration to LNs is dependent on CCR7 in both the steady state and during inflammation[14, 15]. Inhibition of DCs migration toward LNs and decreased T cell responses were observed in a CCR7-deficient mouse model[16]. Also, it was shown that DCs require CCR7 ligands, CCL19 and CCL21, for their migration[17, 18], although CCL19 seems to be redundant[19]. CCL19 is soluble and lacks anchoring residues[20] and CCL21 is also soluble but contains anchoring residues. However, CCL21 is also found immobilized on cells or extracellular matrix[21] but upon contact with DCs, CCL21 is truncated by proteolysis of its anchoring residues and released to act similarly to CCL19[22].

Integrins were reported to be necessary for DCs migration to LNs upon contact sensitization[23, 24]. It was reported that lymphatic endothelial cells express high level of leukocyte adhesion receptors intercellular adhesion molecule 1 (ICAM-1) and vascular cell adhesion molecule 1 (VCAM-1) during inflammation[23]. However, in steady states, it was shown that lymphatic endothelial cells express little ICAM-1 and VCAM-1[23] and pan-integrin-deficient DCs are able to migrate to LNs, so integrins seem dispensable for migration of DCs in steady state[25]. CCR7 and integrins are required for DCs migration to draining LNs but further studies are necessary to delineate why the requirement for integrins is different in steady state and inflammatory conditions.

The mechanisms of migration of intra-tissue resident DCs in lymphoid organs remain less well characterized. It was reported that the chemotactic receptor EBI2 on DCs regulates localization of $CD4^+$ DCs in bridging channels of the marginal zone in the spleen and absence of EBI2 results in defects in T cell activation[26]. $CD11b^+$ DCs and $CD8\alpha^+$ DCs in intestinal Peyer's patches depend on CCR6 and CCR7 for their localization, respectively. $CD11b^+$ DCs require the expression of CCR6 for their recruitment into the subepithelial dome (SED) region and $CD8\alpha^+$ DCs require CCR7 to migrate toward the T cell-rich interfollicular region (IFR), even though the expression of CCR7 was also observed on $CD11b^+$ DCs[27]. Also, migration of splenic DCs toward T cell zone upon inflammation depends on increased expression of CCR7 on mature DCs and gradients of CCR7 ligands, CCL19 and CCL21[28]. Furthermore, DCs in the thymus require the X-C Motif Chemokine Receptor 1 (XCR1) to allow their medullary accumulation. Deletion of XCL1, the XCR1 ligand expressed by medullary thymic epithelial cells, resulted in inhibition of DCs migration to the thymus medulla showing that DCs migration in the thymus depends on XCR1-XCL1 axis[29].

1.1.3. Subset of dendritic cells

DCs can be divided into at least four different subsets, according to their expression of surface markers, $CD8\alpha^+$ DCs and $CD103^+$ DCs, $CD11b^+$ DCs, and $CD317^+$ pDCs. These different subsets of DCs are found in both lymphoid tissues, such as spleens and LNs, and nonlymphoid tissues, such as aortas and intestines.

1.1.3.1. CD8α$^+$ DCs and CD103$^+$ DCs

Phenotype and function of CD8α$^+$ and CD103$^+$ DCs have been better described in comparison to other DCs subsets in murine models[30]. CD8α$^+$ DCs were reported to be one of the DCs populations in lymphoid organs[31], and are referred to as resident DCs that spend their entire lifespan in lymphoid tissues. The CD103$^+$ DCs, one of the migratory DCs subsets, are found in LNs and non-lymphoid organs[32, 33]. CD103$^+$ DCs and CD8α$^+$ DCs share their origin and function so non-lymphoid CD103$^+$ DCs are considered as equivalents of lymphoid CD8α$^+$ DCs[34, 35]. CD8α$^+$ DCs represent about 40% and 15% of DCs in spleen and LNs, respectively, and express CD8α, but not the CD8αβ found in CD8$^+$ T cells[36]. CD103$^+$ DCs account for nearly 25% of DCs in LNs and express no or low levels of CD11b, except the intestinal CD103$^+$CD11b$^+$ DCs. Both CD8α$^+$ DCs and CD103$^+$ DCs express CD135 (Flt3), which is the receptor that binds to Flt3 ligand (Ftl3L), necessary for DCs development[37]. CD135$^{-/-}$ mouse showed significant reduction of both DCs subsets[38]. Both subsets lack of CD11b and macrophage markers CD115, F4/80, CD64, and CX_3CR1. Also both subsets express their own specific markers, such as CD370 (CLAC9A), which is important for efficient cross-presentation of antigen[39], and CD205, which recognizes dying cells[40]. These markers are not expressed by CD11b$^+$ DCs and allow the delivery of antigens to CD8α$^+$ and CD103$^+$ DCs by antibody-mediated antigens delivery.

1.1.3.2. CD11b$^+$ DCs

CD11b$^+$ DCs are the most abundant DCs in lymphoid tissues and non-lymphoid tissues, and lack expression of CD8α. However, the characterization of CD11b$^+$ DCs is less well defined because of the heterogeneity of CD11b$^+$ DCs population. For example CD11b$^+$ DCs can be divided into at least two subsets according to the expression of CD4 and Endothelial cell-specific adhesion molecule (ESAM); CD4$^+$ESAM^{hi} DCs and CD4$^-$ESAM^{lo} DCs. CD4$^+$ESAM^{hi} DCs express higher level of Flt3 and lower level of Csf1R, Csf3R and CCR2 compare to CD4$^-$ESAM^{lo} DCs[41].However, this CD11b$^+$ DCs subset segregation based on the surface markers still does not seem to provide homogenous population because of their heterogeneity of transcriptome profiles[42]. Nevertheless, CD11b$^+$ DCs have common characteristics compared to CD8α$^+$ DCs, such as more efficient in induction of CD4$^+$ T cell immune response. Also CD11b$^+$ DCs are ineffective in cross-presentation[13, 43].

Lymphoid and nonlymphoid tissues contain another subset of CD11b$^+$ DCs which is called moDCs[44]. These cells originate from monocytes, and it was reported that Ly6Chi monocytes contribute to moDCs[45]. moDCs express CD11c, MHCII and CD11b and also present antigen to activate naïve T cells[13, 46]. However, similar to macrophages, moDCs also express CD64, F4/80 and tyrosine protein kinase MER (MERTK)[46, 47, 48]. Also moDCs express DCs specific transcription factor *zbtb46*[49], which

is not expressed by 'TNF-α and iNOS-producing DCs' (TIP DCs) that is now considered to be activated monocytes[44, 49].

1.1.3.3. Plasmacytoid DCs

pDCs are small subset of DC population, which account for less than 0.3% of total splenocytes in steady state[50]. pDCs are found in blood, lymphoid and non-lymphoid organs, and were reported first in humans and later in mice[51, 52]. pDCs share characteristics with DCs, such as development from the same common DCs progenitors (CDPs)[53], FMS-like tyrosine kinase 3 ligand (Flt3L) dependence for its development in the BM[54], and overlapping but distinct transcriptional profile[55]. However, pDCs also have several distinct features from other DCs subsets, such as low expression of CD11c and MHCII in steady state[53], limited potential to prime T cells[56], unique expression of Toll-like receptor (TLR) 7 and 9, and production of large amounts of type I interferon[51, 57]. Also, development of pDCs depends on the helix-loop-helix transcription factor E2-2[58] and deletion of E2-2 leads to conversion into $CD8\alpha^+$ DC-like cells[59] that sustain D-J rearrangement and express CX_3XR1[60].

	Lymphoid tissue				Non-lymphoid tissue	
		Tissue resident DCs			Migratory DCs	
	pDCs	$CD8^+$ DCs	$CD11b^+Esam^{hi}$ DCs	$CD11b^+Esam^{lo}$ DCs	$CD103^+$ DCs	$CD11b^+$ DCs
CD11c	-	++	++	++	+	+
MHCII	-	+	+	+	++	++
CD11b	-	-	+	+	-	+
CD4	+/-	-	+	-	-	-
CD8α	+/-	+	-	-	-	-
CD103	-	-	-	-	+	-
CD205	-	+	-	-	+	-
B220	+	-	-	-	-	-
CD209α	+	-	+	+	-	+/-
CD207	-	+/-	-	-	+	-
XCR1	-	+	-	-	+	-

Table 1. Phenotypic markers of DC subsets in lymphoid and non-lymphoid tissues
pDCs and different DCs subsets in lymphoid and non-lymphoid tissues are divided according to the indicated markers. DCs, dendritic cell; pDCs, plasmacytoid dendritic cells. (Source: adapted from (87))

1.1.4. Priming naïve T cell responses

The development of DCs-specific deletion mouse models, such as CD11c-DTA and CD11c-DTR, allowed to show that DCs are the central key to initiate T cell response[61, 62]. These studies demonstrated that, upon infection, DCs interact with T cells and induce T cell differentiation and clonal expansion. Different subsets of DCs, $CD8\alpha^+$ DCs, $CD103^+$ DCs, and $CD11b^+$ DCs, are found in lymphoid tissues and non-lymphoid tissues and utilize pattern-recognition receptors (PRRs) to recognize pathogen-associated molecular patterns (PAMPs) on microorganisms[63, 64]. It was reported that $CD11b^+$ DCs express higher levels of genes involved in MHC class II antigen presentation pathway compared to $CD8\alpha^+$ DCs[43] and these cells present antigens to $CD4^+$ T cells more efficiently than $CD8\alpha^+$ DCs[43, 65]. On the other hand, $CD8\alpha^+$ DCs and $CD103^+$ DCs can also cross-present antigens to $CD8^+$ T cells. By using Langerin-DTR mouse model, which can deplete both $CD8\alpha^+$ DCs and $CD103^+$ DCs, but not $CD11b^+$ DCs, it was shown that induction of pathogen specific $CD8^+$ T cells relies on $CD8\alpha^+$ DCs[66, 67]. Also DCs instruct T cells by secretion of cytokines; IL-12 and IL-15 by $CD8\alpha^+$ DCs and $CD103^+$ DCs[68, 69, 70, 71], and IL-6 and IL-23 by $CD11b^+$ DC[72, 73]. However, it seems that priming T cells requires original DCs that are directly exposed to pathogens, not the cytokine-stimulated DCs that are not exposed to pathogens[74]. In line with this, T cell stimulation without costimulatory molecules results in tolerance. It was reported that antigens presented by immature DCs do not contribute to T cell polarization and the T cells become antigen-specific tolerogenic[75, 76], which suggest that

T cell response requires three distinct stimuli from DCs: antigens on MHC molecules, costimuliatory signals by B7 family molecules, and cytokines. The relationship is bidirectional, not only DCs instruct T cells but also T cells crosstalk to DCs. It was shown that antigen-presenting DCs in thymus require CD40L expressing T cells for the maturation and prolonged survival of DCs and deletion of autoreactive thymocytes[77, 78]. Also, stimulated T cells by anti-CD3 and anti-CD28 antibodies secrete FMS-like tyrosine kinase 3 ligand (Flt3L) molecule that regulate development of DCs, and can shape DCs compartment[79].

1.2. DCs development

DCs develop from bone marrow progenitors and disseminate to lymphoid and non-lymphoid organs. In the bone marrow, DCs develop from monocytes and DCs committed precursors (MDPs) that also give rise to monocytes[80]. The DC-oriented cell population derived from MDPs is defined as common DCs progenitors (CDPs)[81, 82], which give rise to pre-DCs and pre-pDCs, that then differentiate into DCs and pDCs in lymphoid tissues[81, 83] as well as non-lymphoid tissues where they arrive by the blood[84, 85, 86]. Also, moDCs, another population of $CD11b^+$ DCs, can develop from circulating monocytes[13]. However, further studies are required on DCs development in non-lymphoid tissues since sophisticated studies of pre-DCs differentiation into different DCs subsets are lacking[87].

pDCs have been reported to develop from CDPs originating from common myeloid precursors (CMPs)[81, 82]. Even though pDCs share the developmental origin with DCs, other studies also have shown another origin of pDCs, from common lymphoid progenitors (CLPs). Several studies reported the development of pDCs from CLPs[88, 89], as also suggests a genetic tracing approach following RAG-1 expression by using RAG-1-GFP knock-in mice[90]. However, the pDCs from CLPs showed a lower ability in terms of secretion of type I interferons and T cell activation compared to the ones that originate from CMPs[91]. Further studies about the pDCs specific progenitors in the BM are necessary, but the data suggest that pDCs may differentiate in a less linear fashion than other subsets of DCs. pDCs precursor, CDPs, express CD135/Flt3[82, 92] and depend on cytokine Flt3L for pDCs development in BMs[93]. When Ftl3 is deleted or inactivated by mutation, the number of pDCs is decreased in lymphoid organs[37, 94]. Flt3-Flt3L signaling seems to require activation of mammalian target of rapamycin (mTOR) through phosphoinositide 3-kinase (PI3K)[95].

1.3. Aspects of pDCs function

Early studies reported a minor population of human peripheral blood leukocytes as a source of type I IFNs[96, 97]. Because of the expression of CD4 and morphological similarity to plasma cells, the population was introduced as plasmacytoid T cells[98]. Furthermore, the cells, in early studies, were also described as plasmacytoid monocytes

because of marker expression profile similar to monocytes' [99, 100]. However, it was shown that plasmacytoid cells could differentiate into antigen-presenting cells[101], and later referred to as pDCs[51, 102]. Most pDCs differentiate from CDPs that also bifurcate into $CD8\alpha^+$ DCs, $CD103^+$ DCs, and $CD11b^+$ DCs. Despite similarities between pDCs and other subsets of DCs, pDCs have their own key properties that distinguished them from DCs and other immune cells, which are discussed below.

1.3.1. IFN secretion upon pathogen-mediated infection

The most striking function of pDCs is the secretion of Type I IFNs, especially IFN-α[51, 102]. In respond to stimuli, for example viral infection, pDCs secrete IFN-α up to 1,000-fold more than other immune cells[103] through a signaling pathway involving Toll-like receptors (TLR) TLR7 and TLR9, which sense RNA and DNA viruses[104]. For example, isolated mouse pDCs from the spleen secrete IFN-α when co-cultured with murine cytomegalovirus (MCMV)[105]. Other *in vivo* studies showed that pDCs are responsible for the secretion of IFN-α upon MCMV infection and secretion of IFN-α is mediated through TLR9/MyD88 (primary-response protein 88) signaling[106, 107]. These studies showed that type I IFN response occurs at early time points during viral infection. However, the secretion of type I IFNs from pDCs decreases at later time points and other immune cell types become the source of type I IFNs as well[104]. Furthermore, the role of pDCs in terms of type I IFNs production seems dispensable to

restrain viral infection of vesicular stomatitis virus (VSV) and influenza viruses[108, 109]. Also other studies using lymphocytic choriomeningitis virus (LCMV) and MCMV showed that pDCs are not the optimal host defense in terms of viral clearance and overall survival ratio[106, 107]. In line with these evidences, secretion of type I IFN by pDCs during local systemic viral infections may be only apparent when other tissue-resident cells are eliminated. Previous studies reported that lung-specific macrophages, alveolar macrophages, are the main source of type I IFNs against pulmonary infection by newcastle disease virus (NDV), and only if alveolar macrophages are depleted then pDCs became the source of type I IFNs[110].

Even though several studies didn't show the critical aspect of type I IFNs from pDCs in terms of clearing viruses and overall host survival, other studies reported a critical role of pDC-derived type I IFNs in viral control. For example, isolated pDCs exponentially secreted IFN-α in 24 hours after being exposed to mouse hepatitis virus (MHV) *in vitro* and mice infected with MHV had severe mortality by day 2 upon infection in the IFN α/β receptor (IFNAR) KO mouse model[111]. Another study using LCMV infection model showed E2-2 KO mice, which lack pDC because E2-2 is a transcription factor specific for pDCs development, could not control LCMV infection. This study found that pDCs and IFN-α were necessary for the maintenance of $CD4^+$ T cells against LCMV[112]. In a human study, patients with null mutations in interferon regulatory factor (IRF) 7, the transcription factor responsible for secretion of type I IFNs in pDCs, fail to produce IFN-α and suffer from severe influenza infection[113]. Although these studies indicated an important role of pDCs and type I IFNs, type I IFNs also can be detrimental

to the hosts. One group reported that high levels of IFN-α in mice upon influenza virus resulted in severe lung damages, morbidity and mortality. They found that excessive IFN-α signaling mediated by pDCs induced lung epithelial cell death in a TNF-related apoptosis-inducing ligand (TRAIL) dependent manner, and depletion of pDCs reduced the lung damage[114]. Thus, the role of pDCs and its type I IFNs seems to vary based on the type of viral infection.

The type I IFNs produced in response to acute viral infection mediate mechanisms of repression of viral replication. In several studies of infection with MCMV, VSV and LCMV in mouse models, production of type I IFNs by pDCs is most apparent at early stages of viral infection. However, the secretion of type I IFNs by pDCs is limited in time and becomes less important at later time-points, because other cells start to produce type I IFNs (21884168). Ablation of TLRs signaling in pDCs during LCMV infection does not significantly impair early virus control. In contrast, *Mavs*$^{-/-}$ mice with the same infection severely have compromised type I IFNs production and repression of early virus replication (22447976).

The role of type I IFNs in chronic viral infection is more complex than in acute infection. Chronic HIV infection, for example, contributes to increased type I IFNs production throughout the course of the disease (22975872). pDCs infected by HIV produce type I IFNs persistently, due to early endosomal trafficking of HIV and TLR7 signaling (21339641). Also type I IFNs secretion in HIV-infected pDCs results in expression of IDO-1 in an autocrine fashion through non-canonical NF-κB pathway, and promotes Tregs commitment (22879398) (17910035). Depletion of pDCs in humanized

mice infected with HIV decreases secretion of type I IFNs and allows increased HIV replication (25077616), suggesting that type I IFNs from pDCs suppresses HIV replication. Although type I IFNs induce antiviral response by TRAIL-mediated $CD4^+$ T cells apoptosis and reduction of viral replication (11772539), type I IFNs also drive memory T cell exhaustion in HIV infection by stimulating hyperproliferation (18077723) and telomere shortening by inhibiting telomerase expression (15148341). In line with this, sustained injection of type I IFNs enhances proliferation of simian immunodeficiency virus (SIV) and decreases $CD4^+$ T cells. However, early administration of type I IFNs prevents systemic infection and increases antiviral genes expression (25043006). Thus there is a narrow window of opportunity at early time-points of infection when type I IFNs can inhibit chronic viral infection.

In case of non-infectious diseases, the role of type I IFNs and pDCs has been associated with pathogenesis. In systemic lupus erythematosus (SLE), pDCs produce TLR9-dependent type I IFNs in response to self-DNA-peptide complexes (21389263) (21389264). Also, blockade of type I IFN signaling in BXSB and NZB×NZW lupus-prone mice allows prolonged survival with decreased pathogenesis (23175700) and reduced skin inflammation (21115693), respectively. Activated TLR7 and TLR9 signaling in pDCs induced by self-DNA-peptide complex in psoriasis (17873860) (25332209) and type 1 diabetes (23242473) has also been reported. On the other hand, tolerogenic pDCs were observed in other non-infectious diseases. For example, in the 2,4,6-trinitrobenzenesulfonic acid (TNBS)-induced colitis model, pDCs are responsible for promoting IL-10 producing Tregs commitment (24721570). In line with this, aortic pDCs

in atherosclerosis are responsible for promoting Tregs commitment and inhibit the disease according to the study presented in this thesis. On the other hand, self-DNA-peptide complex stimulates pDCs and promotes atherosclerosis (22388324), and administration of type I IFNs aggravates lesion formation in aorta (14962699). However, it is not known whether aortic pDCs express type I IFNs in atherosclerosis.

1.3.2. TLR signaling

While $CD8\alpha^+$ DCs and $CD11b^+$ DCs express TLR3 or TLR4, respectively, pDCs express TLR7 and TLR9 to recognize viruses and nucleic acids. Specifically, RNA viruses and endogenous RNA are recognized by TLR7, while DNA viruses, or endogenous and bacterial DNA and synthetic cytosine-guanosine-dinucleotide-containing oligonucleotides (CpG ODN) are detected by TLR9[104]. Although the mechanism by which pDCs recognize viruses is not fully understood, some studies have suggested that pDCs require virus-infected cells to recognize the viral infections[115, 116, 117]. One study found that BM-derived pDCs which were exposed to VSV-infected cells recognized VSV in a TLR dependent manner and expressed higher amount of IFN-α and IFN-β compared to free VSV alone[115]. Other studies also showed that human pDCs require hepatitis A virus (HAV)-infected cells to recognize HAV and produce type I IFNs, and it's facilitated by T cell immunoglobulin mucin family member 1 (TIM1) on pDCs[116]. In line with this, pDCs sense viral RNA-containing exosomes that are released from the

hepatitis C virus (HCV)-infected cells[117]. Recently, another interesting study reported a non-cell mediated mechanism where viral-DNA and RNA bound to antinuclear autoantibodies, in the form of DNA-containing immune complexes, are uptaken by Fc receptor FcγRII, which are expressed on pDCs, and induces TLR-dependent type I IFNs expression[118].

Recognition of viruses through TLR7 and TLR9 results in production of type I IFNs and pro-inflammatory cytokines. Regulation of type I IFNs depends on the MYD88–IRF7 signaling pathway; in contrast, secretion of pro-inflammatory cytokines requires MYD88–NF-κB signaling pathway[53]. These two different pathways depend on whether the TLR9 recognize its ligands in early endosomes. Previous studies have reported that type A CpG ODN is retained in the early endosomes spatiotemporally with MYD88–IRF7, which does not occur in other subsets of DCs[119]. Notably, type A CpG ODN complexed with the cationic lipid 1,2-dioleoyloxy-3-trimethylammonium-propane (DOTAP) can be retained in other subsets of DCs and those DCs express type I IFNs. On the other hand, type B CpG ODN is not retained in early endosomes but rather it is transferred to lysosome-associated membrane protein (LAMP)-1-positive endosomes[120]. However, if type B CpG ODN is complexed with DOTAP, type B CpG ODN is also retained in early endosomes and induced type I IFNs by pDCs[119, 120].

The TLR9 signaling pathway requires other molecules to induce the production of type I IFNs. Adapter protein-3 (AP3) is critical for the trafficking of TLR9 to the lysosome-related organelle for IFNs secretion, and the absence of AP3 results in decrease of type I IFNs by pDCs[121, 122]. In addition *Slc15a4*, which encodes the

peptide/histidine transporter 1 (PHT1), was shown to be required for the production of type I IFNs and cytokines[122]. In terms of recognition of viral nucleic acids, *Slc15a4* is upstream of AP3. However, another study indicated that AP3 was not required for the recognition of DNA-containing immune complexes for the secretion of type I IFNs by pDCs; instead, autophagy-related proteins were involved[123]. In line with these data, TLR7 recognize viral replication intermediates by autophagy process to produce type I IFNs[124]. Furthermore, PI3K and mTOR were reported to be important for IRF7 nuclear translocation, but not for NF-κB signaling[125, 126].

In addition to the TLR pathway in pDCs, the mitochondrial antiviral signaling protein (MAVS) pathway is another mechanism leading to the production of type I IFNs upon viral infection (23706667). MAVS is an adaptor protein that localizes to mitochondria where it interacts with the retinoic acid-inducible gene I (RIG-I)-like receptors (RLRs) signaling that initiate expression of antiviral genes (21844353). Stimulation of TLR7 and TLR9 in pDCs requires detection of viral nucleic acids within endosomes, but the MAVS pathway requires activation of cytosolic RNA sensors, RIG-I and MDA5, and results in elicit IRF3 dependent type I IFNs production and other inflammatory cytokines (23706667.) (23706668.). In the case of virus infection, TLR7 and MyD88 are necessary for type I IFNs production in pDCs, whereas MAVS is required for type I IFNs production in most immune cells but not in pDCs (16713980.). Ablation of RIG-I in pDCs had no effect on secretion of type I IFNs upon viral infection either (14976261.) (16039576.), which indicates that production of type I IFNs in pDCs is independent of the MAVS pathway. However, a recent study using a malaria

plasmodium yoelii YM infection model suggests that MAVS in pDCs acts as a negative regulator of TLR7-dependent type I IFN signaling (27793594.). It seems that pDCs in malaria infection utilize the cytosolic RNA sensor MDA5 to recognize long dsRNA (23706667) instead of RIG-I, which is frequently used by other immune cells to recognize viral infections. This new role of MAVS in pDCs may indicate an inhibitory property of type I IFNs signaling.

1.3.3. Antigen-presentation

pDCs have been reported to present antigens to T cells once they are activated, although they are not as efficient as other subsets of DCs[127]. The expression of MHCII on pDCs is normally low, but upon activation, the levels of MHCII as well as the expression of co-stimulatory molecules such as CD80 and CD86 increase[127]. Some studies indicated that pDCs need to be activated through TLR7 and TLR9 to present endogenous or exogenous antigens and activate T cells[128, 129]. Others studies proposed that pDCs could induce immune tolerance in various mouse models. Recently, it was shown that pDCs can capture subcutaneously injected antigens and migrate to the thymus in a CCR9-dependent manner to induce the deletion of antigen-specific thymocytes[130]. Consistent with these observations, Tregs depend on $CCR9^{+}$ pDCs to inhibit antigen-specific immune responses during acute graft-versus-host disease mouse model[131]. The CCR9 expression in pDCs is only found in steady state and once

pDCs are activated in a TLR-dependent fashion, the expression of CCR9 decreases[130]. These studies indicate that antigen presentation by pDCs may result in T cell activation or tolerance based on TLR signaling and further researches are needed to precise the pathways.

1.3.4. pDC-specific receptors

Mouse pDCs express a cell surface markers pattern that differentiates them from other immune cells. Mouse pDCs are positive for B220, LY6C, plasmacytoid dendritic cell antigen 1 (PDCA1) (also known as BST2), and sialic acid-binding immunoglobulin-like lectin H (Siglec-H). in contrast with human pDCs, mouse pDCs express intermediate level of CD11c[104]. Even though PDCA1 and Siglec-H are specific markers for pDCs in steady state, PDCA1 is expressed on other cells once they are exposed to type I IFNs[132] and Siglec-H also found to be expressed in marginal zone macrophages in the spleen and in medullary macrophages in lymph nodes[133]. Other unique markers of pDCs are PDC-TREM and LY49Q. PDC-TREM is expressed by TLR-stimulated pDCs and associate with Plexin-A1. Once the PDC-TREM-binding with Plexin-A1 is blocked by antibody or expression of PDC-TREM is inhibited by shRNA, secretion of IFN-α is diminished. These data support a model wherein PDC-TREM is required for the production of type I IFNs[134]. Another marker, LY49Q, was also reported to be responsible for the production of type I IFNs in pDCs as depletion of LY49Q resulted in

reduction of IFN-α secretion *in vitro* and *in vivo*[135].

Other receptors on pDCs were shown to have Inhibitory activity to restrain the accidental secretion of IFNs. One study reported that paired immunoglobulin-like receptor B (PIR-B) reduce TLR9-mediated type I IFN secretion in pDCs through dephosphorylation of STAT1/STAT2[136]. Epstein-Barr virus induced receptor 2 (EBI2) was also studied by another group and it was found that depletion of EBI2 results in elevated type I IFNs and cytokines from pDCs[137]. Siglec-H was reported to be associated with DNAX-activation protein 12 (DAP12) to regulate type I IFNs response to TLR9 agonist[138]. Recently, receptor protein tyrosine phosphatase sigma (PTPRS) in human and murine pDCs were shown to be downregulated upon pDCs activation and contribute to inhibit spontaneous secretion of type I IFNs[139]. In case of human pDCs, receptor immunoglobulin-like transcript 7 (ILT7) was shown to bind to CD317/BST2, which is expressed by many cell types including pDCs upon type I IFNs stimulation, and repress secretion of type I IFNs and pro-inflammatory cytokines[140]. Interestingly many of these inhibitory receptors on pDCs in mouse and human are less conserved in evolution compare to other type of receptors, so further characterization of other inhibitory receptors and their ligands would yield important understanding about pDCs in various disease models.

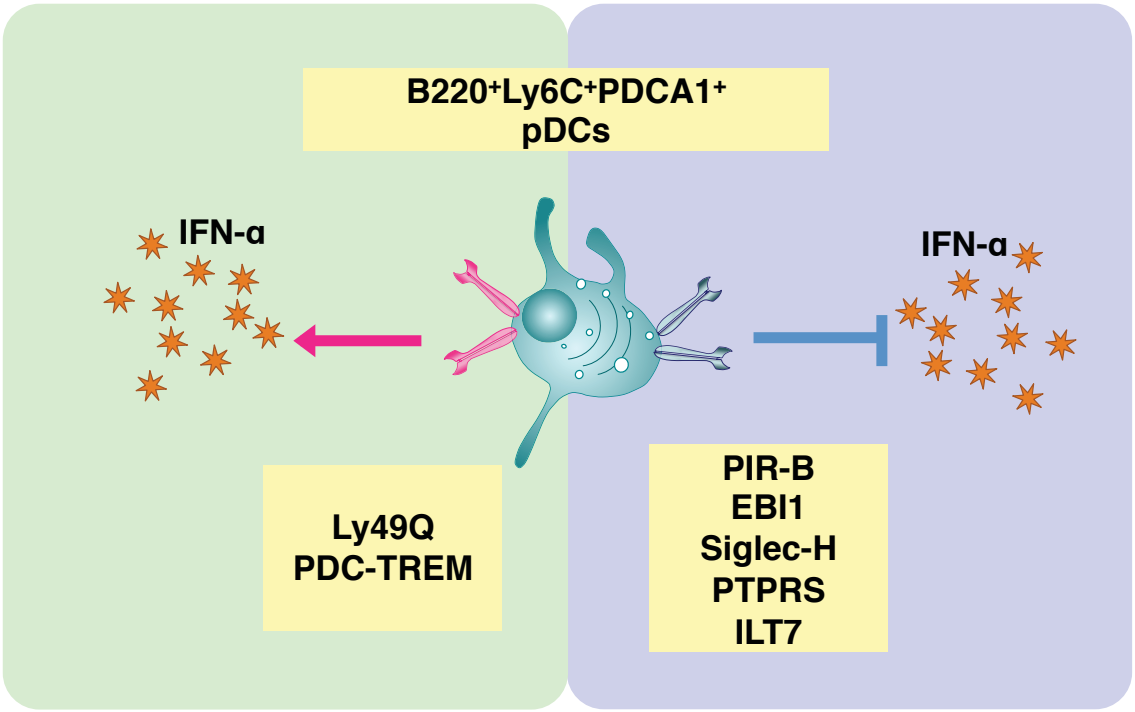

Figure 1.1. pDCs specific Receptors regulating production of IFN-α.
pDCs are positive for B220 and Ly6C, and also express pDCs specific receptors such as PDCA1, Ly49Q, Siglec-H and PTPRS. Ly49Q and PDC-TREM on pDCs are responsible for production of IFN-α. In contrast, PIR-B, EBI1, Siglec-H, PTPRS and ILT7 inhibit secretion of IFN-α and deletion of these markers in pDCs are associated with increased IFN-α production.

1.4. DCs in Atherosclerosis

Atherosclerosis is an inflammatory disease in which apolipoprotein B-containing lipoproteins accumulate in the sub-endothelial layer of the intima of the aorta and promote chronic inflammation facilitated by the innate and adaptive immune response[141]. The lipoproteins promote endothelial cell activation and accumulation of myeloid cells, such as monocytes and DCs, in the arterial intima. These recruited myeloid cells uptake lipoproteins and develop into foam cells. Progression of atherosclerosis is influenced by the innate and adaptive immunity, including DCs that are the critical player of immunity.

1.4.1 Atherosclerosis

Atherosclerosis is one of the main causes of mortality in industrialized countries, estimated at around 15 million deaths per year (20102968) (20404268). Cerebrovascular disease and coronary artery disease are consequences of atherosclerosis, a process that narrows the lumen of arteries by accumulation of atherosclerotic lesions. The atherosclerosis lesions are characterized by lipid deposits in the artery wall, developing preferably at sites where turbulent blood flow occurs (21529710.). The disturbed flow gives rise to endothelial structural deformations by reducing the elastin layer and uncovering negatively charged proteoglycans that can

bind to apolipoprotein B100 (ApoB100) (18506002). Such structural alterations result in accumulation and retention of low-density lipoprotein (LDL) in the sub-endothelial layer when levels of circulating ApoB100-LDL are increased. The trapped LDL particles become susceptible to enzymatic oxidative modifications by myeloperoxidase or lipoxygenases or direct oxidation by reactive oxygen species generated during inflammation (21321594). Oxidized LDL (oxLDL) leads to activation of endothelial cells which produce adhesion molecules, such as E-selectin and VCAM-1, and chemokines to drive intimal infiltration of various immune cells such as monocytes, T cells and DCs. The accumulation of cells and lipids causes obstruction of the lumen of the artery.

1.4.2 Treatment of atherosclerosis

Healthcare systems in many developed countries have been facing a huge burden imposed by the elevated occurrence of atherosclerosis-related disease. Many of the available therapies against atherosclerosis, such as nicotinic acid (21317532), aspirin (19717846) and β-blockers (17606956), are based on mechanisms reducing hypertension and hyperlipidemia or inhibiting platelet aggregation to avoid thrombotic complications. However, these approaches are secondary prevention rather than primary prevention that directly work on inflammatory mechanisms of atherosclerosis development.

Similar to the other therapies for secondary prevention, treatment with statins reduces cholesterol synthesis to lower the levels of circulating LDL. Statins are inhibitors of the enzyme HMG-coA reductase that is also involved in the synthesis of inflammatory mediators, so statins also inhibit inflammation. It has been reported that atorvastatin and rosuvastatin lower levels of high-sensitivity C-reactive protein (hs-CRP) and result in regression of atherosclerosis (16126025) (19329177). The anti-inflammatory actions of statin also reduce and stabilize atherosclerotic plaques because of the beneficial effects on endothelial function and reduction of atherosclerotic lipid lesions (16226165). Statin therapy also decreases the incidence of myocardial infarction, which is one consequence of atherosclerosis disease (16226165).

1.4.3 Atherosclerosis and immune system

Atherosclerotic lesions are characterized by lipids accumulation, infiltration of immune cells, such as T cells, macrophages and neutrophils, and development of fibrous caps. In the early stage of atherosclerosis, lesions consist of lipids deposition in sub-endothelial layer and infiltrated T cells, monocytes and monocyte-derived macrophages (21321594). The monocyte-derived macrophages turn into macrophage-like foam cells as they become loaded with lipids (21529710). Over time, atherosclerotic lesions become a mixture of apoptotic and necrotic cells including foam cells, and cell debris as well as lipids, forming necrotic cores in the plaques. The necrotic cores of the lesions

are covered by fibrous caps composed of collagen and vascular smooth muscle cells (SMCs). The shoulder regions of fibrous caps become heavily infiltrated by neutrophils, T cells and macrophages, which produce pro-inflammatory mediators (18039117). Also infiltrated macrophages replace SMCs and thin fibrous caps that are susceptible to rupture and the formation of a thrombus.

1.4.4. Role of DCs in atherosclerosis

In the steady state, DCs exist in immature state with distinguishable features, such as lower expression of costimulatory molecules CD40, CD80 and CD86, and MHC class II compare to mature DCs, but higher capacity of endocytosis and phagocytosis[142]. These characteristics, in contrast, become largely reversed upon DCs maturation, when DCs migrate to draining LNs to present antigens to T cells. Also TLR-mediated DCs maturation requires TLR signaling adaptor myeloid differentiation MYD88 activation[143, 144]. Interestingly, several studies have demonstrated that DCs accumulate in the lesion of atherosclerosis in mouse and human, and the number of aortic DCs increases as atherosclerosis progress[145, 146, 147, 148]. To investigate the role of DCs in atherosclerosis, one study used mice lacking costimulatory molecule CD80 and CD86 and observed reduced atherosclerosis[149]. In line with this, once DCs are depleted using CD11c-DTR mouse model, atherosclerosis was diminished[146]. These studies indicate that DCs may be pro-atherosclerosis. Other studies, furthermore, suggested that DCs in

atherosclerosis lesions may be compromised for migrating to draining LNs[150], even though DCs are functional in terms of T cell stimulatory capacity[151]. It was suggested that CCR7 might be responsible for impairing migration ability of DCs[141] since blockage of CCR7 signaling by injection of antibodies against the CCR7 ligands, CCL19 and CCL21, prevents migration of aortic DCs to draining LNs and development of atherosclerosis[152]. These data suggested a potential role of defective DCs migration in hypercholesterolemic conditions, such as increasing the secretion of inflammatory cytokines and local activation of T cells.

Even though DCs can induced T cell immunity, DCs also control another aspect of immunity; the induction of Tregs, a small population of $CD4^+$ T cells that repress inflammation[153, 154]. Tregs were reported to repress atherosclerosis-induced inflammation in aorta of a mouse model, and antibody-mediated depletion of Tregs by anti-CD25 antibody resulted in increased atherosclerotic lesions[155]. DCs express costimulatory molecules CD80 and CD86 and deletion of these molecules inhibits Tregs development[156]. In line with this, specific deletion of Myd88 in DCs resulted in decreased number of Tregs, as well as effector T cells, but increased atherosclerotic lesions which indicate role for Tregs to suppress atherosclerosis[157].

Aortic DCs consist of two subsets, $CD103^+$ DCs and $CD11b^+$ DCs, which could have different effects on atherosclerosis. $CD103^+$ DCs were reported to be tolerogenic and inhibit atherosclerosis through the induction of Tregs. $CD103^+$ DCs depend on Flt3 signals and depletion of Flt3 decreased the number of Tregs and increased atherosclerotic lesions in the aorta[148]. The tolerogenic character of $CD103^+$ DCs in gut

and lung was also reported in other studies[158, 159]. On the other hand, the exact role of aortic CD11b$^+$ DCs in atherosclerosis is not known yet because there are no precise genetic tools to deplete CD11b$^+$ DCs with no effects to monocytes and macrophages. However, a previous study, which transiently depleted both CD103$^+$ DCs and CD11b$^+$ DCs with CD11c-DTR mouse model, showed reduced atherosclerosis[146]. Furthermore, CD11b$^+$ DCs constitute most of aortic DCs, suggesting that CD11b$^+$ DCs may promote the development of atherosclerosis. On the other hand, aortic CCL17$^+$ DCs seems to exacerbate atherosclerosis by inhibit Treg development. CCL17$^+$ DCs prevent the differentiation of T cells into Tregs and deletion of CCL17 resulted in increased numbers of Tregs, which led to decrease of atherosclerotic lesions in *Apoe*$^{-/-}$ mouse model[160]. However, whether CCL17$^+$ DCs and CD11b$^+$ DCs are the same population remains unknown.

1.4.5. Role of pDCs in atherosclerosis

pDCs constitute a very small percentage of the total DCs in spleen[50] and only few studies have addressed the function of pDCs in atherosclerosis, with conflicting results. The main feature of pDCs is the secretion of the type I IFNs, which are known to be pro-atherogenic[161]. It was also reported that the levels of type I IFNs transcript in human patient samples correlate positively with plaque severity score[162]. Once pDCs were depleted with anti-PDCA-1 antibody, atherosclerosis lesions are reduced[163, 164].

Also another study showed that depletion of pDCs by deletion of pDCs specific transcription factor, E2-2, reduced atherosclerosis lesions[165]. On the other hand, another study showed a tolerogenic effect for pDCs in atherosclerosis, since depletion of pDCs exacerbated atherosclerotic lesions in *Ldlr*$^{-/-}$ mouse model[166]. However, because PDCA-1 is expressed not only by pDCs but also on other cell types, including macrophages, during inflammation[167], anti-PDCA-1-mediated depletion of pDCs could also have depleted macrophages in the lesions. The E2-2 KO mouse model was reported to have a larger CD8α^{+} DCs-like cell population[59] which is atheroprotective, so further investigations are necessary to elucidate the function of pDCs in atherosclerosis.

1.5. Rationale and objectives of this thesis

Throughout the introduction of this thesis I have discussed about the general function of DCs, their development and their role in atherosclerosis. Even though extensive research has focused on the function of myeloid cells in atherosclerosis in human patients and mouse models, our current knowledge of the fundamental mechanisms of the impact and function of DCs in atherosclerosis still remains limited.

Our laboratory and others have reported the existence of functional aortic DCs and their functions in atherosclerosis[148, 168, 169]. On the other hand, only few studies have focused on the role of pDCs in atherosclerosis; with some reporting that pDCs worsened atherosclerosis[163, 164, 165] and another one reporting that pDCs were protective

against atherosclerosis[166]. Even though pDCs are well known to induce immune response against viral infection by secretion of type I IFNs, pDCs were also reported to induce immune tolerance by inducing Tregs in several studies that showed that depleting pDCs in various disease models resulted in severe pathogenesis[130, 131, 170]. In addition, previous studies showed gaps in their data, such as demonstrating the actual presence of pDCs and their spatial-temporal information in the aorta. As a result, the precise role of pDCs in atherosclerosis has not been comprehensively shown and remains elusive. Therefore, the fundamental premise of this study was to elucidate the functions of pDCs in aorta during atherosclerosis.

1.5.1. Main hypothesis

1) Aortic pDCs may regulate development of atherosclerosis in association with Tregs.
2) Human aortic pDCs in hu-NSG mice and patients may be associated with Tregs in the same manner as mouse aortic pDCs.

1.5.2. Objectives

1) To determine the presence of authentic aortic pDCs in mouse or human, and provide spatial-temporal information about pDCs in aortas from healthy versus diseased individuals, which is critical to understand the role of pDCs

during atherosclerosis progression.

2) To determine the role of authentic aortic pDCs in atherosclerosis because previous studies analyzed the pDCs not from the aortas but from spleens, lymph nodes, and bone marrow in general.
3) To determine the critical molecules in pDCs that are responsible for the regulation of atherosclerosis and maintenance of Tregs.

2. RESULTS

2.1. Identification of pDCs and DCs in normal mouse aorta

Despite constituting a very low proportion of splenocytes (<0.4%; **Figure 2.1.A**), pDCs are central to mounting innate immune responses against most viruses through their production of type I IFNs. We had previously sought to identify pDCs as $CD11c^{+}B220^{+}CD19^{-}$ cells in the normal aorta but found that these cells were very scarce [148]. To overcome this and better identify pDCs, we further optimized our multicolor flow cytometry procedure and applied it to cell suspensions obtained from at least 10–15 pooled healthy mouse aortas, including the aortic root (with valves), ascending aorta, aortic arch, and descending aorta (**Figure 2.1.B**). $CD45^{+}$ leukocytes were first separated from macrophages (MΦs, $CD11b^{+}CD64^{+}$), which are a major source of autofluorescence among aortic $CD45^{+}$ cells (**Figure 2.1.C**), and these cells

were further separated from DCs ($CD11c^+MHCII^+$), monocytes ($CD11b^{hi}Ly6C^{hi}$), granulocytes ($CD11b^+Ly6C^{int}Ly6G^+$), T cells ($CD3^+$), B cells ($CD19^+$), and natural killer (NK) cells ($CD49b^+$)[171, 172]. After all of these non-pDCs populations had been removed, the remaining cells (~0.05% of total $CD45^+$ cells) were found to represent a distinct population of cells bearing a pDCs phenotype (**Figure 2.1.B**). Similar to splenic pDCs, these aortic pDCs expressed high levels of PDCA-1/BST2/CD317, lymphocyte antigen 6 complex (Ly6C), FMS-related tyrosine kinase 3 (Flt3)/CD135, B220/CD45R, Siglec-H (**Figure 2.1.D**), and Clec9A compared with aortic B cells (**Figure 2.1.E**), but lesser amounts of other leukocyte markers specific for granulocytes, B cells, T cells, and NK cells (**Figure 2.1.F**). In addition, pDCs did not express monocyte or MΦ-specific markers, such as CD11b, CX_3CR1, F4/80, CD115/MCSF-R, CD14, CD64, CD206 and MerTK (**Figures 2.1.G** and **2.1.H**). Notably, these pDCs also lacked expression of the DC-specific markers Zbtb46, XCR1 and CD103, and expressed low levels of CD11c and MHCII compared with DCs (**Figure 2.1.I**) [49, 148, 173]. We also observed, after separation of MΦs ($CD11b^+CD64^+$), two subsets of aortic DCs; $CD103^+$ DCs and $CD11b^+$ DCs (**Figure 2.1.J**). The two DCs subsets were negative for the expression of other leukocyte markers specific for T cells, B cells, granulocytes, and pDCs (**Figure 2.1.K**). Interestingly two subsets of DCs showed different marker expressions. $CD103^+$ DCs in aorta expressed higher amount of Zbtb46, Clec9A, and XCR1 compare to $CD11b^+$ DCs, but CD14, CX_3CR1, and CD172a were only expressed in $CD11b^+$ DCs (**Figure 2.1.L**). To further distinguish pDCs from other immune cells by functional criteria, we bathed aortic cell suspensions in serum-containing RPMI medium with 1 μm fluorescent YG

microspheres for 1hour to test whether pDCs had the phagocytic activity of MΦs. pDCs, DCs, and B cells were poorly phagocytic (took up 0-1 bead), whereas MΦs were highly phagocytic (> 3-5 beads) (**Figure 2.1.M**). When sorted out, pDCs were round or spherical shapes separable from MΦs and the dendritic morphology of DCs.

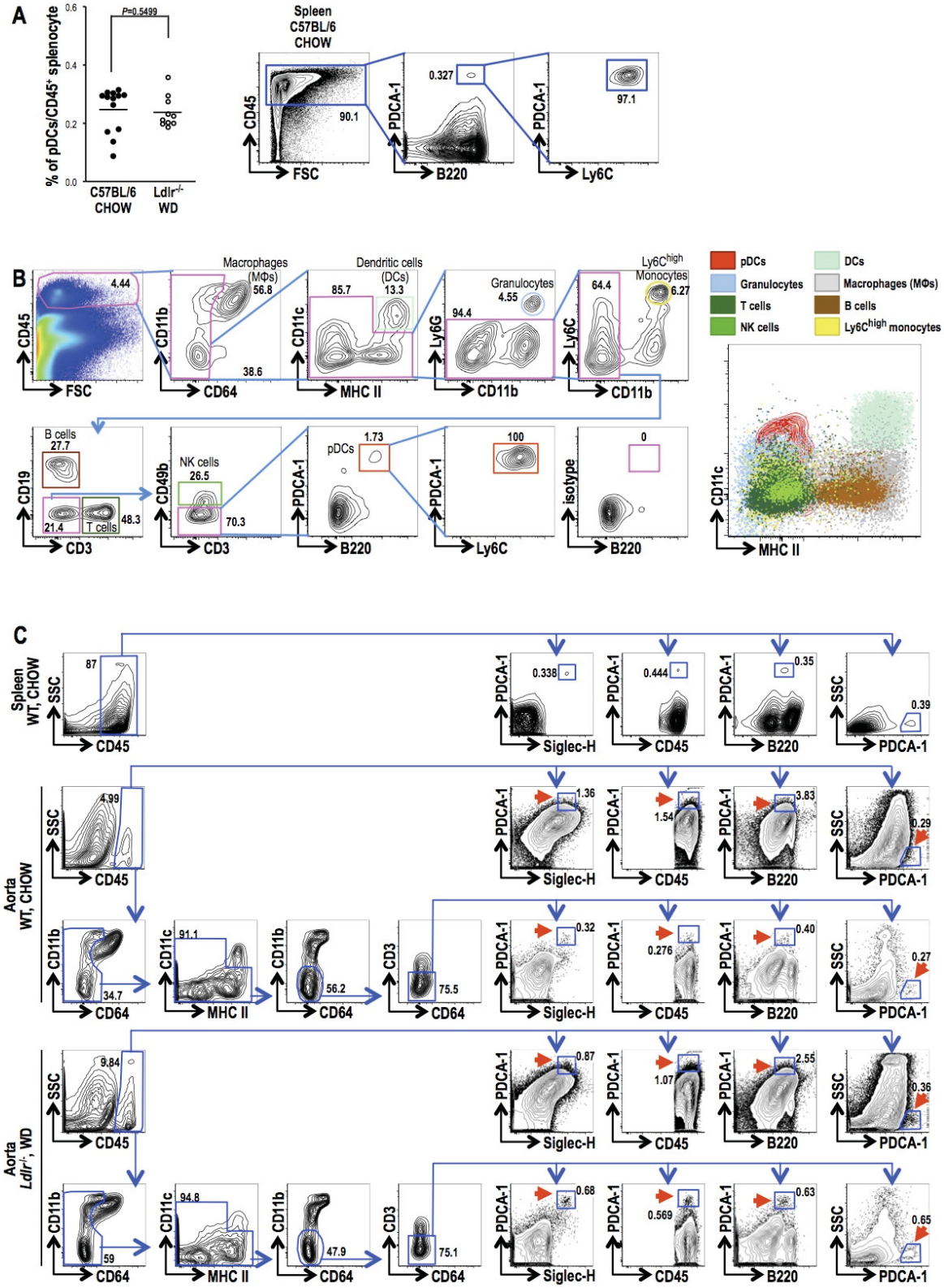
A
% of pDCs/CD45+ splenocyte
P=0.5499
C57BL/6 CHOW
Ldlr-/- WD
Spleen C57BL/6 CHOW
CD45
FSC
90.1
PDCA-1
B220
0.327
Ly6C
97.1
B
CD45
FSC
4.44
CD11b
CD64
Macrophages (MΦs)
56.8
38.6
CD11c
MHC II
Dendritic cells (DCs)
85.7
13.3
Ly6G
CD11b
Granulocytes
4.55
94.4
Ly6C
CD11b
Ly6Chigh Monocytes
64.4
6.27
CD19
CD3
B cells
27.7
21.4
T cells
48.3
CD49b
CD3
NK cells
26.5
70.3
PDCA-1
B220
pDCs
1.73
PDCA-1
Ly6C
100
isotype
B220
0
pDCs
Granulocytes
T cells
NK cells
DCs
Macrophages (MΦs)
B cells
Ly6Chigh monocytes
CD11c
MHC II
C
Spleen WT, CHOW
SSC
CD45
87
PDCA-1
Siglec-H
0.338
CD45
0.444
B220
0.35
PDCA-1
SSC
0.39
Aorta WT, CHOW
4.99
1.36
1.54
3.83
0.29
CD11b
CD64
34.7
CD11c
MHC II
91.1
CD11b
CD64
56.2
CD3
CD64
75.5
0.32
0.276
0.40
0.27
Aorta Ldlr-/-, WD
9.84
0.87
1.07
2.55
0.36
59
94.8
47.9
75.1
0.68
0.569
0.63
0.65

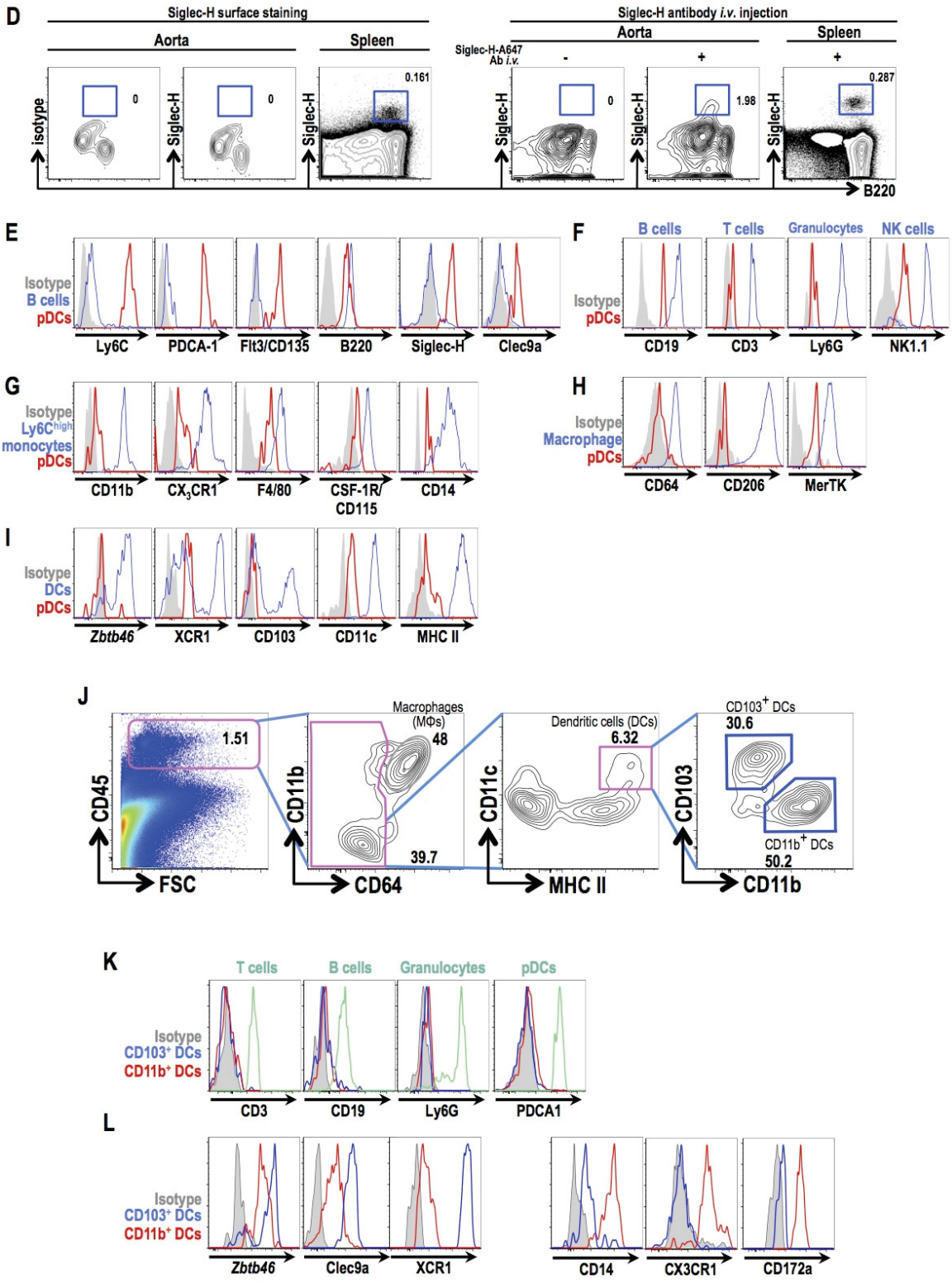
D
Siglec-H surface staining
Aorta
Spleen
Siglec-H antibody i.v. injection
Aorta
Spleen
Siglec-H-A647 Ab i.v.
-
+
+
isotype
Siglec-H
0
0
0.161
0
1.98
0.287
B220
E
Isotype
B cells
pDCs
Ly6C
PDCA-1
Flt3/CD135
B220
Siglec-H
Clec9a
F
B cells
T cells
Granulocytes
NK cells
Isotype
pDCs
CD19
CD3
Ly6G
NK1.1
G
Isotype
Ly6C^high monocytes
pDCs
CD11b
CX3CR1
F4/80
CSF-1R/ CD115
CD14
H
Isotype
Macrophage
pDCs
CD64
CD206
MerTK
I
Isotype
DCs
pDCs
Zbtb46
XCR1
CD103
CD11c
MHC II
J
Macrophages (MΦs)
Dendritic cells (DCs)
CD103+ DCs
1.51
48
39.7
6.32
30.6
CD11b+ DCs
50.2
CD45
FSC
CD11b
CD64
CD11c
MHC II
CD103
CD11b
K
T cells
B cells
Granulocytes
pDCs
Isotype
CD103+ DCs
CD11b+ DCs
CD3
CD19
Ly6G
PDCA1
L
Isotype
CD103+ DCs
CD11b+ DCs
Zbtb46
Clec9a
XCR1
CD14
CX3CR1
CD172a

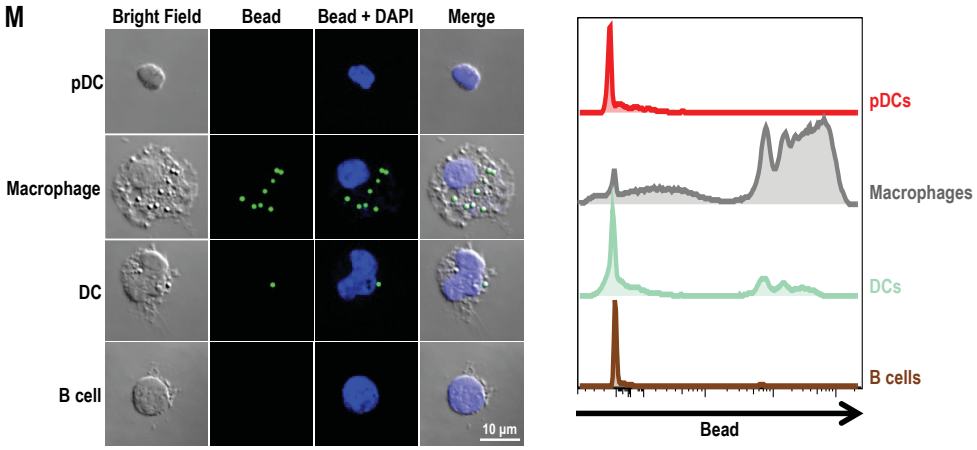
M
Bright Field
Bead
Bead + DAPI
Merge
pDC
Macrophage
DC
B cell
10 µm
pDCs
Macrophages
DCs
B cells
Bead

Figure 2.1. Identification of pDCs and DCs under steady state in mouse aortas.

(A) Left: frequency of pDCs in the steady-state spleen and atherosclerotic spleen (bar = mean, n ≥ 9); Right: gating strategy for pDCs in spleen.

(B) Gating strategy for aortic macrophages (MΦs), dendritic cells (DCs), B cells, T cells, NK cells, granulocytes, Ly6C^{high} monocytes, and pDCs from collagenase-digested aortic cells from 10–15 pooled C57BL/6 mouse (WT) aortas. The liberated cells were surface stained for the indicated markers and analyzed by FACS. The subpopulation of aortic leukocytes are visualized on the dot blot (right) according to the expression of CD11c and MHCII. SSC^{low} and FSC^{low} dead cells and doublet cells were gated out and analyzed with FlowJo (TriStar).

(C) Gating strategy for pDCs in spleens and aortas, compared with previously published strategy. Note that macrophages (MΦs) removal is critical for enumeration of pDCs.

(D) Detection of Siglec-H expression by injection of anti-Siglec-H-Alexa647 antibody. WT mice were injected *i.v.* with 15 µg of Siglec-H-Alexa647 (clone: 551) and sacrificed 14–18 hours post injection. Aortic pDCs were gated from CD45$^+$CD11b$^-$CD64$^-$B220$^+$Ly6C$^+$ cells. Surface staining of Siglec-H did not reveal a clear population (left), but injection of anti-Siglec-H prior to collagenase treatment yielded a specific population of Siglec-H$^+$ cells (right). Note that Siglec-H surface expression is higher in the spleen and is still detectable after collagenase treatment.

(E–I) Aortic pDCs (red lines) were analyzed for surface markers and compared with other aortic cell populations (blue lines) and isotypes (grey filled lines). All markers were surface stained except CD206 and Clec9a, which were stained intracellularly; *Zbtb46* (*Zbtb46*$^{+/+}$ [WT] and *Zbtb46*$^{gfp/+}$) and *Cx$_3$cr1* (*Cx$_3$cr1*$^{+/+}$ [WT] and *Cx$_3$cr1*$^{gfp/+}$) reporter mice were used for evaluating the expression of these molecules in aortic pDCs. Representative marker histograms from at least three experiments are shown, and each histogram is from 6–10 pooled WT aortas.

(E) pDC-specific markers compared to B cells.

(F) Expression of specific markers for B, T, and NK cells and granulocytes in pDCs.

(G) Expression of specific markers for Ly6C^{high} monocytes in pDCs.

(H) Expression of macrophages (MΦs)-specific markers in pDCs.

(I) Expression of DC-specific markers in pDCs.

(J) Gating strategy for aortic macrophages (MΦs), dendritic cells (DCs), and two subsets of DCs from collagenase-digested aortic cells from 2 pooled C57BL/6 mouse (WT) aortas. The liberated cells were surface stained for the indicated markers and analyzed by FACS. SSC^{low} and FSC^{low} dead cells and doublet cells were gated out and analyzed with FlowJo (TriStar).

(K and L) Aortic CD103$^+$ DCs (blue lines) and CD11b$^+$ DCs (red lines) were analyzed for surface markers and compared with other aortic cell populations (green lines) and isotypes (grey filled lines). All markers were surface stained except Clec9a, which were stained intracellularly; *Zbtb46* (*Zbtb46*$^{+/+}$ [WT] and *Zbtb46*$^{gfp/+}$) and *Cx$_3$cr1* (*Cx$_3$cr1*$^{+/+}$ [WT] and *Cx$_3$cr1*$^{gfp/+}$) reporter mice were used for evaluating the expression of these molecules in aortic DCs subsets.

(K) Expression of specific markers for T cells, B cells, granulocytes, and pDCs (green lines) in CD103$^+$ DCs (blue lines) and CD11b$^+$ DCs (red lines).

(L) *Left:* Expression of CD103$^+$ DCs specific markers; *Right:* Expression of CD11b$^+$ DCs specific markers.

(M) Morphology and phagocytic activity of aortic pDCs. Aortic cells from 40 pooled WT aortas were incubated with 1 µm Fluoresbrite YG microspheres (green) for 1 hour and stained with markers as in (B). Cells were sorted out, cytospined to assess morphology (left) and counterstained for DAPI (blue) and phagocytic activity was assessed by FACS (right).

2.2. Flt3L treatment increases pDCs numbers in the aorta

Given the higher expression of Flt3/CD135 in aortic pDCs (**Figure 2.1.B**), we next asked whether Flt3L, a cytokine crucial for DCs development, could expand this population. We previously reported that Flt3L treatment selectively increased $CD11c^{+}MHCII^{+}$ DCs[148]. Similarly, Flt3L treatment increased DCs and pDCs in the spleen (**Figures 2.2.A** and **2.2.B**). In these mice, the absolute number and percentage of aortic pDCs were increased (**Figure 2.2.C**). However, MΦs, which are dependent on CD115, did not show any significant expansion (**Figure 2.2.C**, **bottom**). To rule out nonspecific effects, we next tested Flt3L on Flt3-deficient (*Flt3*$^{-/-}$) mice. Whereas Flt3L treatment increased the number of aortic pDCs in wild-type (WT) mice, this effect was completely absent in *Flt3*$^{-/-}$ mice (**Figures 2.2.D** and **2.2.E**). To further identify the anatomical location of pDCs in the aortic wall, we surgically separated adventitia from aorta. In the normal aorta, pDCs were not detected in the adventitia, but were present in the intima (**Figure 2.2.F**). Treatment with Flt3L slightly increased the number of pDCs in the adventitia but most increases were restricted to the intima. To further confirm the anatomical location of pDCs, an *en face* preparation of the aorta was stained for immunofluorescence (IF) with the pDCs marker Siglec-H and co-stained for CD11c. We had previously reported that DCs are enriched in the intimal space, based on staining with CD11c only (**Figure 2.2.H**)[148, 168]. Notably, Siglec-H^{+} cells were only detected in the intima and their morphology was spherical—clearly distinguishable from the dendritic morphology of DCs (**Figure 2.2.G**). To further define the exact location of these cells,

we separated aortas into aortic root, aortic arch including the ascending aorta, and descending aorta. This analysis revealed that most pDCs were localized in the sinus area of the normal aorta (**Figures 2.2.I** and **2.2.H**), an area known to be atherosclerosis prone where most of both DCs subsets are located (**Figure 2.2.J**).

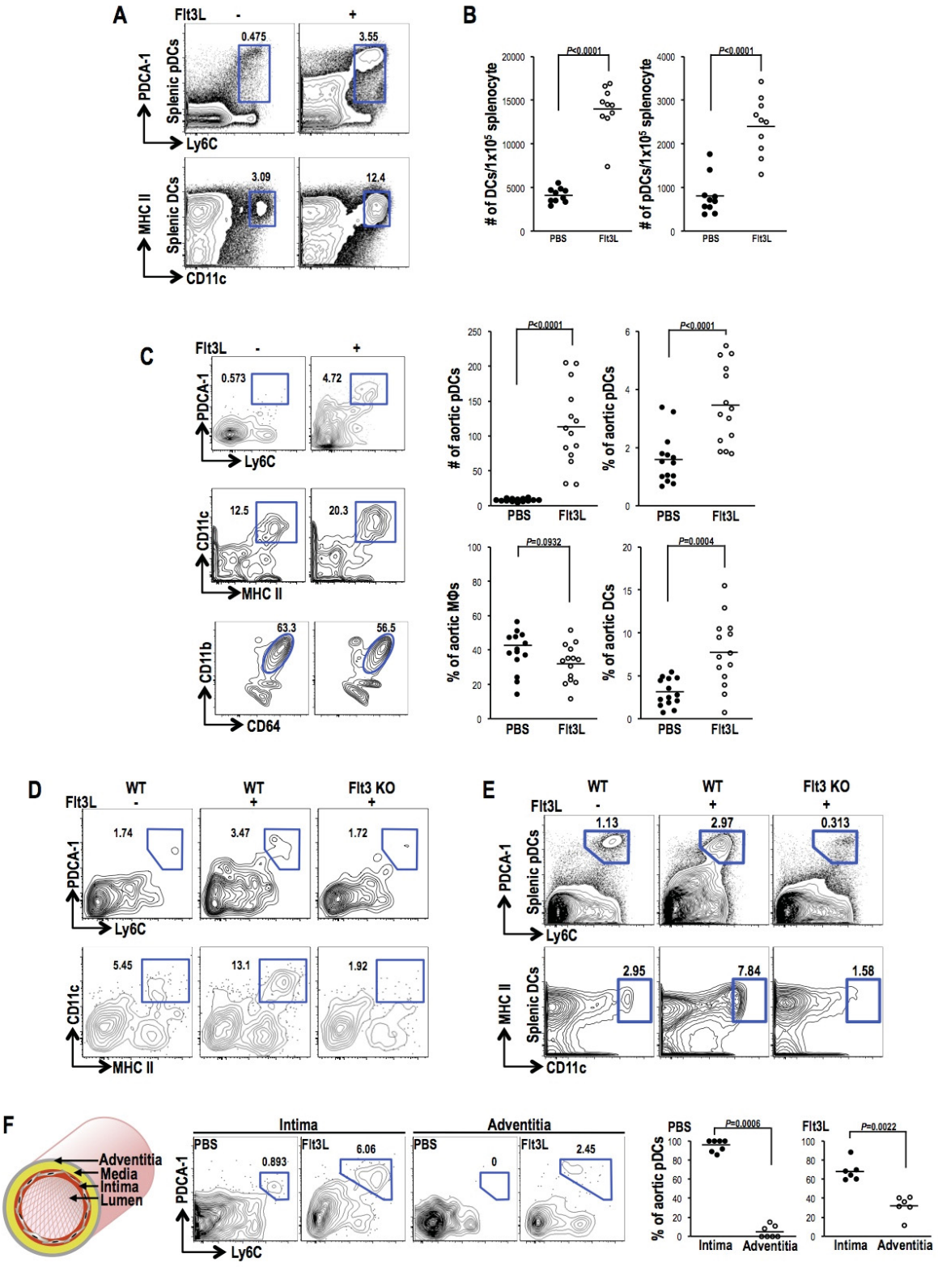
A
Flt3L - +
0.475
3.55
PDCA-1
Splenic pDCs
Ly6C
3.09
12.4
MHC II
Splenic DCs
CD11c
B
P<0.0001
# of DCs/1x10^5 splenocyte
PBS
Flt3L
P<0.0001
# of pDCs/1x10^5 splenocyte
C
Flt3L - +
0.573
4.72
12.5
20.3
63.3
56.5
CD11b
CD64
P<0.0001
# of aortic pDCs
P<0.0001
% of aortic pDCs
P=0.0932
% of aortic MΦs
P=0.0004
% of aortic DCs
D
WT - WT + Flt3 KO +
Flt3L
1.74
3.47
1.72
5.45
13.1
1.92
E
WT - WT + Flt3 KO +
Flt3L
1.13
2.97
0.313
2.95
7.84
1.58
F
Adventitia
Media
Intima
Lumen
Intima
Adventitia
PBS
Flt3L
0.893
6.06
0
2.45
P=0.0006
P=0.0022
% of aortic pDCs
Intima
Adventitia

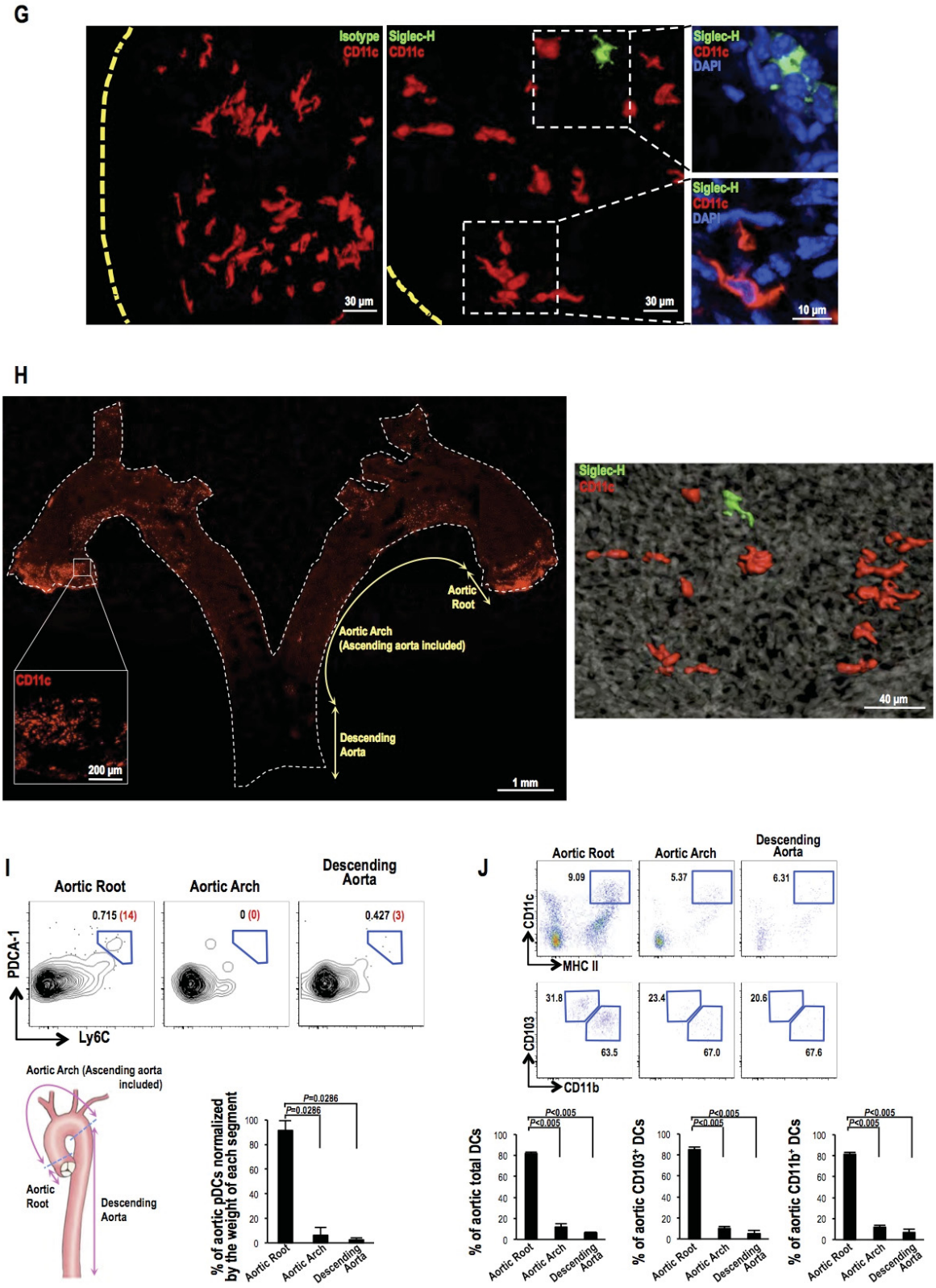
G
Isotype
CD11c
30 µm
Siglec-H
CD11c
30 µm
Siglec-H
CD11c
DAPI
Siglec-H
CD11c
DAPI
10 µm
H
CD11c
200 µm
Aortic Root
Aortic Arch
(Ascending aorta included)
Descending Aorta
1 mm
Siglec-H
CD11c
40 µm
I
Aortic Root
Aortic Arch
Descending Aorta
0.715 (14)
0 (0)
0.427 (3)
PDCA-1
Ly6C
Aortic Arch (Ascending aorta included)
Aortic Root
Descending Aorta
% of aortic pDCs normalized by the weight of each segment
P=0.0286
P=0.0286
Aortic Root
Aortic Arch
Descending Aorta
J
Aortic Root
Aortic Arch
Descending Aorta
9.09
5.37
6.31
CD11c
MHC II
31.8
63.5
23.4
67.0
20.6
67.6
CD103
CD11b
% of aortic total DCs
% of aortic CD103+ DCs
% of aortic CD11b+ DCs
P<0.005
P<0.005
Aortic Root
Aortic Arch
Descending Aorta

Figure 2.2. Flt3/Flt3L-dependent aortic pDCs and DCs localize to atherosclerosis-prone areas.

(A-C) WT mice were injected intraperitoneally (*i.p.*) with PBS alone or with 2 μg of Flt3L/day for 9 consecutive days.

(A) Representative FACS plots of pDCs and DCs from spleens of mice injected with PBS or Flt3L.

(B) Quantification of DCs and pDCs from spleens (bar = mean).

(C) Absolute numbers and percentages (%) of aortic pDCs, DCs, and macrophages (MΦs) were quantified by FACS. *Left:* representative FACS plot of aortic pDCs (top), DCs (middle) and macrophages (MΦs) (bottom); *Right:* quantification of absolute numbers of aortic pDCs per aorta and % of aortic pDCs, DCs, and macrophages (MΦs) among aortic $CD45^+$ cells (bar = mean; n = 14).

(D-E) WT mice and Flt3/Flk2/CD135-deficient mice were injected intraperitoneally (*i.p.*) with PBS alone or with 2 μg of Flt3L/day for 9 consecutive days.

(D) Aortic pDCs and DCs were quantified from WT mice and *Flt3*$^{-/-}$ mice. Representative FACS plots from at least three experiments.

(E) pDCs and DCs from spleens, analyzed from mice in (D).

(F-H) Localization and distribution of aortic pDCs.

(F) Aortas from WT mice injected with PBS (n = 7) or Flt3L (n = 6) were surgically separated into intima and adventitia. Representative FACS plots (middle) and quantitation (right, bar = mean). Each value (dot) is from 5-7 pooled aortas (PBS-injected) or 2-3 pooled aortas (Flt3L-injected).

(G) Z-stacked confocal microscopy images of an *en face* IF with Siglec-H (pDC, green), CD11c (DC, red) and counterstained with DAPI (nuclei, blue) in the aortic intima. Aortas from WT mice, without (left) or with (right) Siglec-H-Alexa-488 Ab injection, were stained with an anti-Alexa-488 antibody to visualize Siglec-H^+ cells (yellow dashed lines: borders of aortic valves).

(H) *Left*: distribution of aortic $CD11c^+$ cells (red). Inset shows the Siglec-H^+ cell area in (G). *Right*: Z-stacked confocal microscopy image of the inset from the left panel. Siglec-H^+ cells (pDCs, green) and CD11c+ cells (DCs, red) are visualized from aortic intima (auto-fluorescent internal elastic lamina, grey).

(I) Distribution of aortic pDCs in each aortic segment (aortic root, aortic arch, and descending aorta) from WT mice were analyzed. *Top*: representative FACS plot of pDCs in each segment of the aorta (%, black; cell numbers, red); *Bottom*: % of aortic pDCs normalized by the weight of each aorta segment (graph = mean ± SD; n = 10 mice/experiment; 4 experiments).

(J) Distribution of aortic total DCs and their two subsets in each aortic segment (aortic root, aortic arch, and descending aorta) from WT mice were analyzed. *Top*: representative FACS plot of DCs in each segment of the aorta; *Middle*: representative FACS plot of $CD103^+$ DCs and $CD11b^+$ DCs in each segment of the aorta; *Bottom*: % of aortic total DCs, $CD103^+$ DCs, and $CD11b^+$ DCs in each segment, normalized by total numbers of DCs, $CD103^+$ DCs, and $CD11b^+$ DCs, respectively (graph = mean ± SD; 4 experiments).

2.3. Aortic pDCs are bona fide pDCs that secrete IFN-α

It is well established that pDCs secrete type I IFN upon TLR7 or -9 ligation[174]. Previous studies had failed to measure IFN-α in the mouse aorta[163, 164, 165, 166]. Given the scarcity of pDCs, we reasoned that a method for obtaining more aortic pDCs was needed to successfully assay for secreted IFN-α. First, we expanded pDCs by treating them with Flt3L. Then, we compared the capacity of splenocytes, which typically contain ~0.4% pDCs in WT mice (**Figure 2.1.A**), with single-cell suspensions prepared from hearts and aortas of 10 WT mice, treated with Flt3L. Notably, cells obtained from hearts and aortas secreted detectable IFN-α when challenged with TLR9 agonist, synthetic oligodinucleotides containing CpG motifs (CpG ODNs, now after CpG) (**Figures 2.3.A** and **2.3.B**). To further identify the types of aortic cells that secreted IFN-α, we performed intracellular staining (ICS) for IFN-α and analyzed cells by fluorescence-activated cell sorting (FACS). Of the total aortic IFN-α^+ cell population, more than 80% were pDCs, similar to LNs pDCs (**Figure 2.3.C**). Within each cell type (aortic pDCs and LNs pDCs), 5-7% of cells produced IFN-α^+ (**Figure 2.3.D**). To further confirm these *in vitro* results, we next questioned if aortic pDCs upregulate the expression of PDC-TREM, a pDC-specific receptor responsible for increased production of type I IFNs[134]. When CpG was injected intravenously (*i.v.*) for 9-12 hours, LNs pDCs did preferentially upregulate PDC-TREM (**Figure 2.3.E**). Of note, we observed inducible expression of PDC-TREM in native aortic pDCs (**Figure 2.3.E**). Therefore, pDCs identified in the normal mouse aorta are functional pDCs with a morphology clearly distinguishable from that of other DCs

and possess the unique capacity to produce IFN-α *in vivo*.

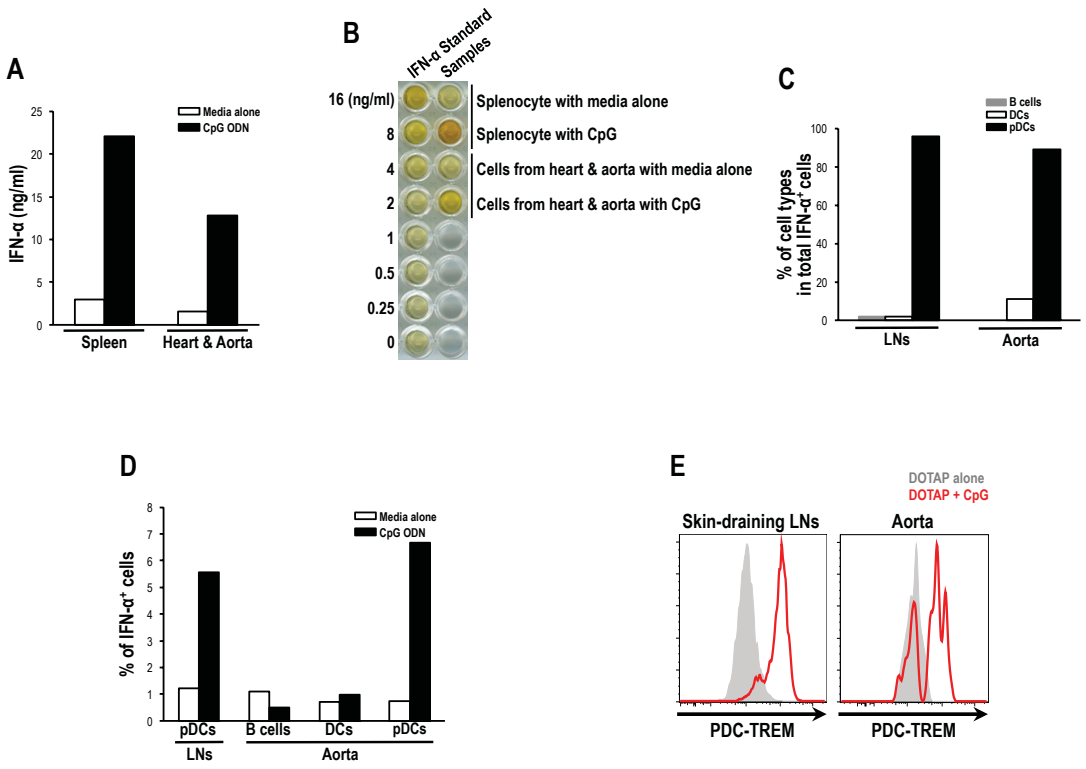

Figure 2.3. Aortic pDCs secrete type I IFN upon TLR9 ligation.

(A) Single cells from spleens and pooled hearts and aortas from Flt3L-treated WT mice were incubated *in vitro* with 10 μg/mL of CpG for 48 hours. IFN-α in the supernatant was measured by ELISA.

(B) ELISA plate image, related to (A).

(C) IFN-α$^+$ cells were measured at the single-cell level by incubating all cells from each organ with media alone or 10 μg/mL of the CpG for 3 hours followed by an additional 6 hours incubation with 10 μg/mL of brefeldin A (BFA). After cell surface staining and ICS for IFN-α, total IFN-α$^+$ cells, defined as CD45$^+$CD64$^-$IFN-α$^+$ cells, were enumerated. Aortic pDCs, CD45$^+$CD64$^-$CD11b$^-$ B220$^+$PDCA-1$^+$Ly6C$^+$IFN-α$^+$; skin-draining LNs pDCs, B220$^+$PDCA-1$^+$Ly6C$^+$IFN-α$^+$. Graph is representative of two independent experiments.

(D) Percentage of IFN-α$^+$ skin-draining LN cells and aortic cells from WT mice (n = 30) were analyzed after *in vitro* stimulation with CpG. WT mice were injected *i.p.* with 2 μg of Flt3L per day for nine consecutive days. Total cells from each organ were incubated with media alone or with 10 μg/mL of CpG for 3 hours followed by an additional 6 hours incubation with 10 μg/mL of Brefeldin A (BFA). Aortic pDCs, CD45$^+$CD64$^-$CD11b$^-$B220$^+$PDCA-1$^+$Ly6C$^+$IFN-α$^+$; skin- draining LN pDCs, B220$^+$PDCA-1$^+$Ly6C$^+$IFN-α$^+$, related to (C).

(E) PDC-TREM expression in skin-draining LNs pDCs and native aortic pDCs. 6-7 mice were injected *i.v.* with CpG (10 μg/mouse) complexed to DOTAP (30 μl/mouse) or DOTAP alone. 9-12 hours later, LNs and aortas were harvested and pooled to stain pDCs with anti-PDC-TREM antibody (See gating strategy in Figure 2.1.B). Histogram is representative of two independent experiments.

2.4. pDCs are present in humanized mice aortas

Our ability to analyze human aortas was constrained by the paucity of pDCs as well as limited availability of human tissues. Therefore, we next assessed whether human pDCs could be identified in the steady-state mouse aorta reconstituted with human stem cells (HSCs). To this end, we used NOD/SCID/γc-null (NSG) mice whose BM is reconstituted from purified human cord blood HSCs (hu-mice hereafter). pDCs in these mice can be easily detected in peripheral blood as cells that are negative for monocyte/MΦ markers (CD14, CD64, CD16) and the B cell marker CD19, but positive for HLA-DR, CD123 and BDCA2 (**Figure 2.4.A**)[175]. pDCs were detectable in aortas isolated from these mice and were further increased in number by Flt3L treatment (**Figures 2.4.B** and **2.4.C**). To test systemic IFN-α secretion in hu-mice, we injected CpG *i.v.* and measured serum IFN-α levels over a 12 hours period. Functional human IFN-α was detected in the blood of hu-mice as early as 4 hours after CpG ligation (**Figure 2.4.D**). We next asked whether pDCs in the hu-mice aorta could produce functional IFN-α. To this end, we incubated aortic cell suspensions from hu-mice with CpG (10 μg/ml) for 9 hours. For the last 6 hours, Brefeldin A (BFA) was added to block secretion of IFN-α. Notably, pDCs produced IFN-α and also showed upregulated surface expression of CCR7 and CD83 upon TLR9 ligation, whereas other BDCA3$^+$ DCs in the same culture well did not (**Figure 2.4.E**). These results suggest that pDCs in the hu-mice aorta are authentic pDCs with the capacity to produce copious amounts of IFN-α (**Figure 2.4.E**). pDCs were also detected in the aortas of hu-BLT mice, another hu-

mice model transplanted with HSCs isolated from fetal liver, and donor-matched thymus (**Figure 2.4.F**). To localize these pDCs in the hu-mice aorta, we needed an additional reliable, single marker to stain tissue samples. To this end, we chose lysosome-associated membrane protein 5 (LAMP5), a newly discovered marker for pDCs[176]. We found that LAMP5 expression was restricted to human pDCs (**Figure 2.4.G**)[177]. Moreover, LAMP5 staining was sufficient to mark $CD123^+BDCA2^+BDCA4^+$ pDCs in human peripheral blood (**Figure 2.4.H**); this was further confirmed using pDCs from hu-mice BM (**Figures 2.4.I** and **2.4.J**). Using an anti-LAMP5 antibody, we found that pDCs were localized in the aortic root (sinus) of hu-mice (**Figure 2.4.K, left**), where numerous $HLA\text{-}DR^+$ cells were also found (**Figure 2.4.K, right)**. Notably, pDCs were only detected in the intimal space of the normal hu-mice aorta (**Figure 2.4.L**). These pDCs were also easily detected in non-atherosclerotic human aortas (**Figures 2.4.M** and **2.4.N**).

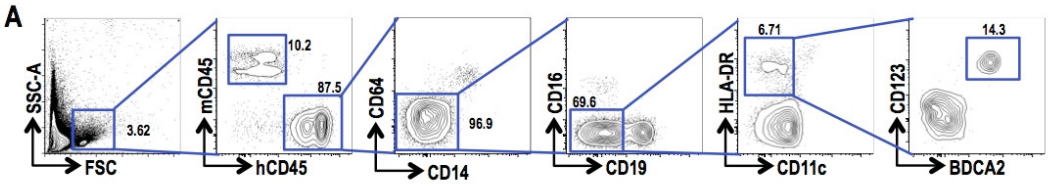
A
SSC-A
FSC
3.62
mCD45
hCD45
10.2
87.5
CD64
CD14
96.9
CD16
CD19
69.6
HLA-DR
CD11c
6.71
CD123
BDCA2
14.3

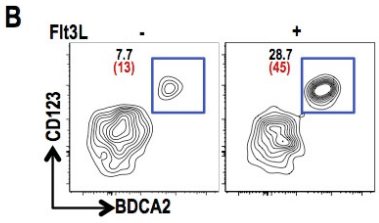
B
Flt3L
-
+
7.7
(13)
28.7
(45)
CD123
BDCA2

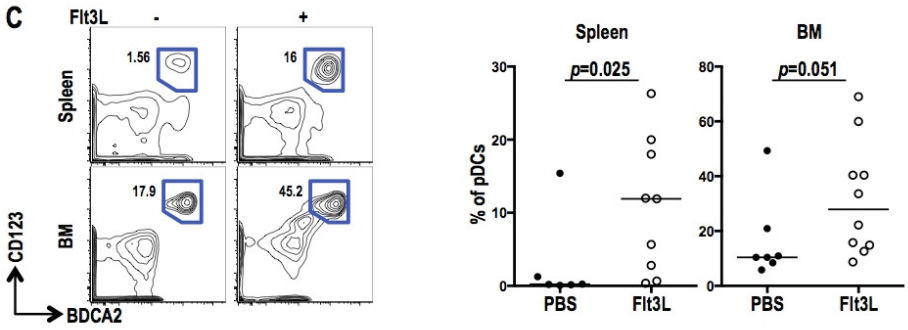
C
Flt3L
-
+
Spleen
BM
1.56
16
17.9
45.2
CD123
BDCA2
Spleen
BM
p=0.025
p=0.051
% of pDCs
PBS
Flt3L
PBS
Flt3L

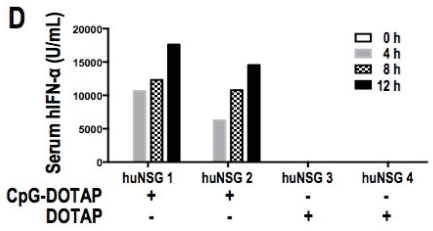
D
Serum hIFN-α (U/mL)
0 h
4 h
8 h
12 h
huNSG 1
huNSG 2
huNSG 3
huNSG 4
CpG-DOTAP
DOTAP

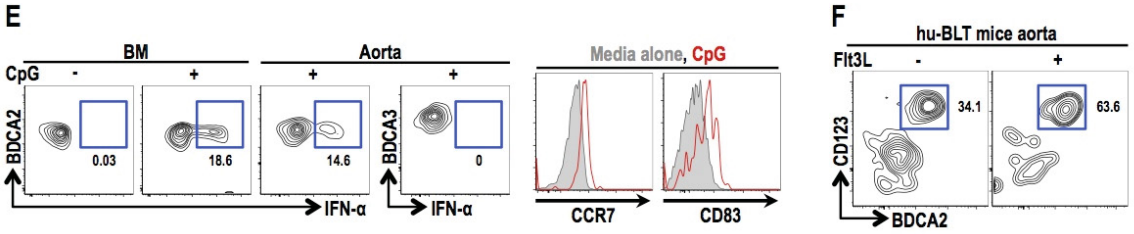
E
BM
Aorta
CpG
BDCA2
IFN-α
0.03
18.6
14.6
BDCA3
IFN-α
0
Media alone, CpG
CCR7
CD83
F
hu-BLT mice aorta
Flt3L
CD123
BDCA2
34.1
63.6

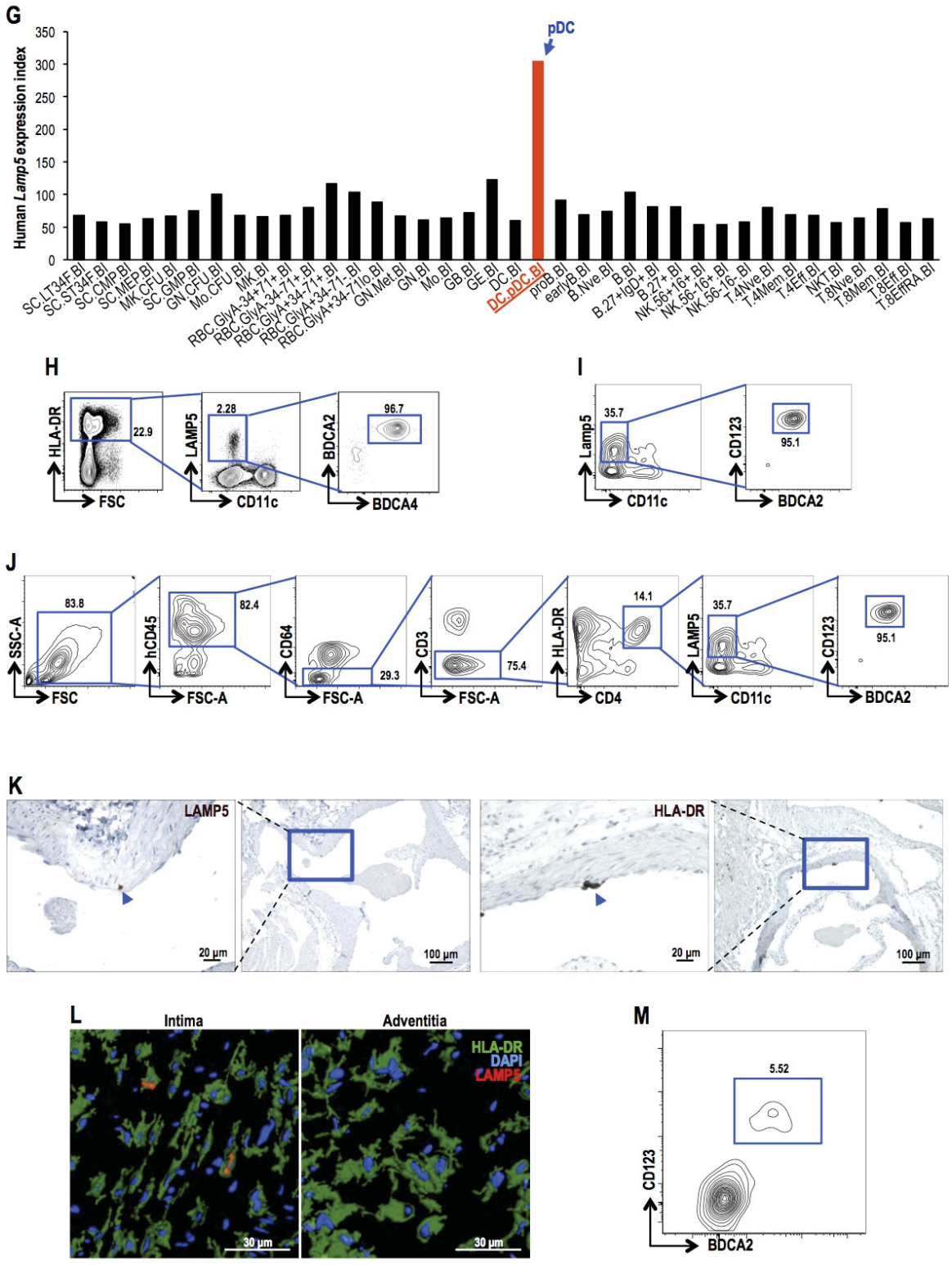
G
Human Lamp5 expression index
pDC
SC.LT34F.BI
SC.ST34F.BI
SC.CMP.BI
SC.MEP.BI
MK.CFU.BI
SC.GMP.BI
GN.CFU.BI
Mo.CFU.BI
MK.BI
RBC.GlyA-34+71+.BI
RBC.GlyA-34-71+.BI
RBC.GlyA+34-71+.BI
RBC.GlyA+34-71-.BI
RBC.GlyA+34-71lo.BI
GN.Mat.BI
GN.BI
Mo.BI
GB.BI
GE.BI
DC.BI
DC.pDC.BI
proB.BI
earlyB.BI
B.Nve.BI
B.BI
B.27+IgD+.BI
B.27+.BI
NK.56+16+.BI
NK.56-16+.BI
NK.56-16-.BI
T.4Nve.BI
T.4Mem.BI
T.4Eff.BI
NKT.BI
T.8Nve.BI
T.8Mem.BI
T.8Eff.BI
T.8EffRA.BI
H
HLA-DR
22.9
FSC
LAMP5
2.28
CD11c
BDCA2
96.7
BDCA4
I
Lamp5
35.7
CD11c
CD123
95.1
BDCA2
J
SSC-A
83.8
FSC
hCD45
82.4
FSC-A
CD64
29.3
FSC-A
CD3
75.4
FSC-A
HLA-DR
14.1
CD4
LAMP5
35.7
CD11c
CD123
95.1
BDCA2
K
LAMP5
20 μm
100 μm
HLA-DR
20 μm
100 μm
L
Intima
Adventitia
HLA-DR
DAPI
LAMP5
30 μm
30 μm
M
5.52
CD123
BDCA2

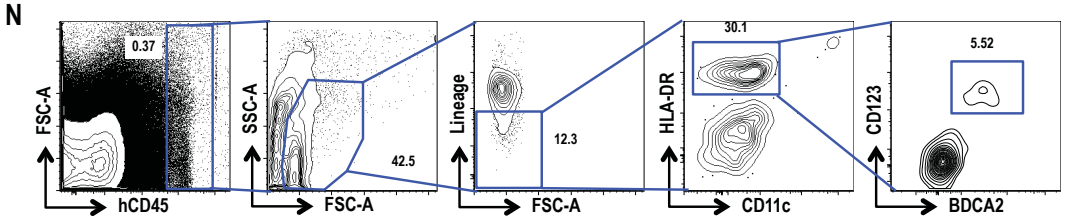

Figure 2.4. Identification and localization of aortic pDCs in the humanized mouse and human patient.

(A-L) Hu-mice were injected *i.p.* with 2 µg of Flt3L/day for 9 consecutive days.

(A) Gating strategy for human pDCs from hu-mice blood.

(B) Representative FACS plots of aortic pDCs of hu-mice with or without Flt3L treatment (%, black; cell numbers, red).

(C) *Left*: representative FACS plots, showing increased numbers of pDCs in the spleens and bone marrow (BM) from hu-mice, analyzed in (B). *Right:* percentage of pDCs in spleens and BM after PBS or Flt3L treatment (bar = mean).

(D) Secretion of functional IFN-α in serum of hu-mice. Hu-mice were injected *i.v.* with 10 µg of CpG encapsulated with DOTAP or DOTAP alone. Serum was collected at 0, 4, 8 and 12 hours after injection.

(E) CpG-stimulated IFN-α$^+$ and expression of CCR7 and CD83 in human pDCs in BM and aortas (6 pooled) from hu-mice. Cells from BM and aortas were incubated with media alone or with 10 µg/mL of CpG for 3 hours followed by additional 6 hours incubation with 10 µg/mL of BFA. BDCA2$^+$ aortic pDCs and BDCA3$^+$ aortic DCs were from the same sample.

(F) Increase in human pDCs in aortas from hu-BLT mice upon Flt3L treatment. Flt3L treatment also increased aortic pDCs in other hu-mice strains in addition to hu-NSG mice.

(G) Expression of the *LAMP5* gene in human immune cells compared to the other indicated cell types. The data were acquired and modified from the Immgen database (http://www.immgen.org).

(H) Gating strategy for pDCs in human peripheral blood.

(I) Hu-mice BM cells were immunostained with the indicated antibodies.

(J) Gating strategy for pDCs in hu-mice BM.

(K) Paraffin-embedded sections of aorta from Flt3L-injected hu-mice, IHC for LAMP5 and HLA-DR (brown) and counterstained with hematoxylin. Arrowheads indicate LAMP5$^+$ (left) and HLA-DR$^+$ (right) cells.

(L) Z-stacked confocal microscopy images of Flt3L-injected hu-mice aortas, stained for LAMP5 (red), HLA-DR (green), and DAPI (blue).

(M) Single cells from collagenase-digested aorta from a human patient were stained for the human pDC-specific markers, CD123 and BDCA2. Aortic cells were gated from a CD45$^+$ lineage (CD14, CD19, CD56)$^-$ HLA-DR$^+$ cell population.

(N) Gating strategy for pDCs in human non-atherosclerotic patient aorta.

2.5. pDCs specifically expand in the intimal layer of atherosclerotic aortas in mice

It was previously reported that aging increases the accumulation of intimal DCs (**Figure 2.5.A**)[178]. However, we found no correlation between pDCs number and mouse age (**Figure 2.5.B**). We and others have observed that western-type diet (WD)-induced atherosclerosis increases the number of DCs in the aorta[148, 178]. Indeed, the total number of DCs increased in WD-fed *Ldlr*$^{-/-}$ mice (**Figure 2.5.C**, **bottom**), and about 70% of DCs were CD11b^{+} DCs in atherosclerosis and CD103^{+} DCs were only about 15% (**Figure 2.5.D)**. Interestingly, CD103^{-}CD11b^{-} DCs also increased upon WD and consisted about 15% out of total DCs. Notably, we observed an increase in pDCs in the aortas of these mice, but not in other organs such as the spleens, para-aortic LNs, and mediastinal LNs (**Figures 2.5.C** and **2.5.E** and **2.5.F**). Importantly, similar to the distribution of DCs, pDCs were mostly enriched in the intimal layer where atherosclerosis develops (**Figures 2.5.G - 2.5.J**), and their distribution was further expanded into the descending aorta region where lesions develop in the later stage of atherosclerosis (**Figure 2.5.K**). When tested for type I IFNs response by TLR9 ligation, these aortic pDCs in atherosclerotic lesions were functional in terms of PDC-TREM upregulation (**Figure 2.5.L**). To further confirm type I IFN production, we sorted cells from atherosclerotic aorta for qPCR and only aortic pDCs expressed IFN-β1 at single cell level (**Figure 2.5.M**).

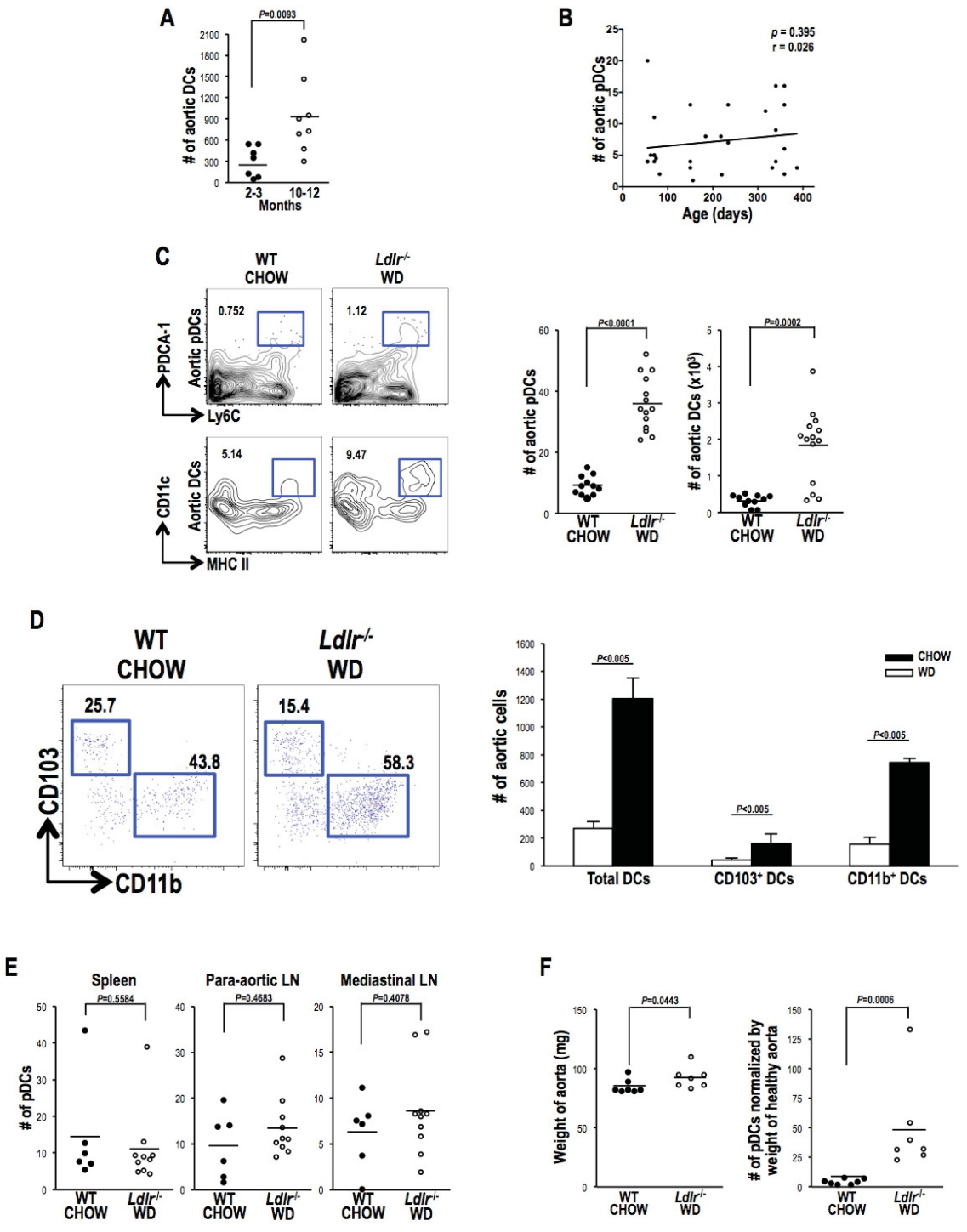
A
P=0.0093
# of aortic DCs
2100
1800
1500
1200
900
600
300
0
2-3
10-12
Months
B
p = 0.395
r = 0.026
# of aortic pDCs
25
20
15
10
5
0
0
100
200
300
400
Age (days)
C
WT
CHOW
Ldlr-/-
WD
0.752
1.12
PDCA-1
Aortic pDCs
Ly6C
5.14
9.47
CD11c
Aortic DCs
MHC II
P<0.0001
# of aortic pDCs
60
40
20
0
WT
CHOW
Ldlr-/-
WD
P=0.0002
# of aortic DCs (x10³)
5
4
3
2
1
0
WT
CHOW
Ldlr-/-
WD
D
WT
CHOW
Ldlr-/-
WD
25.7
43.8
15.4
58.3
CD103
CD11b
# of aortic cells
1600
1400
1200
1000
800
600
400
200
0
P<0.005
P<0.005
P<0.005
CHOW
WD
Total DCs
CD103+ DCs
CD11b+ DCs
E
Spleen
Para-aortic LN
Mediastinal LN
P=0.5584
P=0.4683
P=0.4078
# of pDCs
50
40
30
20
10
0
40
30
20
10
0
20
15
10
5
0
WT
CHOW
Ldlr-/-
WD
F
P=0.0443
Weight of aorta (mg)
150
100
50
0
WT
CHOW
Ldlr-/-
WD
P=0.0006
# of pDCs normalized by weight of healthy aorta
150
125
100
75
50
25
0
WT
CHOW
Ldlr-/-
WD

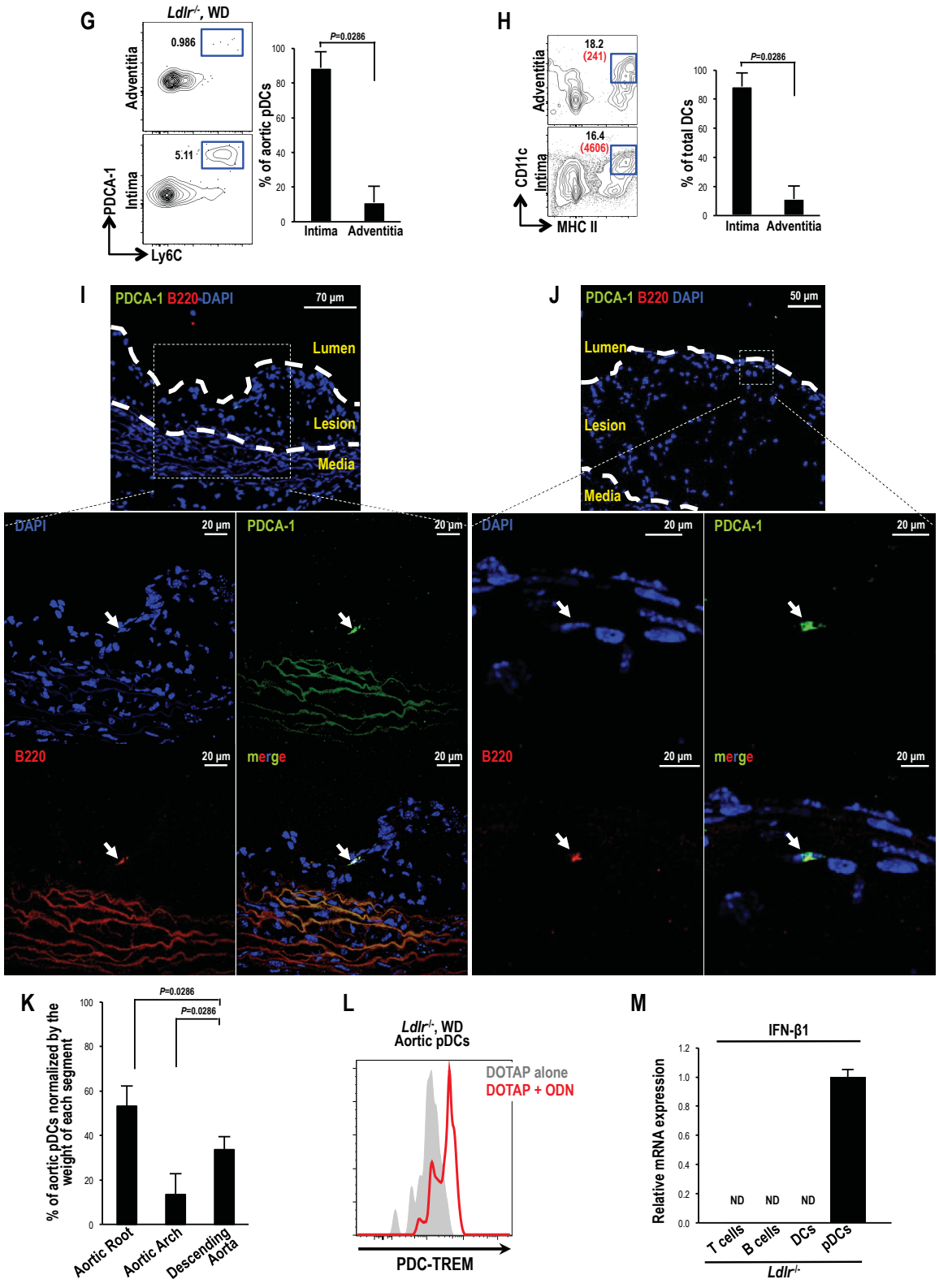
G
Ldlr-/-, WD
0.986
5.11
Adventitia
Intima
PDCA-1
Ly6C
P=0.0286
% of aortic pDCs
Intima
Adventitia
H
18.2
(241)
16.4
(4606)
CD11c
MHC II
% of total DCs
I
PDCA-1 B220 DAPI
70 μm
Lumen
Lesion
Media
J
50 μm
DAPI
PDCA-1
B220
merge
20 μm
K
% of aortic pDCs normalized by the weight of each segment
Aortic Root
Aortic Arch
Descending Aorta
L
Ldlr-/-, WD
Aortic pDCs
DOTAP alone
DOTAP + ODN
PDC-TREM
M
IFN-β1
Relative mRNA expression
ND
T cells
B cells
DCs
pDCs
Ldlr-/-

Figure 2.5. pDCs expand exclusively in the atherosclerotic aorta.

(A) Absolute numbers of aortic DCs from WT mice at different ages was measured (bar = mean; n ≥ 7/group).

(B) Absolute numbers of aortic pDCs in WT mice at different ages were quantified by FACS (n = 27).

(C) Absolute numbers of aortic pDCs and DCs from WT mice fed a normal diet (CHOW) and *Ldlr*$^{-/-}$ mice fed WD for 10 wk, quantified by FACS. *Left:* representative FACS plots of aortic pDCs and DCs, where numbers in the plot denote the % of cells; *Right:* absolute numbers of aortic pDCs and DCs per aorta (bar = mean; n ≥ 11).

(D) Absolute numbers of aortic DCs and their two subsets of DCs from WT mice fed a normal diet (CHOW) and *Ldlr*$^{-/-}$ mice fed WD for 10 wk, quantified by FACS. *Left:* representative FACS plots of aortic CD103^{+} DCs, and CD11b^{+} DCs where numbers in the plot denote the % of cells; *Right:* absolute numbers of aortic total DCs, CD103^{+} DCs, and CD11b^{+} DCs per aorta (bar = mean ± SD; n = 4).

(E) Absolute numbers of pDCs per 1 × 10^{4} CD45^{+} cells from spleen, para-aortic LN, and mediastinal LN from the mice in (C) (bar = mean; n ≥ 6).

(F) Weights of aortic segments, and absolute numbers of aortic pDCs normalized by the weights of aortas aortic segments from WT mice fed normal diet (CHOW) and *Ldlr*$^{-/-}$ mice fed WD for 12 wk. (bar = mean; n = 7/group).

(G) Aortic pDCs in intima and adventitia were measured from *Ldlr*$^{-/-}$ mice fed WD for 12 wk. *Left:* representative plots of aortic pDCs; *Right:* % of aortic pDCs in each layer of the aorta (bar = mean ± SD; n = 4).

(H) Aortic DCs in intima and adventitia were measured from *Ldlr*$^{-/-}$ mice fed WD for 12 wk. *Left:* representative FACS plot of aortic DCs; *Right:* percentage of aortic DCs among total aortic DCs (bar = mean; n = 4). Note the specific increase in DCs in the intima.

(I and J) Cross-sections from atherosclerotic aorta were immunostained for PDCA-1 (green), B220 (red) and counterstained with DAPI (blue). PDCA-1^{+}B220^{+} aortic cells (pDCs) are indicated by arrows. Atherosclerotic aortas were from *Ldlr*$^{-/-}$ mice fed WD for 7 wk.

(K) Distribution of aortic pDCs in the aortic root, aortic arch, and descending aorta. Aortic pDCs were measured from *Ldlr*$^{-/-}$ mice fed WD for 12 wk. % of aortic pDCs normalized by the weight of each aorta segment (bar = mean ± SD; 4 experiments).

(L) PDC-TREM expression in aortic pDCs. *Ldlr*$^{-/-}$ mice fed WD for 6 months were injected *i.v.* with CpG (10 µg/mouse) complexed to DOTAP (30 µl/mouse) or DOTAP alone.

(M) Relative mRNA expression of IFN-β1 from sorted out aortic immune cells. Aortic cells were isolated from WD-fed *Ldlr*$^{-/-}$ mice (9 wk). Data were normalized to *TBP* (bar = mean ± SD). Representative of two independent experiments.

2.6. pDCs depletion in *Ldlr*$^{-/-}$ mice reconstituted with BDCA2-DTR BM aggravates atherosclerosis

To explore the role of pDCs in disease, we generated atherosclerotic mice lacking pDCs by reconstituting *Ldlr*$^{-/-}$ mice with BM from BDCA2-DTR mice. It was previously reported that pDCs can be inducibly and selectively depleted by injecting BDCA2-DTR mice with DT[179]. These mice were fed WD for 12 weeks, with or without DT treatment, to deplete pDCs (**Figure 2.6.A**). To understand the role of pDCs in the development of atherosclerosis, we measured lesion size in the aortic sinuses of these mice. The average lesion size in pDC-depleted mice was significantly increased by 47% (**Figure 2.6.B**). In line with this, levels of the inflammatory cytokine TNF-α were increased in pDC-depleted mice aorta (**Figure 2.6.C**), whereas there was no significant change in IFN-α levels (**Figure 2.6.D**). We also found that lipid profiles were not significantly changed in these mice (**Figure 2.6.E**). These results suggest that pDCs function to reduce inflammation and immunity but do not play a role in systemic lipid metabolism.

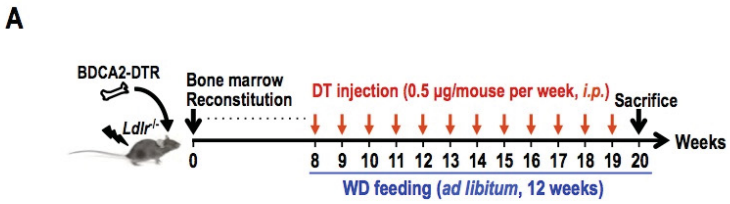
A
BDCA2-DTR
Ldlr-/-
Bone marrow
Reconstitution
DT injection (0.5 μg/mouse per week, i.p.)
Sacrifice
Weeks
0
8 9 10 11 12 13 14 15 16 17 18 19 20
WD feeding (ad libitum, 12 weeks)

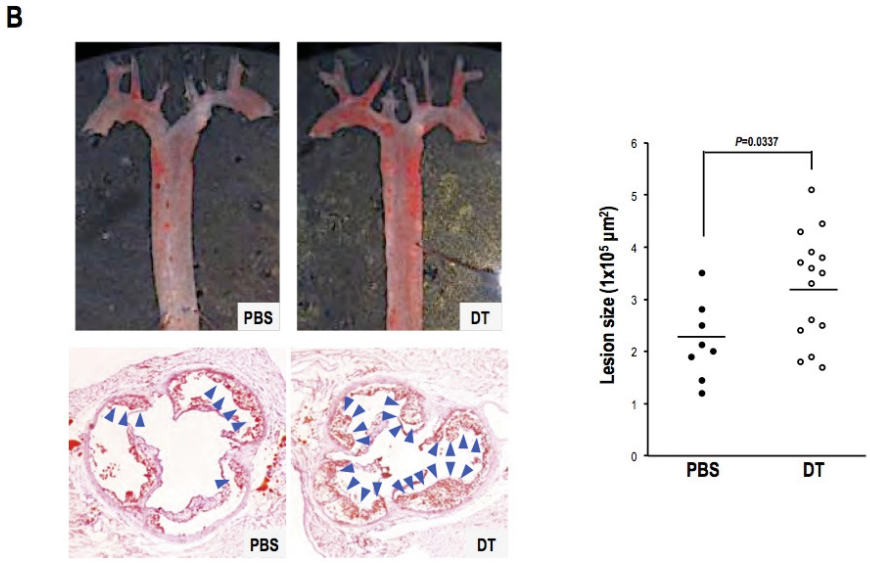
B
PBS
DT
PBS
DT
P=0.0337
Lesion size (1x10⁵ μm²)
PBS
DT

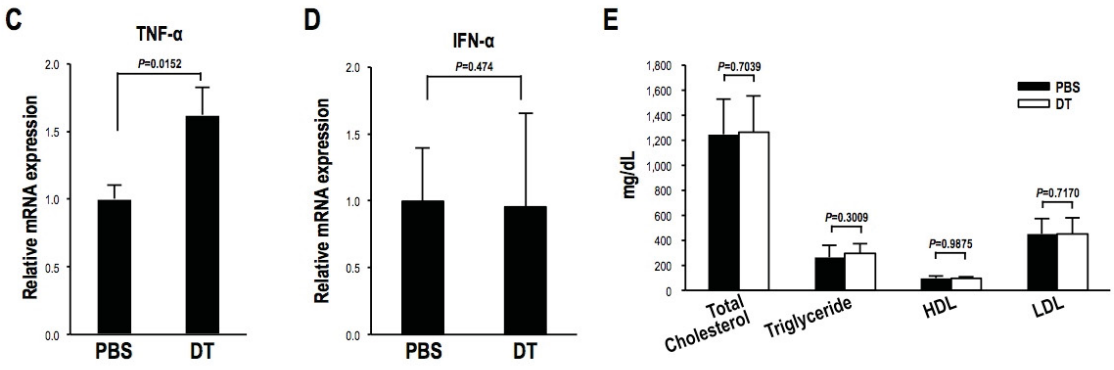
C
TNF-α
P=0.0152
Relative mRNA expression
PBS
DT
D
IFN-α
P=0.474
Relative mRNA expression
PBS
DT
E
P=0.7039
P=0.3009
P=0.9875
P=0.7170
mg/dL
PBS
DT
Total Cholesterol
Triglyceride
HDL
LDL

Figure 2.6. Aortic pDCs protect aortas from atherosclerosis.
(A-E) Lethally irradiated *Ldlr*$^{-/-}$ mice were reconstituted with BM from BDCA2-DTR mice.
(A) After 8 wk, reconstituted *Ldlr*$^{-/-}$ mice were fed WD and injected with PBS alone (n = 8) or with DT/ week (n = 15) for 12 wk.
(B) *Left:* representative images of Oil Red O staining of atherosclerotic lesions in *en face* aorta preparation (top), with atherosclerotic lesions in the sinus indicated by blue arrowheads (bottom); *Right*: quantification of atherosclerotic lesion size (bar = mean).
(C) TNF-α mRNA expression levels in the aorta, measured by qPCR. Data were normalized to *β-actin* (bar = mean ± SD; n = 6).
(D) Relative IFN-α mRNA expression levels in the aorta samples from (C), measured by qPCR. Data were normalized to *β-actin* and bars represent mean ± SD (n = 6).
(E) Lipid profile in serum was measured from the samples in (B) (bar = mean ± SD).

2.7. Treatment with a pDC-targeting antibody depletes MΦs

An antibody-mediated cell-ablation approach employing pDC-depleting antibodies was widely used to study *in vivo* function of pDCs[167]. In this regard, a monoclonal antibody against BST-2 (bone marrow stromal cell antigen 2), had previously been used to investigate the role of pDCs in atherosclerosis[163, 164, 166]. However, none of these previous reports clearly demonstrated specific ablation of pDCs in the mouse aorta. Thus, given our demonstration of a specific increase in pDCs numbers in atherosclerosis-prone areas of the mouse aorta and the atheroprotective role of pDCs, we were interested in revisiting this previously applied approach. As expected, based on previous studies, treatment with anti-PDCA1 resulted in specific depletion of pDCs in spleen and LNs, assessed by monitoring the pDCs markers Siglec-H and Ly6C (**Figure 2.7.A** and **2.7.B**). Surprisingly, validation of this depletion strategy, in conjunction with a FACS analysis, to cells prepared from atherosclerotic aortas revealed that more than 50% of cells in the atherosclerotic aorta were positive for PDCA-1 (**Figure 2.1.C**). Most of these cells were found to be $CD11b^{+}CD64^{+}$ MΦs (**Figure 2.7.C**). This finding is consistent with the fact that, although PDCA-1 is known to be restricted to pDCs under steady-state conditions, it is expressed promiscuously upon stimulation with type I IFN or IFN-γ[132]. Because the concentration of inflammatory cytokines is elevated in the atherosclerotic lesion, it is likely that PDCA-1 is expressed on multiple cell types. Therefore, we next questioned whether treatment with an anti-

PDCA-1 antibody also affects the MΦs population. We found that PDCA-1 mAb treatment depleted more than 50% of MΦs (**Figure 2.7.D**).

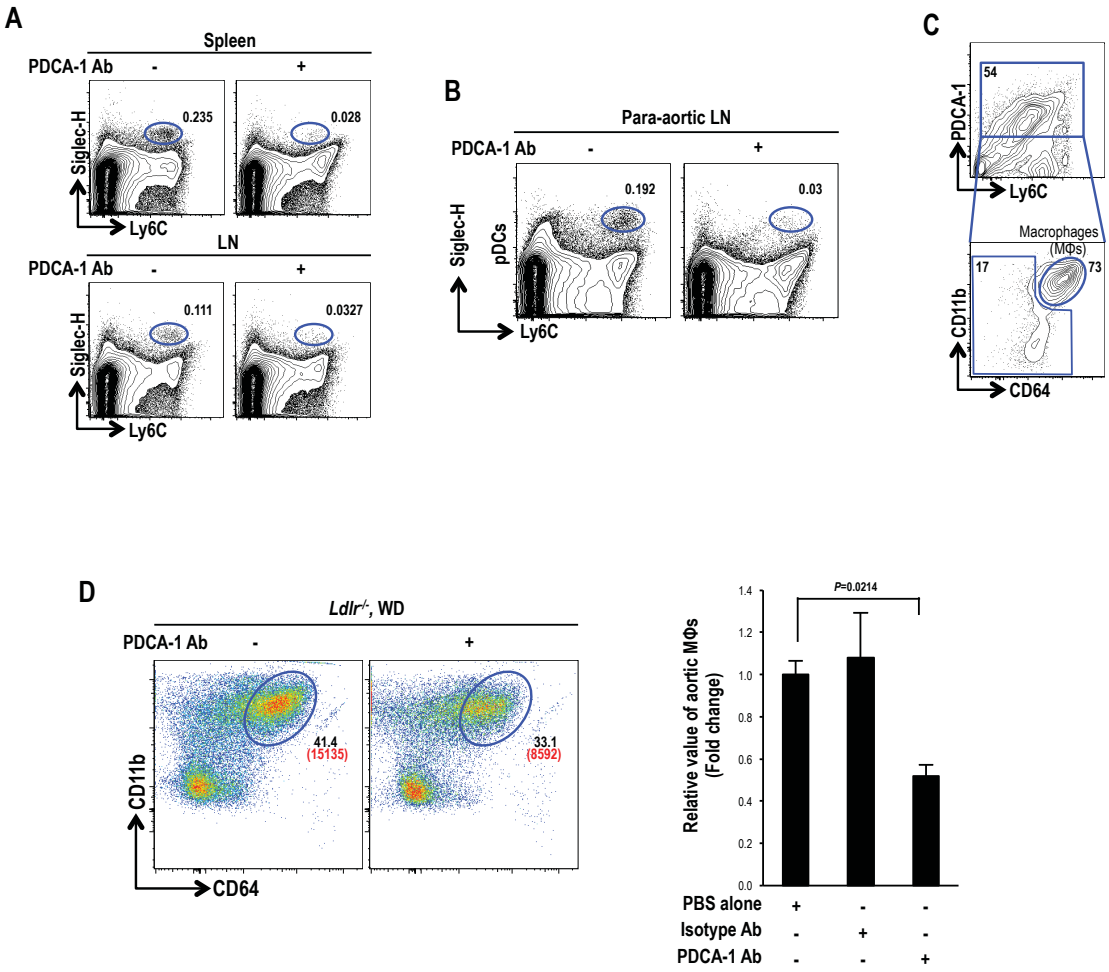

Figure 2.7. Antibody medicated depletion of aortic pDCs also reduce aortic macrophages.

(A-C) Antibody-mediated depletion of pDCs. *Ldlr*$^{-/-}$ mice fed WD for 12–14 wk were injected *i.v.* with PBS alone or 250 µg of PDCA-1 antibody or isotype control twice at 36 hours intervals.

(A) Selective depletion of pDCs of spleen and skin-draining LNs.

(B) pDCs in para-aortic LNs were depleted as pDCs-specific antibody, PDCA-1 (Clone: 927), was injected in mice in (A).

(C) CD45^{+} cells were analyzed for PDCA-1, Ly6C, CD11b, and CD64. A majority of PDCA-1^{+} aortic cells were macrophages (MΦs).

(D) Aortic macrophages (MΦs) in the aortic cell population from the mice in (A) were determined by immunostaining for CD45, CD11b, and CD64. *Left:* representative FACS plot of aortic cells (%, black; cell numbers, red); *Right:* relative number of aortic macrophages (MΦs) (normalized to the PBS group) from PBS alone, isotype, and PDCA-1 antibody groups (graph = mean ± SD; n ≥ 3; *P*-values determined by one-way ANOVA).

2.8. Selective depletion of aortic pDCs in steady state and atherosclerotic *Ldlr*$^{-/-}$ mice reconstituted with BDCA2-DTR BM

The off-target effects of the antibody-based depletion strategies, noted above, highlight the need for a more selective and inducible pDC-depletion model to precisely address the impact of pDCs in atherogenesis. Accordingly, we next sought to determine whether BDCA2-DTR mice could be used to ablate aortic pDCs. Treatment of these mice with DT specifically eliminated splenic and LNs pDCs (**Figure 2.8.A**), as reported. Importantly, this treatment also selectively eliminated aortic pDCs in steady state (**Figure 2.8.B**), without significantly affecting MΦs or DCs (**Figure 2.8.C**). To explore the specificity of the BDCA2-DTR strain in atherosclerosis, we generated atherosclerotic mice lacking pDCs by reconstituting *Ldlr*$^{-/-}$ mice with BM from BDCA2-DTR mice and fed WD as described in **Figure 2.6.A**. DT treatment successfully depleted splenic and LNs pDCs in these mice (**Figure 2.8.D**). Of note, aortic pDCs were selectively depleted (**Figures 2.8.E** and **2.8.F**), not affecting MΦs and DCs (**Figure 2.8.G**).

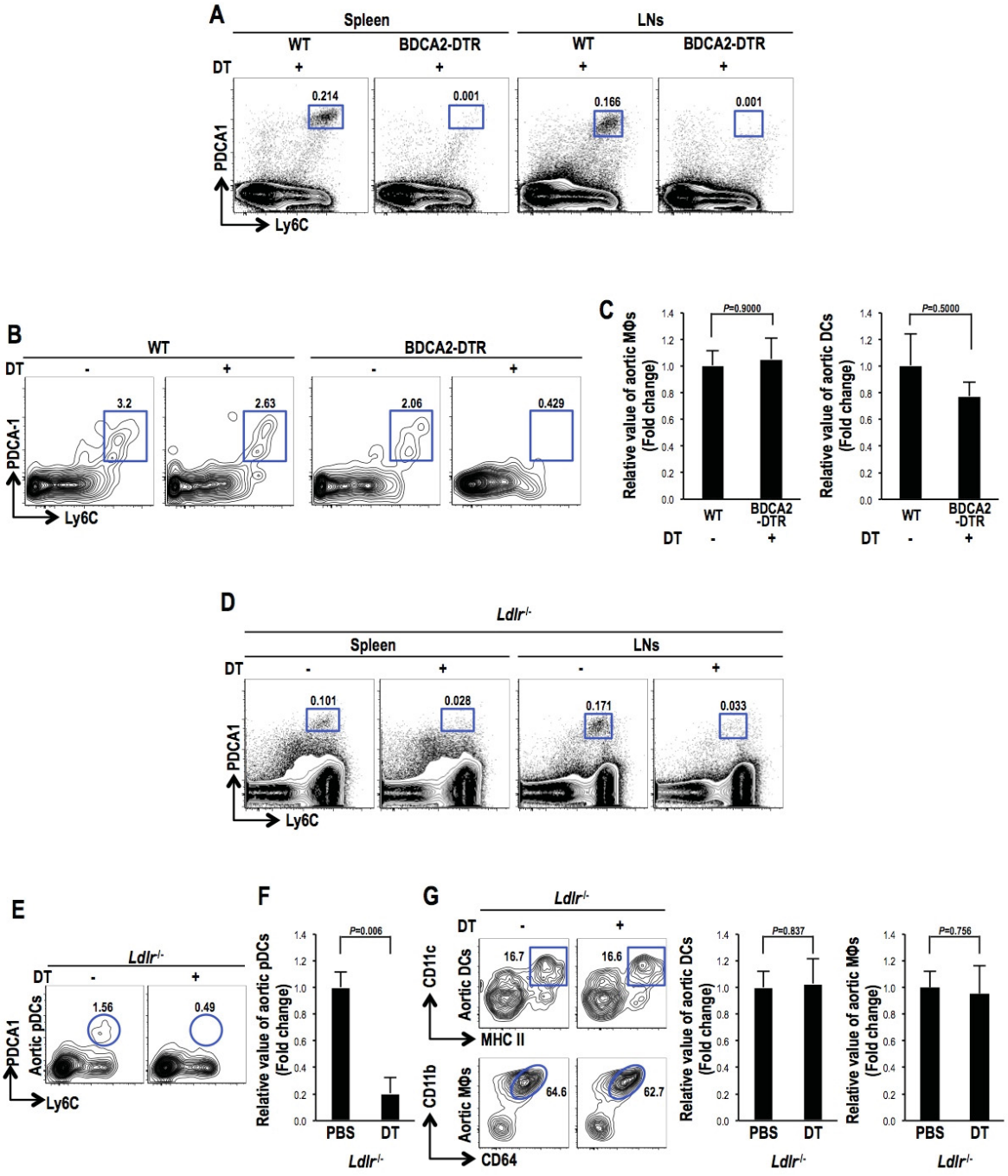
A
Spleen
LNs
WT
BDCA2-DTR
WT
BDCA2-DTR
DT
+
+
+
+
0.214
0.001
0.166
0.001
PDCA1
Ly6C
B
WT
BDCA2-DTR
DT
-
+
-
+
3.2
2.63
2.06
0.429
PDCA-1
Ly6C
C
P=0.9000
Relative value of aortic MΦs (Fold change)
WT
BDCA2 -DTR
DT
-
+
P=0.5000
Relative value of aortic DCs (Fold change)
WT
BDCA2 -DTR
DT
-
+
D
Ldlr-/-
Spleen
LNs
DT
-
+
-
+
0.101
0.028
0.171
0.033
PDCA1
Ly6C
E
Ldlr-/-
DT
-
+
1.56
0.49
PDCA1
Aortic pDCs
Ly6C
F
P=0.006
Relative value of aortic pDCs (Fold change)
PBS
DT
Ldlr-/-
G
Ldlr-/-
DT
-
+
16.7
16.6
CD11c
Aortic DCs
MHC II
64.6
62.7
CD11b
Aortic MΦs
CD64
P=0.837
Relative value of aortic DCs (Fold change)
PBS
DT
Ldlr-/-
P=0.756
Relative value of aortic MΦs (Fold change)
PBS
DT
Ldlr-/-

Figure 2.8. Selective and inducible pDC-ablation in BDCA2-DTR transgenic mice strain.

(A) Selective depletion of pDCs from the spleens and lymph nodes of C57BL/6 and BDCA2-DTR mice. Mice were injected *i.p.* with 0.5 µg of DT twice at 24 hours intervals (n = 4).

(B) Selective and inducible depletion of aortic pDCs in BDCA2-DTR mice. Aortic cells were previously gated from the $CD45^{+}CD64^{-}CD11b^{-}CD11c^{low}$ population. Mice were from (A).

(C) Relative number of aortic macrophages (MΦs) (left) and DCs (right) from (B) (graph = mean ± SD; n = 4).

(D-G) Selective depletion of pDCs from *Ldlr*$^{-/-}$ mice reconstituted with BM cells of BDCA2-DTR mice. Reconstituted *Ldlr*$^{-/-}$ mice were fed WD for 12 wk and injected *i.p.* with PBS or DT as described in Figure 2.6.A (graph = mean ± SD; n ≥ 5). Selective depletion pDCs from the spleens and lymph nodes (D). Selective depletion of aortic pDCs upon DT (E and F). No influence of DT on aortic DCs and macrophages (MΦs) (G).

2.9. Spatio-temporal correlation of Tregs and pDCs expansion during atherosclerosis

It has previously been shown that atherosclerosis is exacerbated in *Flt3*$^{-/-}$ mice, presumably because of a reduction in Tregs frequency in these mice [148]. However, measuring Treg frequency in the mouse aorta is very demanding, and only a few papers have tried to demonstrate the presence of Tregs in this tissue [180, 181]. By further optimizing our method, which importantly includes the essential step of MΦ elimination (**Figures 2.9.A - 2.9.C**), we were able to reliably and precisely quantify Tregs in the aorta. We found that Treg numbers were increased in the atherosclerotic mouse aorta (**Figure 2.9.D**), but not in other tissues such as spleen and LNs (data not shown). These Tregs were mainly localized in the intimal area of the atherosclerotic aorta (**Figure 2.9.E**). To further dissect the kinetics of Treg and pDCs expansion, we measured the number of pDCs and Tregs during WD intake in *Ldlr*$^{-/-}$ mice (0, 4, 8 and 12 weeks). As we previously reported, DCs numbers rose according to disease development (data not shown). Notably, both pDCs and Tregs numbers showed similar pattern of increase (**Figure 2.9.F**). In steady state, Tregs were largely restricted to the sinus area of the aorta, a distribution similar to that of pDCs (**Figure 2.9.G**, **left**). However, following WD, Tregs had expanded and were distributed throughout atherosclerotic aorta with similar distribution to that of pDCs (**Figure 2.9.G**, **Right**). This spatio-temporal correlation suggests a possible link between pDCs and Tregs in

atherosclerosis. In line with this, pDCs were essential to mediate tolerance to vascularized allograft and acute graft-versus-host disease[131, 170].

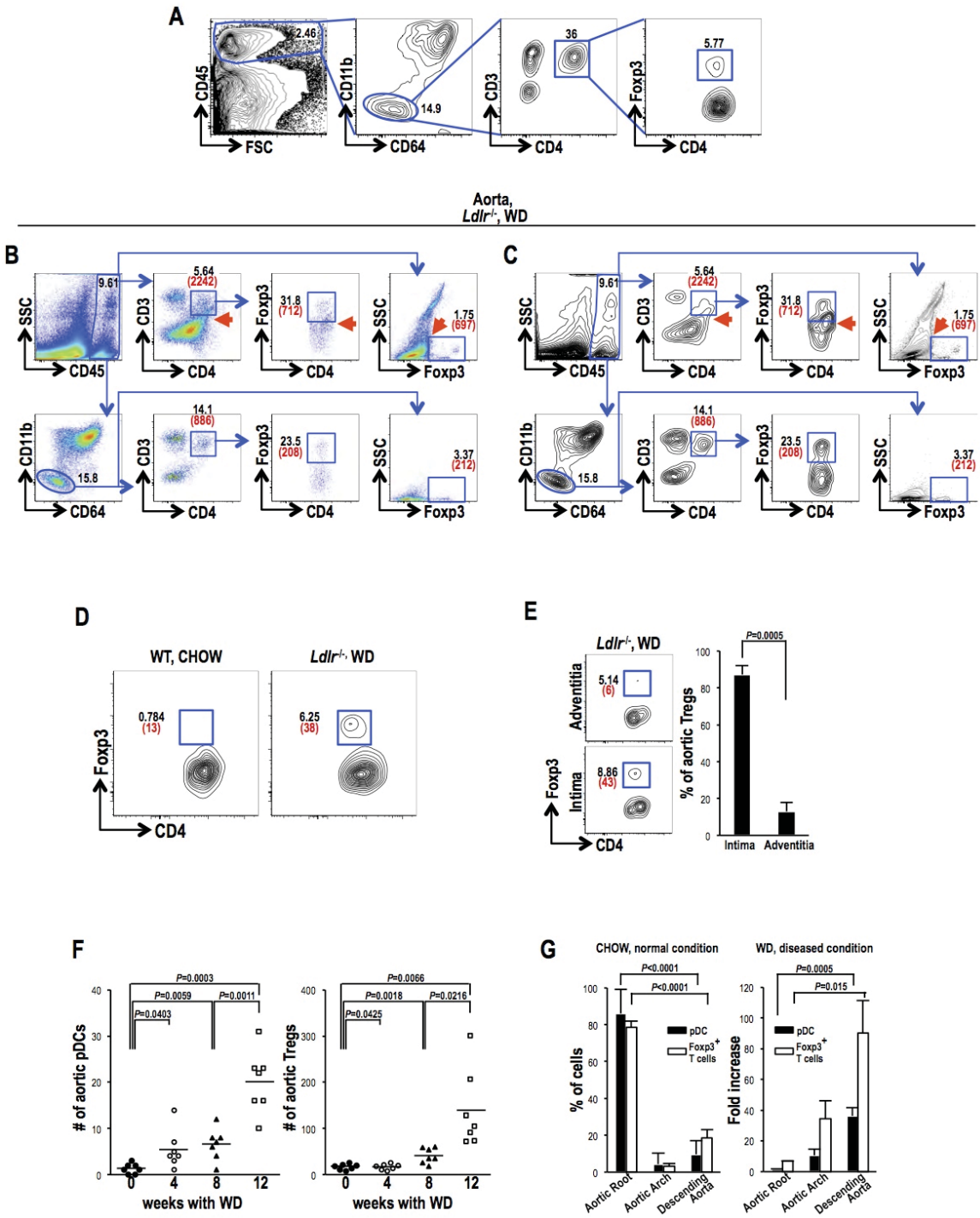
A
2.46
CD45
FSC
CD11b
14.9
CD64
CD3
36
CD4
Foxp3
5.77
CD4
Aorta,
Ldlr-/-, WD
B
SSC
9.61
CD45
CD3
5.64
(2242)
CD4
Foxp3
31.8
(712)
CD4
SSC
1.75
(697)
Foxp3
CD11b
15.8
CD64
CD3
14.1
(886)
CD4
Foxp3
23.5
(208)
CD4
SSC
3.37
(212)
Foxp3
C
SSC
9.61
CD45
CD3
5.64
(2242)
CD4
Foxp3
31.8
(712)
CD4
SSC
1.75
(697)
Foxp3
CD11b
15.8
CD64
CD3
14.1
(886)
CD4
Foxp3
23.5
(208)
CD4
SSC
3.37
(212)
Foxp3
D
WT, CHOW
Ldlr-/-, WD
Foxp3
0.784
(13)
6.25
(38)
CD4
E
Ldlr-/-, WD
Adventitia
5.14
(6)
Intima
8.86
(43)
Foxp3
CD4
P=0.0005
% of aortic Tregs
100
80
60
40
20
0
Intima
Adventitia
F
P=0.0003
P=0.0059
P=0.0011
P=0.0403
# of aortic pDCs
40
30
20
10
0
0
4
8
12
weeks with WD
P=0.0066
P=0.0018
P=0.0216
P=0.0425
# of aortic Tregs
400
300
200
100
0
0
4
8
12
weeks with WD
G
CHOW, normal condition
WD, diseased condition
P<0.0001
P<0.0001
% of cells
100
80
60
40
20
0
pDC
Foxp3+ T cells
Aortic Root
Aortic Arch
Descending Aorta
P=0.0005
P=0.015
Fold increase
120
100
80
60
40
20
0
pDC
Foxp3+ T cells
Aortic Root
Aortic Arch
Descending Aorta

Figure 2.9. Aortic Tregs and pDCs accumulate concomitantly in the atherosclerotic aorta.

(A) Gating strategy for Tregs from collagenase-digested mouse aortas. Liberated cells were stained intracellularly for CD4 and Foxp3 and analyzed by FACS. Numbers in FACS plots represent the % of cells in the indicated gate.

(B-C) Comparison of aortic Treg gating strategies. *Top:* without macrophages (MΦs) removal; *Bottom:* with macrophages (MΦs) removal. Same cells are shown in pseudo-color plots (B) and in contour plots (C). See contamination of macrophages (MΦs) (top, arrows), which results in incorrect enumeration of Tregs. Percentages (black) and absolute cell numbers (red parentheses) are shown in FACS plots.

(D) Aortic $CD4^+Foxp3^+$ T cells were analyzed from WT mice fed CHOW and *Ldlr*$^{-/-}$ mice fed WD for 14 wk (%, black; cell numbers, red).

(E) Distribution of Tregs in intima and adventitia of aortas of *Ldlr*$^{-/-}$ mice fed WD for 12 wk. *Left:* representative FACS plots of aortic $CD4^+Foxp3^+$ T cells (%, black; cell numbers, red).; *Right:* quantitation of the % of aortic $CD4^+Foxp3^+$ T cells (graph = mean ± SD; n = 4).

(F) Absolute numbers of aortic pDC and $CD4^+Foxp3^+$ T cells were analyzed from *Ldlr*$^{-/-}$ mice fed WD for 0, 4, 8 and 12 wk (bar = mean; n = 7/group).

(G) Distribution of aortic pDCs and $CD4^+Foxp3^+$ T cells in the aortic root, aortic arch, and descending aorta of CHOW-fed WT and WD-fed *Ldlr*$^{-/-}$ mice after 12 wk. *Left:* distribution of the % of each aortic population in WT mice; *Right:* fold increase in each population in WD-fed *Ldlr*$^{-/-}$ mice normalized by WT value (graph = mean ± SD; n ≥ 3).

2.10. Aortic pDCs express IDO-1 and induce antigen-specific Tregs

Given the close relationship between Treg and pDCs numbers during atherogenesis, we next investigated the tolerogenic capacity of aortic pDCs[182]. Of note, local expression of IDO-1, an enzyme critical for the induction of Tregs, was elevated in atherosclerotic aorta (**Figure 2.10.A)**. To identify IDO-1^{+}cells, we sorted out cells from atherosclerotic aorta for single-cell gene expression analysis. Importantly, we found a higher expression of IDO-1 in pDCs (**Figure 2.10.B**). In line with this, aortic pDCs expressed CCR9 and IDO-1 (**Figure 2.10.C**). To further test that IDO-1 expression by pDCs causes local Treg generation in atherosclerotic aorta, we reconstituted *Ldlr*$^{-/-}$ mice with BMs from WT and *Ido1*$^{-/-}$ mice. We did not detect a statistically significant difference of Treg number in the spleen of either WT or *Ido1*$^{-/-}$ *mice*. However, atherosclerotic aorta from *Ido1*$^{-/-}$ mice possessed reduced Treg numbers compared with WT (40% reduction) (**Figure 2.10.D**). In keeping with this, depletion of pDCs in atherosclerotic mice resulted in a reduction in Treg numbers only in affected aortas, not in lymphoid organs such as spleen and LNs (**Figure 2.10.E**). In addition, the level of IL-10, a cytokine that is a hallmark of Tregs, was decreased in pDC-depleted aortas (**Figure 2.10.F**). Previously, antigen-presentation by pDCs was reported to promote proatherogenic T cell immunity [163, 165]. However, these conclusions were largely based on *in vitro* experimentations with splenic or BM derived pDCs. To assess the antigen-specific T cell response in atherosclerotic aorta, we established *Ldlr*$^{-/-}$ mice reconstituted with OT-II transgenic mice BM. To selectively deliver an antigen to pDCs, we genetically cloned and

engineered anti-SiglecH antibody fused with ovalbumin (OVA) (**Figure 2.10.G**). In these mice, we injected anti-SiglecH-OVA *i.v.* to target aortic pDCs. Of note, antigen presentation by aortic pDCs in atherosclerotic environment induced OVA-specific Tregs (**Figure 2.10.H**). Together, these results demonstrate a direct functional link between the presence of IDO-1^{+} pDCs and the regulation of Treg generation in atherosclerotic aorta.

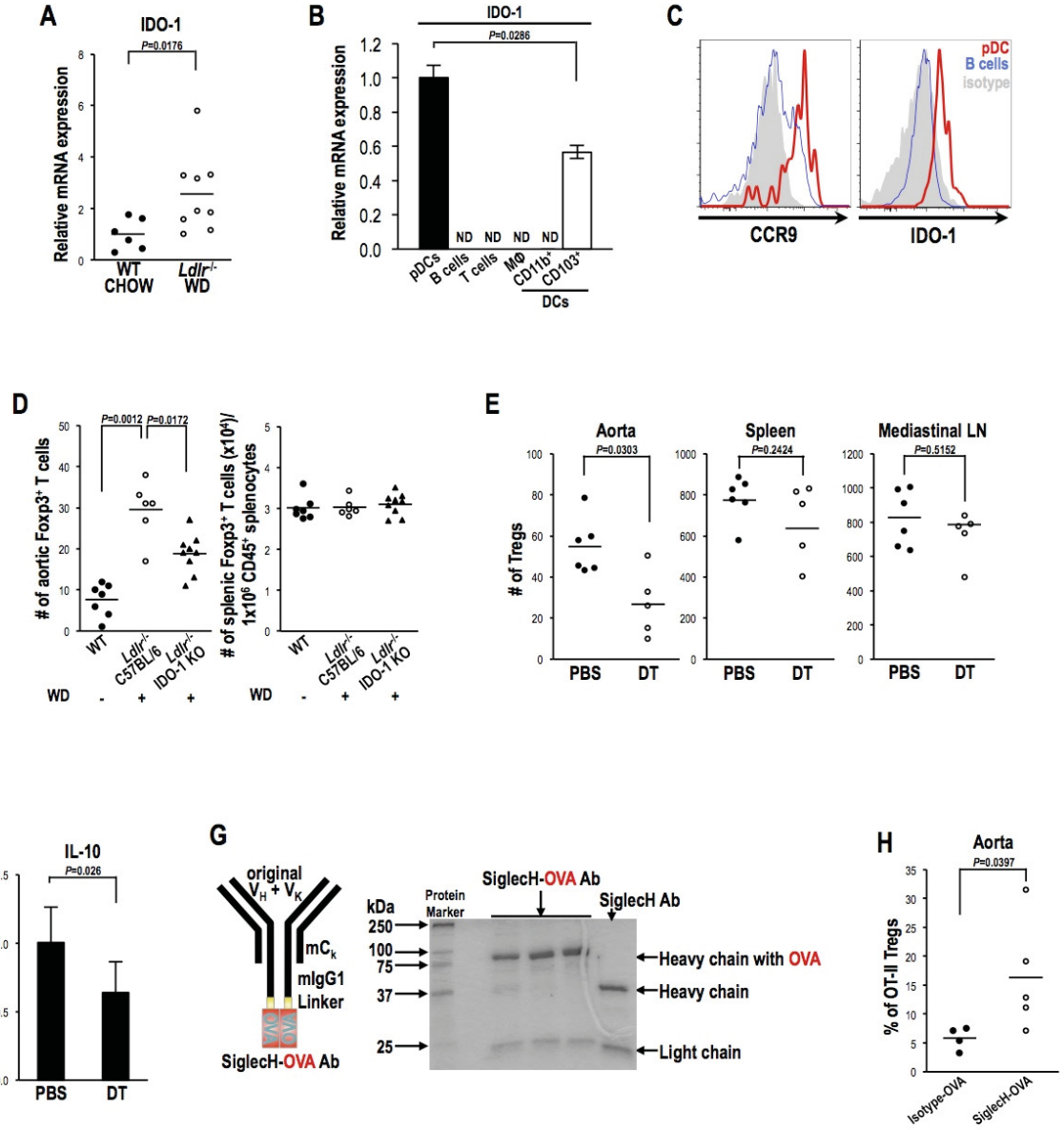
A
IDO-1
P=0.0176
Relative mRNA expression
WT CHOW
Ldlr-/- WD
B
IDO-1
P=0.0286
Relative mRNA expression
ND ND ND ND
pDCs
B cells
T cells
MΦ
CD11b+
CD103+
DCs
C
pDC
B cells
isotype
CCR9
IDO-1
D
P=0.0012
P=0.0172
# of aortic Foxp3+ T cells
WT
Ldlr-/- C57BL/6
Ldlr-/- IDO-1 KO
WD
# of splenic Foxp3+ T cells (x10⁴)/ 1x10⁶ CD45+ splenocytes
E
Aorta
P=0.0303
Spleen
P=0.2424
Mediastinal LN
P=0.5152
# of Tregs
PBS
DT
F
IL-10
P=0.026
Relative mRNA expression
PBS
DT
G
original VH + VK
mCk
mIgG1
Linker
SiglecH-OVA Ab
kDa
Protein Marker
SiglecH-OVA Ab
SiglecH Ab
250
100
75
37
25
Heavy chain with OVA
Heavy chain
Light chain
H
Aorta
P=0.0397
% of OT-II Tregs
Isotype-OVA
SiglecH-OVA

Figure 2.10. Interaction of aortic Tregs and CCR9$^+$IDO-1$^+$ pDCs is essential for Tregs homeostatic maintenance.

(A) IDO-1 mRNA expression levels in the aorta from WD-fed *Ldlr*$^{-/-}$ mice for 7 wk, measured by qPCR. Data were normalized to *β-actin* (bar = mean ± SD; n = 9).

(B) Relative IDO-1 mRNA expression from FACS-sorted aortic immune cells from WD-fed *Ldlr*$^{-/-}$ mice for 9 wk. Data were normalized to *TBP* (bar = mean ± SD).

(C) Comparison of CCR9 and IDO-1 expression in pDCs and B cells in aortas from WD-fed *Ldlr*$^{-/-}$ mice for 12 wk.

(D-H) Lethally irradiated *Ldlr*$^{-/-}$ mice were reconstituted with BM from WT mice or *Ido1*$^{-/-}$ mice (D), BDCA2-DTR mice (E and F), OT-II mice (H).

(D) Absolute numbers of CD4$^+$Foxp3$^+$ T cells in aortas and splenic CD4$^+$Foxp3$^+$ T cells per 1 x 10^6 CD45$^+$ splenocytes from indicated mice (bar = mean; n ≥ 6). Reconstituted *Ldlr*$^{-/-}$ mice were fed WD for 3 wk.

(E and F) Reconstituted *Ldlr*$^{-/-}$ mice were fed WD and injected *i.p.* with PBS or DT/week for 12 wk.

(E) Absolute numbers of CD4$^+$Foxp3$^+$ T cells per 1 × 10^4 CD45$^+$ cells in aortas, spleens and mediastinal LNs (bar = mean; n ≥ 5).

(F) Relative IL-10 mRNA expression levels in the aorta, measured by qPCR. Data were normalized to *β-actin* (bar = mean ± SD; n = 6).

(G) Schematic presentation of genetically cloned anti-SiglecH-OVA antibody is presented (left) and the integrity of purified anti-SiglecH-OVA and anti-SiglecH antibodies are confirmed by staining with Coomassie blue (right). VH for heavy chain variable region; Vk for light chain variable region; mCk for light chain constant region; mIgG1 for mouse IgG1 isotype region; Linker for 17 amino acids for fusion flexibility.

(H) % of Foxp3$^+$ cells in aortic OT-II CD3$^+$CD4$^+$ T cells were measured from reconstituted *Ldlr*$^{-/-}$ mice fed WD for 4 wk. Mice were injected with 10 μg of Isotype-OVA (n = 4) or SiglecH-OVA (n = 5) *i.v.* and sacrificed 3 days post injection (bar = mean).

2.11. Tregs regulate the homeostasis of pDCs in atherosclerotic aortas

While Tregs are important for atheroprotection[148, 155, 157], there is no report on the impact of Treg-depletion in regulating the homeostasis of pDCs in diseased aorta. To this end, we established selective Treg depletion model with *Ldlr*$^{-/-}$ mice reconstituted with Foxp3-DTR mice BMs[183]. As expected, WD expanded pDCs and Tregs in the aorta (**Figure 2.11.A**). Of note, constitutive *in vivo* ablation of Treg during the course of WD decreased aortic pDCs (**Figure 2.11.A**), demonstrating an important role of Tregs to maintain the homeostasis of pDCs in diseased aorta.

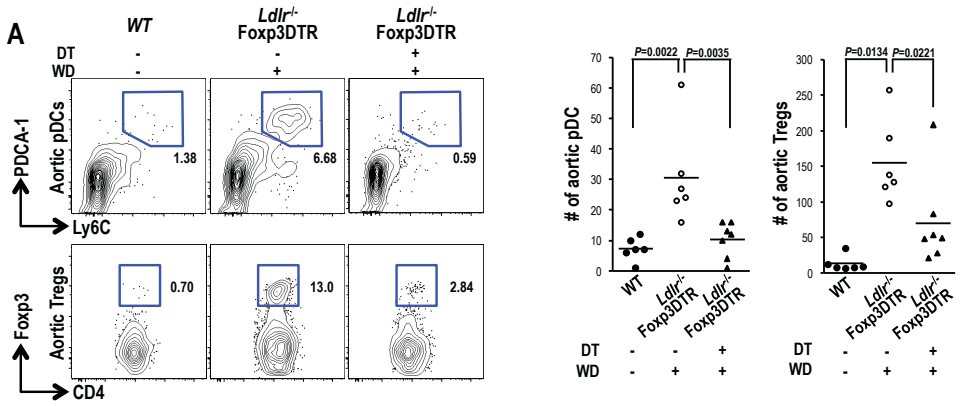

Figure 2.11. Homeostasis of aortic pDCs depend on Tregs in atherosclerosis.

(A) Lethally irradiated *Ldlr*$^{-/-}$ mice were reconstituted with BM from Foxp3-DTR mice. Aortic pDCs and CD3^{+}CD4^{+}Foxp3^{+} T cells were from reconstituted *Ldlr*$^{-/-}$ mice fed WD and injected *i.v.* with PBS or DT/week for 4 wk. *Left*: representative FACS plots of aortic pDCs and CD3^{+}CD4^{+}Foxp3^{+} T cells; *Right*: quantification of absolute numbers of aortic pDCs and CD3^{+}CD4^{+}Foxp3^{+} T cells per aorta (bar = mean; n ≥ 6).

2.12. Aortas from human atherosclerotic patients contain authentic pDCs that colocalize with Tregs

We next sought to extend these findings to humans, investigating whether aortas from human atherosclerotic patients also contain pDCs. Indeed, human atherosclerotic aortas contained pDCs ($CD123^+BDCA2^+BDCA4^+$) (**Figure 2.12.A**). Upon CpG challenge, these human pDCs secreted IFN-α (**Figure 2.12.B**) and exhibited CCR7 and CD86 upregulation (**Figure 2.12.C**), further suggesting that these cells are authentic pDCs. In the diseased aorta, we could easily detect these pDCs by virtue of their positive staining for both BDCA2 and LAMP5 (**Figures 2.12.D** and **2.12.E**). Interestingly, there was a positive correlation between pDCs numbers and the severity of atherosclerosis (**Figure 2.12.F**) comparable to that observed in the mouse model (**Figure 2.9.F**). Given the close relationship between Tregs and pDCs observed in the diseased mouse aorta, we further investigated patient aortas for the presence of Tregs. As was the case in the mouse model, Tregs were detected in the aortas of atherosclerosis patients, labeled by Foxp3 and Helios (**Figures 2.12.G** and **2.12.H**)[184], where they were colocalized with pDCs in plaques (**Figures 2.12.I** and **2.12.J**). In addition, pDCs in plaque areas also expressed the Treg-inducing enzyme, IDO-1, as determined by FACS (**Figures 2.12.K** - **2.12.M**) and immunohistochemistry (IHC) of sections (**Figure 2.12.N**). Furthermore, these pDCs were colocalized with $Foxp3^+$ Tregs in the diseased aortas, as determined by monitoring for LAMP5 (**Figures 2.12.O** and

2.12.P) and BDCA2 (**Figure 2.12.Q**) expression. Notably, ~48% of pDCs were observed together with Tregs, reinforcing their direct functional link (**Figure 2.12.R**).

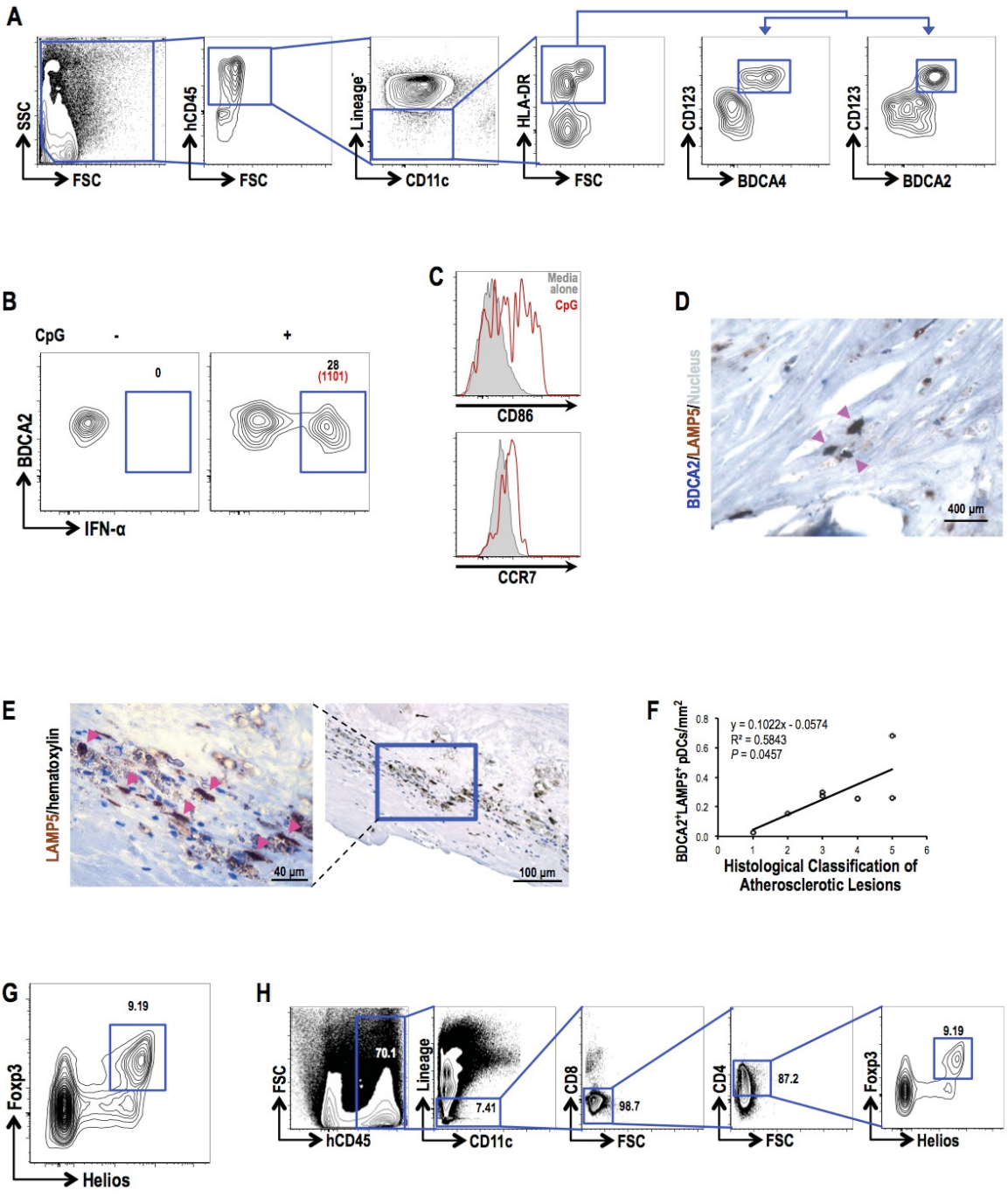
A
SSC
FSC
hCD45
FSC
Lineage-
CD11c
HLA-DR
FSC
CD123
BDCA4
CD123
BDCA2
B
CpG
-
+
0
28
(1101)
BDCA2
IFN-α
C
Media alone
CpG
CD86
CCR7
D
BDCA2/LAMP5/Nucleus
400 μm
E
LAMP5/hematoxylin
40 μm
100 μm
F
y = 0.1022x - 0.0574
R² = 0.5843
P = 0.0457
BDCA2+LAMP5+ pDCs/mm2
Histological Classification of Atherosclerotic Lesions
G
9.19
Foxp3
Helios
H
70.1
FSC
hCD45
Lineage-
7.41
CD11c
CD8
98.7
FSC
CD4
87.2
FSC
9.19
Foxp3
Helios

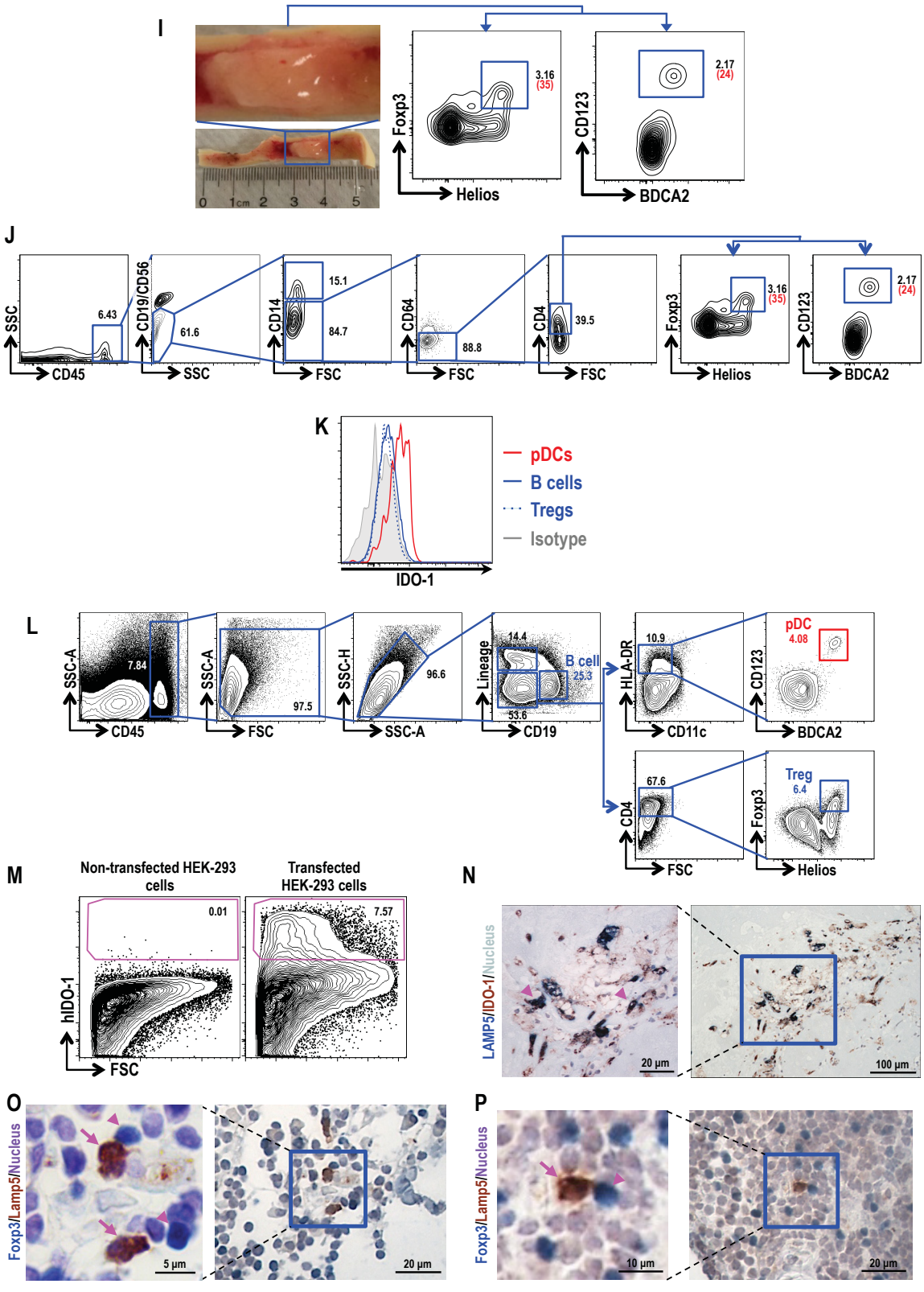
I
Foxp3
Helios
3.16
(35)
CD123
BDCA2
2.17
(24)
J
SSC
CD45
6.43
CD19/CD56
SSC
61.6
CD14
FSC
15.1
84.7
CD64
FSC
88.8
CD4
FSC
39.5
Foxp3
Helios
3.16
(35)
CD123
BDCA2
2.17
(24)
K
IDO-1
pDCs
B cells
Tregs
Isotype
L
SSC-A
CD45
7.84
SSC-A
FSC
97.5
SSC-H
SSC-A
96.6
Lineage
CD19
14.4
B cell
25.3
53.6
HLA-DR
CD11c
10.9
CD123
BDCA2
pDC
4.08
CD4
FSC
67.6
Foxp3
Helios
Treg
6.4
M
Non-transfected HEK-293 cells
Transfected HEK-293 cells
hIDO-1
FSC
0.01
7.57
N
LAMP5/IDO-1/Nucleus
20 μm
100 μm
O
Foxp3/Lamp5/Nucleus
5 μm
20 μm
P
Foxp3/Lamp5/Nucleus
10 μm
20 μm

Figure 2.12. Functional pDCs and Tregs in human atherosclerotic aorta.

(A) Gating strategy for human pDCs from human patients aorta. Abs for CD3, CD14, CD16 and CD19 were used for lineage-removal.

(B) IFN-α production by aortic pDCs from human atherosclerotic patients. Aortic cells were incubated with media alone or with 10 µg/mL of CpG for 3 hours followed by additional 6 hours incubation with 10 µg/mL of BFA (%, black; cell numbers, red).

(C) Expression of CCR7 and CD86 in cells from the human sample in (B) gated from media-alone-treated pDCs and CpG-treated IFN-α$^+$ pDCs.

(D) Paraffin-embedded sections from human atherosclerotic aorta were stained for IHC with LAMP5 (brown) and BDCA2 (blue), and counterstained with hematoxylin. LAMP5$^+$ cells (pDCs) are indicated by arrowheads.

(E) Paraffin-embedded sections of human atherosclerotic aorta were stained for pDCs (LAMP5+, brown, arrowhead) and counterstained with Hematoxylin.

(F) Correlation between numbers of human aortic pDCs and histological classification of atherosclerotic lesions from patients.

(G) Tregs from a human patient with atherosclerosis.

(H) Gating strategy for Tregs (from G) from human patients with atherosclerosis (Lineage: CD14, CD16, CD19 and CD56).

(I) Fatty plaques from atherosclerotic human aortic tissue were isolated and subjected for analysis of pDC and Treg cells (%, black; cell numbers, red).

(J) Gating strategy for the detection of Tregs (from I) in fatty plaques from atherosclerotic human aortic tissue. Dissociated aortic cells were gated based on ICS for CD45, CD19, CD56, CD14, CD64, CD4, Helios, Foxp3, CD123 and BDCA2.

(K) Analysis of IDO-1 expression in pDCs, B cells, and Treg cells from human patients with atherosclerosis.

(L) Gating strategy and distribution of pDCs, B cells and Tregs (from K) from human patients with atherosclerosis (Lineage: CD14, CD16, CD56 and CD64).

(M) Specificity of IDO-1 antibody used. Related to (K). Human IDO-1 cDNA was transfected into HEK-293 cell line. Non-transfectant and IDO-1 transfectant were fixed and stained for hIDO-1.

(N) Localization of LAMP5$^+$IDO-1$^+$ pDCs in human atherosclerotic aorta.

(O-Q) Colocalization of LAMP5$^+$ pDCs (O and P, arrows) or BDCA2$^+$ pDCs (Q, arrows) with Foxp3$^+$ Treg cells (arrowheads).

(R) IHC analysis of cell-to-cell contact between pDCs and Tregs in human atherosclerotic aortas (n = 7). Double IHC for BDCA2 and FoxP3 were performed to visualize pDCs and Tregs in human atherosclerosis. The BDCA2$^+$ pDCs contacting Foxp3$^+$ Tregs have been counted under light microscopy and shown as the % of pDCs with or without contacting Tregs.

3. Discussion

3.1. Aortic pDCs in steady and atherosclerosis

In this study, we provide the first comprehensive IHC, flow cytometry and functional analyses of both human and mice pDCs in the aorta at both steady state and at the inflammatory stage during atherosclerosis. pDCs in the aorta have plasma cell morphology and are distinguishable from typical conventional dendritic cells (cDCs), which contain numerous dendrites. As previously described, pDCs, alongside with most DCs and T cells, are mainly located in the intimal areas of the aortic roots, a location that is prone to atherosclerosis development. The phenotype of aortic pDCs is very similar to that of pDCs in spleen, including the expression of PDCA-1/Bst-2/CD317, Siglec-H, Ly6C, B220 and Clec9a, as well as the Flt3/CD135-dependence of their generation. In contrast, aortic pDCs lack or express lower levels of classical DCs and monocyte/MΦ markers and markers of other lymphocyte lineages, such as B cells, T cells, NK cells, and granulocytes. Importantly, pDCs isolated from aorta have the capacity to produce large quantities of type I IFN upon stimulation through TLR9. As a result, IFN-α secreting native aortic pDCs upregulate surface expression of PDC-TREM *in vivo*. Thus, aortic pDCs are equivalent in many functional respects to pDCs identified in other tissues. Notably, none of these functional features of aortic pDCs has been previously described under steady state conditions. To further identify mouse equivalents of human aortic pDCs under normal conditions, we harnessed hu-mice

reconstituted with human hematopoietic stem cells, thereby possessing human immune cells in their aortas. With two widely used hu-mice models (hu-NSG and BLT), we were able to identify $CD123^{+}BDCA2^{+}BDCA4^{+}$ authentic human pDCs in the mouse aorta. Similar to mouse aortic pDCs, human aortic pDCs produced IFN-α upon TLR9 ligation and were mainly found in the intima, where HLA-DR^{+} DCs also reside. Our observation in humanized mice further indicates the usefulness of these models to recapitulate normal human aorta. In addition, pDCs were also found in samples of healthy human aorta.

These steady-state findings allowed us to explore mouse aortic pDCs under inflammatory conditions. One mildly inflammatory condition is aging, and it has previously been reported that the number of aortic DCs increases with increasing age [178]. We did not detect any significant change in the number of pDCs with age (up to 400 days). We did, however, find a remarkable increase in aortic pDCs numbers upon feeding WD to atherosclerosis-prone *Ldlr*$^{-/-}$ mice. Notably, this increase was only observed in the aorta, and not in other lymphoid organs, such as the spleen and even aorta-draining LNs (para-aortic and mediastinal). Anatomically, the increase in pDCs number was mainly restricted to the intimal space, further corroborating the possible role of pDCs in atherosclerosis.

The number of pDCs in aorta is low in steady state but, according to our study, increase in aorta of mice with induced atherosclerosis. The increased number of aortic pDCs is spatio-temporally correlated with increased atherosclerotic lesions. The accumulation of pDCs at the lesions and around the necrotic core has been observed

by other studies (22388324) (22936340). Combined, these evidences indicate trafficking of pDCs into the lesions. SMCs in aorta express CXC ligand (CXCL) 12 after arterial injury and expression of CXCL12 can be detected in atherosclerosis lesions (10666407). We did not test the expression of the CXCL12 receptor CXCR4 on aortic pDCs in the plaques, but it is known that CXCR4 promotes migration of pDCs to CXCL12-expressing tumors, where the recruited pDCs are associated with compromised T cell responses (11726975.) pDCs depend on CCR5 and CXCR3 for the migration into inflamed tissues (12444109) (16147979), but further experiments are needed to determine the expression of CCR5 and CXCR3 in aortic pDCs. On the other hand, our study found that aortic pDCs express CCR9, which is necessary for the recruitment of pDCs to the thymus (22444632) and small intestine (17404233.). CCR9 in pDCs permits pDCs' chemotaxis to its ligand CCL25 in the thymus and defines tolerogenic pDCs (22444632.). Our study shows that increased number of aortic Tregs depends on $CCR9^{+}$ aortic pDCs, but the expression of CCL25 in plaques was not tested. Thus, it is reasonable to postulate that accumulated aortic pDCs are tolerogenic and is in line with our study.

Although mechanistic studies in the mouse are informative, the identification of aortic pDCs in humans equivalent to those in mice would facilitate translational applications. To this end, we examined the aortas of human patients. Remarkably, human patient aortas contained functional pDCs similar to their mouse counterparts. First, these pDCs underwent maturation and produced IFN-α following stimulation with TLR9 agonist. Second, there was a positive correlation between pDCs number and the

severity of atherosclerosis closely recapitulating our mouse studies. Finally, these human aortic pDCs also expressed IDO-1 and colocalized with Tregs in plaque tissues. These preliminary evidences suggest that our results in the mice are probably equivalent or representative of what happens in humans.

3.2. Role of pDCs in innate vs adaptive immunity

In addition to the secretion of type I IFNs, pDCs also express IL-12 and other inflammatory chemokines, which regulate both innate and adaptive immune responses. pDCs quickly express type I IFNs during viral infections to allow other cells to express IFN-stimulated genes against viral infection, and maturate DCs for efficient antigen presentation and cross-presentation to naïve T cells (19227367.) (14502286). Also type I IFNs, IL-12 and IL-18 from pDCs enhance NK cell-mediated cytotoxicity and secretion of IFN-γ (11420036.).

On the other hand, pDCs also influence adaptive immunity by supporting $CD8^+$ T cell cytolytic activity (16824119.) and T-helper 1 (Th1) polarization of $CD4^+$ T cells (12563297.). Furthermore, expression of IDO-1 (21804557) (15356121) and inducible T cell co-stimulator ligand (ICOSL) (17200410) in pDCs promote Tregs commitment, and production of type I IFNs, IL-6, B cell-activating factor (BAFF) and A proliferation-inducing ligand (APRIL) (21333555) in pDCs drive the generation of plasma cells and antibody secretion (23635775).

Even though the role of DCs (19893012.) (22078798.) (15096453) (21633167) and NK cells (24469537) in atherosclerosis was thoroughly investigated, the impact of pDCs onto the function of DCs and NK cells in aorta is largely unknown. On one side, production of anti-double-stranded DNA antibody (22388324) and splenic T-cell activation (22936340) in atherosclerosis seems dependent on aortic pDCs. On the other hand, our study and another study by the Biessen group (22021930) found a tolerogenic role for pDCs. Interestingly, both groups also observed the expression of IDO-1 in aortic pDCs and their tolerogenic role, but with different effects of IDO-1. Our group observed IDO-1$^+$ pDCs increase number of aortic Tregs but Biessen group reported IDO-1$^+$ pDCs decrease CD4$^+$ T cell proliferation. A different microenvironment in the plaques of each study may explain the difference. pDCs exposed to IFN-γ inhibit T cell proliferation and induce T cell apoptosis, but pDCs exposed to TGF-β generate more Tregs (21804557). Interestingly, both of these T cell responses require IDO-1 induction, but the pDCs exposed to TGF-β doesn't require IDO-1 enzymatic activity to generat Tregs. We also used 1-methyltryptophan (1-MT), an inhibitor of IDO-1 enzymatic activity, but we did not observe any effect of 1-MT and failed to affect the generation of Tregs. The two different pathways of tolerogenic pDCs may exist in atherosclerosis and their relative contribution may depend on the experimental model used. It would be worthwhile to assess if aortic pDCs in atherosclerosis act differently in response to IFN-γ and TGF-β.

3.3. Tolerogenic property of pDCs and Tregs

pDCs are known to induce peripheral and central tolerance in various studies, such as studies using vascularized cardiac allografts model[170] and graft-versus-host disease model[131]. Also another study reported pDCs mediate oral tolerance[185] and tolerogenic property of pDCs seems depend on CCR9[130]. Also our study found that aortic pDCs prevent atherosclerosis. Then we questioned how aortic pDCs could reduce atherosclerosis and one possible explanation was by induction of Tregs. For example, it was known that depletion of Tregs has been shown to aggravate atherosclerosis[155, 186]. It was also reported that Treg numbers reach a peak at 4 weeks after WD-induced atherogenesis, although remain decreased at later stages of atherosclerosis[180]. However, none of these previous studies have reported the enumeration of Tregs in the aorta using an unbiased approach, such as FACS. In addition, most studies in the field have relied on measuring Tregs in spleen and LNs of atherosclerotic mice or mRNA expression and IHC for Foxp3 in the aorta[181]. To fill this gap, we devised a new approach for precisely enumerating aortic Tregs, both in steady state and during atherosclerosis development, without using *Foxp*3-reporter strain[187]. Of importance, removal of autofluorescent MΦs was an essential step. Using this approach, we found a positive correlation between pDCs and Treg numbers during atherosclerosis development. Anatomically, both pDCs and Tregs were found in the intima of aortic roots under normal conditions but were distributed throughout lesions that developed in atherosclerosis. Again, this phenomenon was restricted only to the atherosclerotic aorta and did not manifest in the other lymphoid tissues tested such as spleen and draining

LNs. Notably, aortic pDCs expressed two markers of tolerogenic pDCs: CCR9 and IDO-1. In line with this, depletion of pDCs during atherosclerosis resulted in decreased Treg numbers only in the aorta, with a concomitant reduction in IL-10 levels. To further investigate the local role of aortic pDCs in Treg generation, we made *Ido1*$^{-/-}$ atherosclerosis-prone mice. Indeed, *Ido1*$^{-/-}$ deficient atherosclerotic aorta possessed 40% lesser Treg number, compared with WT. However, there was no statistically significant difference of Treg number in the spleen of WT and *Ido1*$^{-/-}$ mice. To further pursue the outcome of pDCs-targeted antigen delivery, we used pDC-targeting antibody fused with OVA. Importantly, antigen presentation by pDCs resulted in the induction of OT-II Tregs in atherosclerotic aorta. In addition, selective ablation of Tregs by Foxp3-DTR mice decreased pDCs numbers in atherosclerotic aorta, suggesting essential interaction of IDO-1^{+} pDCs and Tregs for the homeostasis of these cell-populations in diseased aorta.

3.4. pDCs: a potential target to cure atherosclerosis

Atherosclerosis-related disease impose a large burden onto the healthcare system of various countries. Besides the currently available drugs for atherosclerosis-related disease, new emerging concepts for the treatment can be suggested by recent studies, including ours. One main source of infiltrating immune cells are the circulating monocytes that employ the chemokine receptors CCR2 and CCR5 to invade

atherosclerotic plaques and differentiate into macrophages in the lesions (17200719) (17200718). Ablation of CCR2 or CCR5 decreases atherosclerosis by reduced blood monocytosis and macrophage accumulation (18347211) (16763157) (18165355), and blockade of CCR2 or CCR5 can be a plausible therapy. Recently the anti-CCR2 antibody MLN1202 was shown to be a promising solution for patients with cardiovascular disease (21247529). Maraviroc, an antagonist of CCR5, can be another suitable candidate for atherosclerosis treatment. The safety of maraviroc has been well established by several studies because it is used as against HIV, that uses CCR5 as a receptor (20118962). Thus, it may be a possible addition to the currently available therapies.

Another experimental strategy is the DC vaccination approach using atherosclerotic antigen-pulsed DCs that can induce adaptive immunity against atherogenic inflammation. Although the optimal atherosclerotic antigen for DC vaccination remains unclear, injecting tolerogenic IL-10–exposed DCs pulsed with ApoB100 before WD reduces atherosclerosis development (21357823). The ApoB100-loaded tolerogenic DCs inhibit proliferation of effector T cells and increase the generation of Tregs, and other studies also confirmed the same result using IL-10–exposed tolerogenic DCs in different system (17627284) (11895781). This is in line with our study showing tolerogenic effects of pDCs by increased number of Tregs in atherosclerosis, and points to pDCs as potential targets to slow down or cure atherosclerosis. Although our study didn't test the effects of pDCs on the proliferation of effector T cells, us and another group (22021930) found the expression of IDO-1 in

pDCs from atherosclerosis-induced mice. The mechanism that controls the expression of IDO-1 in pDCs is not clear yet. However, pDCs stimulation with the inhibitory ligands CTLA4-Ig (12902462) or CD200-Ig (15356121.), induces the expression of IDO-1, and administration of ligand-dependent tolerogenic pDCs seems worthwhile to assess its effects on plaque progression. On the other hand, administration of lipopolysaccharide-exposed, aldehyde-modified LDL-pulsed DCs aggravates atherosclerosis (19897195), but lipopolysaccharide-exposed, oxLDL-pulsed DCs reduce atherosclerosis (19819882). These contradictory results indicate that several factors including the degree of atherosclerosis and hyperlipidemia, atherosclerotic antigens and timing of DC administration may shape atherosclerosis progression, and further experiments are needed to test tolerogenic pDCs as therapeutics.

3.5. pDCs depletion methods in mice

Based on the results obtained using pDC-depleting antibodies or constitutive depletion of pDCs, previous studies had suggested a contradictory role for pDCs in atherosclerosis[163, 164, 165]. However, there are potential issues that cloud the interpretation of these studies. First, it is reported that anti-PDCA-1 antibodies, clone 927 and clone 120G8, that are pDC-specific in steady state might cross-react with other cell types under inflammatory conditions because other cell types also express PDCA-1 under stimulation with type I IFNs[132]. This promiscuous binding of anti-pDCs antibodies

could conceivably cause these antibodies to affect additional cell types critical for atherogenesis, yielding ambiguous phenotypes in atherosclerosis. Indeed, we found that these antibodies target not only aortic pDCs but also aortic MΦs in atherosclerosis induced mice, resulting in more than 50% depletion of MΦs, even when administered *i.v.* twice. Aortic macrophages are known to be pro-atherogenic because foam cells are derived from macrophages. Second, it was reported that the constitutive removal of E2-2 transcription factors in a DC-restricted fashion depletes pDCs. However, in this mutant mouse, there is a compensatory increase in DC-like cells[59] which could also reflect a conversion of E2-2–deficient pDCs into DCs. $CD8\alpha^+$ DCs are equivalents of $CD103^+$ DCs in non-lymphoid organs, and $CD103^+$ DCs are known to inhibit atherosclerosis[148]. Given this, further analysis of the atherosclerosis phenotype in a DC-specific E2-2–deficient mice background will be required to allow any solid conclusions to be drawn. Given these caveats, it is reasonable to conclude that the specific contribution of pDCs to atherosclerosis *in vivo* has not yet been investigated in detail. To address these unfulfilled gaps, we used BDCA2-DTR mice, in which the DT receptor is only expressed in mouse pDCs, enabling us to achieve selective and inducible pDC-depletion upon DT administration. Using this strain, we confirmed that DT administration depletes only pDCs in the aorta, sparing aortic MΦs and DCs. This model afforded us with an unequivocal opportunity to answer questions regarding the potential role of pDCs in atherosclerosis. Notably, mice without pDCs developed severe atherosclerosis (47% more than non-DT treated group). However, there was no change in serum lipid profile. Furthermore, there was no significant change in IFN-α mRNA levels in pDC-depleted

aortas compared with non-depleted aortas. This led us to seek an immune-modulatory function of aortic pDCs.

3.6. The hurdle to overcome in aorta study: Macrophages

Although previous studies focused on aortic pDCs and DCs provide informative data about their role in atherosclerosis, contribution of a certain cell type in their FACS analysis was largely neglected; Aortic macrophages[180]. Macrophages are different from other immune cells because they show high phagocytic activity and are largely autofluorescent owing to foamy cytoplasm[161, 188, 189]. If macrophages are not separated in FACS analysis as shown in their previous studies, interpretation and identification of pDCs and DCs may be hampered partially because of macrophages' autofluorescence and expression of DCs and pDCs markers on macropahges. It was reported that some macrophages express CD11c[190]. Furthermore, pDCs markers, PDCA1 and Siglec-H are found to be expressed on macrophages exposed to type I IFNs and marginal zone macrophages in the spleen, respectively[132, 133]. Especially $CD11b^+$ DCs are known to be heterogeneous and $CD11b^+$ DCs population may also contain macrophages if macrophages are not separated in FACS analysis. Macrophages express high levels of CD64 and MerTK, so it is necessary to use those two markers in combination with CD11b or F4/80 in order to separate macrophages from the analysis of DCs and pDCs in aortas.

3.7. Future prospects and experiments

Throughout this dissertation I have reviewed the previous studies on pDCs and DCs and their implications on atherosclerosis, and described our study about the role of aortic pDCs in atherosclerosis. Our study showed that aortic pDCs in steady state and in atherosclerosis are functional pDCs, secrete type I IFNs, and inhibit atherosclerosis by inducing Tregs. A previous study reported that IFN-α levels in serum did not change in atherosclerosis-induced mice or in human patients compared to the steady state[166]. In contrast, another group showed that IFN-α levels in serum and mRNA levels in aortas increased in atherosclerosis induced mice[163]. In our report, we found that isolated aortic pDCs, were able to secrete IFN-α upon CpG, TLR9 agonist, stimulation *ex vivo*, so are functional. However, we do not know if aortic pDCs secret type I IFNs upon atherosclerosis, although we observed aortic pDCs in atherosclerosis induced mice expressing higher level of PDC-TREM upon type A CpG ODN injection *in vivo* compared to controls, which suggest that aortic pDCs in atherosclerosis may not be activated. Also, we observed that aortic pDCs in atherosclerosis are $CCR9^{+}$, which is known to be downregulated upon TLR9 stimulation[130], therefore we presume that aortic pDCs in atherosclerosis are in an immature state. We obtained only indirect evidence indicating aortic pDCs may not secrete type I IFNs in atherosclerosis, thus further studies will be required to confirm if aortic pDCs express type I IFNs in atherosclerosis.

Our study and previous studies focused on the function of pDCs at the early stage of atherosclerosis by inducing both pDCs depletion and atherosclerosis on the same time point, but further study is needed to analyze the role of aortic pDCs at the late stage of atherosclerosis, when it becomes a chronic state. For example, recent studies showed pDCs maturation in chronic diseases such as systemic lupus erythematosus and psoriasis[191, 192, 193]. However, we observed that aortic pDCs in mice fed WD for 12 weeks were $CCR9^+$ and $IDO\text{-}1^+$, indicating that aortic pDCs even in chronic atherosclerosis are not mature. Since we did not directly test whether depletion of pDCs in already established atherosclerosis, for example by depleting pDCs after 12 weeks of WD feeding, would reduce aortic Tregs and aggravate atherosclerosis, it would be interesting to address the direct association between aortic pDCs and Tregs at the late stage of atherosclerosis.

We observed that aortic pDCs inhibit atherosclerosis by regulating aortic Tregs in aorta. Also other studies reported tolerogenic properties for pDCs in various mouse models and showed that the induction of Tregs depends on pDCs. It is interesting to note that $CCR9^+$ pDCs can migrate to the thymus with antigens uptaken from peripheral tissues[130]. Those $CCR9^+$ pDCs in thymus participate in the deletion of antigen-specific thymocytes and contribute to immune tolerance. The same study showed that pDCs depend on CCR9 for their migration into thymus. We did not examine whether aortic pDCs may regulate the deletion of thymus T cells specific for atherosclerosis-related antigens. We did not test either the migration of aortic pDCs in atherosclerosis from aorta to the thymus, even though another study showed that the migration of DCs in

mice with atherosclerosis is compromised[150]. Additional studies will be required to examine the possible role of pDCs in clonal deletion in the thymus and, also, the importance of aortic pDCs versus aortic DCs in terms of atherosclerosis regulation. In addition to pDCs in atherosclerosis, we also observed increase of $CD103^{-}CD11b^{-}$ DCs and it would be interesting to test whether these population would turn into $CD11b^{+}$ DCs, which is the major aortic DCs population in atherosclerosis, and $CCL17^{+}$ DCs, which exacerbate atherosclerosis.

3.8. Conclusion

On the basis of our findings, we propose that the aortic pDCs described herein have two roles. First, they are part of the innate response initiated upon microbial stimulation (e.g., TLR7 and TLR9 ligation), a response consistent with their rapid production of type I IFN. Confirming this role will require additional studies *in vivo* in the future. The second is that of an immune modulator. Accordingly, during atherogenesis, aortic pDCs increase in number and become one of the dominant cell types, thereby inducing Tregs and balancing the adverse effects of cytopathic T cells. Therefore, future therapeutic strategies harnessing tolerogenic pDC-based atheroprotective vaccines will be promising and beneficial for atherosclerosis in humans.

4. Materials and methods

Mice

C57BL/6, *Ldlr*$^{-/-}$ [194], CX3CR1-GFP, Zbtb46-GFP, OT-II, Foxp3- DTR/GFP, *Ido1*$^{-/-}$, NSG (NOD/SCID/γc-null) mice were purchased from The Jackson Laboratory (Bar Harbor, ME). *Flt3*$^{-/-}$ mice[195] (I. Lemischka, Mount Sinai School of Medicine) were a generous gift of M. Nussenzweig. BDCA2-DTR mice[179] were from M. Colonna (Washington University, St. Louis, MO). For humanized mice, NSG mice reconstituted with human CD34^{+} cells (hu-mice) or NSG mice reconstituted with human CD34^{+} cells and surgically implanted with human thymus (Hu-BLT mice) were used. All mice were fed ad libitum a normal diet (CHOW) or western-type diet (WD) (AIN-76A; Carbohydrates 49.9%, Protein 17.4%, Fat 20%, Cholesterol 0.15%) (TestDiet, St. Louis, MO) under specific pathogen-free conditions. To expand the number of pDCs, mice were injected *i.p.* with 2 μg of human FLT3 ligand (hFlt3L; Celldex Therapeutics) per day for 9 consecutive days. All mice were bred under specific pathogen-free conditions at the Institut de Recherches Cliniques de Montre´al (IRCM). All mouse experiments were performed according to guidelines of the Canadian Council on Animal Care.

Human Samples

Peripheral blood samples and aortic tissues were obtained from healthy adult donors or patients after receipt of written informed consent in accordance with the Declaration of Helsinki and research protocols approved by the research ethics review board of the

IRCM and Montréal Heart Institute. Peripheral blood mononuclear cells were isolated by Ficoll-Paque centrifugation (GE Healthcare). Collagenased aortic cells were isolated by Percoll gradient (GE Healthcare), and cultured in RPMI-1640 media supplemented with 10% FBS. To obtain human tissues to make hu-mice and for atherosclerotic tissues, written informed consent was obtained from donors. This study was approved by the ethical committee of CHU (Centre Hospitalier Universitaire) Sainte-Justine (CER#2126 and #1995) and the Montreal Heart Institute.

Single-Cell Isolation and Flow-Cytometric Analysis

Aortic single cells were isolated according to a previously described method[148], with minor modifications. Mouse aortas were incubated with the enzyme mixture containing 675 U/mL collagenase I, 18.75 U/mL collagenase XI, and 9 U/mL hyaluronidase (Sigma) in Ca^{+}/Mg^{+} containing Hank's balanced salt solution for 40 min at 37°C with gentle shaking. The adventitia was carefully separated from the mouse aorta with microforceps after incubation of the whole aorta in the enzyme mixture for 15 min at 37°C. The isolated adventitia and intima/medial tissues were then incubated separately in the new enzyme mixture for 25 min at 37°C. Human aortic samples were incubated in the same enzyme mixture, additionally containing 54 U/mL DNase (Sigma) for 40 min at 37°C with gentle shaking. Mouse spleen and LNs were digested in 400 U/mL of collagenase D (Roche) in RPMI-1640 for 30 min at 37°C. $Foxp3^{+}$ T cells were stained using a Foxp3 staining buffer set (eBioscience), according to a previously described method[196]; all other intracellular staining was performed using a

fixation/permeabilization solution kit (BD Biosciences). Stained cells were acquired or sorted using a LSRFortessa flow cytometer or FACSAria III (BD Biosciences), respectively, and analyzed with FlowJo (Tree Star). Sorted cells were cytospined at 500 rpm for 5 min using Cytospin4 (Thermo Scientific) for phagocytosis analysis.

En Face IF and Confocal Microscopic Analysis

C57BL/6 and hu-mice aortas were perfused with cold PBS and fixed in 4% formaldehyde for 40 min. After careful removal of the perivascular fat and cardiac muscle tissues, the aortas were dissected longitudinally and permeabilized with 0.2% Triton X-100 for 20 min. Siglec-H-Alexa 488 (secondary Ab: anti-Alexa 488), CD11c, HLA-DR, and LAMP5 were immunostained using an Alexa 488 and an Alexa 555 TSA kit (Invitrogen) according to the manufacturer's protocol. Detection of Siglec-H was done by injection of 15 mg of anti-Siglec-H-Alexa 488 Ab *i.v.*, and the mice were sacrificed 14–18 hr post-injection. Confocal images were acquired along the z axis using an LSM 710 laser-scanning confocal microscope (Carl Zeiss), and *Z*-stacked images were analyzed with Imaris software (Bitplane).

BM Chimeras

Marrow from BDCA2-DTR mice, *Ido1*$^{-/-}$ mice, OT-II mice, or Foxp3-DTR mice were injected *i.v.* into lethally irradiated (2 3 5 Gy, 3 hours apart) *Ldlr*$^{-/-}$ mice. After 8 weeks, mice were fed either chow or WD and injected with PBS or DT (Sigma; 0.5 mg per mouse per week intraperitoneally [*i.p.*] for BDCA2-DTR; and 1 mg per mouse per week

i.v. for Foxp3-DTR) for the indicated period.

Statistics

All statistical significance between two groups was tested using a Mann-Whitney test with two-tailed p values. One-way ANOVA was used for comparisons of three groups in Figures 4A, 5C, and S7B. R-squared value was obtained from linear regression analysis. Data are presented as mean ± SD.

Antibodies and Reagents.

Antibodies to mouse Foxp3 and IDO-1 and human Foxp3 and IDO-1 for FACS analysis were from eBioscience, and the antibody to human LAMP5 was a generous gift from YJ. Liu (MedImmune, MD). The antibody to human IFN-α for FACS analysis was from Miltenyi Biotec. The antibody for mouse IFN-α (for intracellular staining and ELISA) was from PBL Assay Science. Single or double immunostaining was performed using antibodies to human LAMP5 from BioLegend, human HLA-DR from Dako, human BDCA2 from Genetex, human IDO-1 from Novus Biologicals and/or human Foxp3 from eBioscience. Anti-Siglec-H (clone: 551) and anti-PDCA-1 (clone: 927) antibodies were from M. Colonna and were purified in house and labeled using an Alexa Fluor antibody labeling kit (Invitrogen) according to the manufacturer's protocol. All other antibodies were from BioLegend. All single cells were incubated in culture supernatant from the 2.4G2 hybridoma (Fc Receptor Block, ATCC: HB-197) prior to staining with the indicated antibodies. 10 μg of Type A TLR9 agonist CpG ODN 2216 (InvivoGen) were

mixed with 30 µl of DOTAP (Roche) according to the manufacturer's instructions, and injected *i.v.*. Injected mice were sacrificed 9-12 hours post injection and expression level of PDC-TREM was compared.

Assessment of Atherosclerosis in Mouse and Human.

For mouse, the heart and aorta were perfused via each ventricle with cold phosphate-buffered saline (PBS) and fixed in cold 4% paraformaldehyde. After fixation, hearts were embedded in OCT and frozen. For analysis of aortic sinus plaque, cryosections were stained overnight with Oil Red O (Sigma) and digitized (TSView). For *en face* analysis, an aortic segment from the ascending aorta to the descending aorta was used. After removal of the perivascular tissues, the aortas were split longitudinally, pinned onto flat black silicone plates, and stained with 0.5% Oil Red O in propylene glycol for 7 hours. After staining, aortas were destained with 85% propylene glycol in distilled water. The atherosclerotic lesion area was digitized and calculated using the TSView program (ver.7.1.1.5). Plasma lipids, including total cholesterol, triglyceride, low-density lipoprotein and high-density lipoprotein, were determined using an automated blood chemical analyzer (Hitachi). For human aortic atherosclerosis grading, histopathological classification was analyzed according to foam cells and tissue disruption[197].

Immunohistochemistry.

After fixation with 4% paraformaldehyde overnight, aortas from humanized mice and human atherosclerotic patients were processed using standard procedures, embedded

in paraffin, and sectioned (5-µm thick). After performing antigen retrieval by autoclaving in a citric acid solution, sections were singly or doubly immunostained with the indicated antibodies. Immunoreactive proteins were visualized using an ImmPRESS-AP anti-rabbit Ig polymer detection kit, a VECTOR blue alkaline phosphatase substrate kit, an ImmPRESS HRP anti-mouse Ig polymer detection kit, a VECTOR NovaRED peroxidase substrate kit (Vector Labs) and a Polink-1 HRP Broad for DAB Kit (GBI Labs), as appropriate. In addition, M.O.M Elite Peroxidase kits (Vector Labs) were used for double immunostaining involving two mouse primary antibodies. All experiments were performed according to the manufacturer's instructions. Nuclei were counterstained with hematoxylin solutions.

Cell Culture.

For analysis of IFN-α secretion into culture media, cells from pooled aortas and hearts and spleens from C57BL/6 mice were incubated with media alone or with 10 µg/mL of Type A TLR9 agonist CpG ODN 2216 (InvivoGen) for 48 hours. For flow cytometric analysis of IFN-α, cells from aortas and skin-draining LNs from C57BL/6 mice were incubated with media alone or with 10 µg/mL of Type A TLR9 agonist CpG ODN 2216 for 3 hours, followed by an additional 6 hours incubation with addition of 10 µg/mL of Brefeldin A (Sigma). For phagocytosis assay, aortic cells from Flt3L injected C57BL/6 mice were incubated with Fluoresbrite YG Carboxylate Microspheres 1.0 µm (Polysciences) at 37°C for 1 hour. Then, cells were incubated in Fc Receptor Block and stained with antibodies at 4°C for cell sorting. All mouse cells were incubated in RPMI

1640 containing 5% FBS, 1x antibiotic-antimycotic, GlutaMAX and MEM nonessential amino acids, and 2-mercaptoethanol (Gibco). HEK-293 cell line was cultured in DMEM containing 10% FBS, 1x antibiotic-antimycotic, GlutaMAX and MEM nonessential amino acids. HEK-293 cell line was transfected with human IDO-1 expression vector (BPS Bioscience) using Lipofectamine 2000 (Invitrogen).

ELISA and QUANTI-Blue Reporter Assays.

Mouse IFN-α levels in cell supernatants were measured by sandwich enzyme-linked immunosorbent assay (ELISA). Culture supernatants were incubated with a rat monoclonal anti-IFN-α (RMMA-1 clone) and rabbit polyclonal anti-IFN-α (PBL Assay Science) antibody on Maxisorp plates (Nunc) and developed with tetramethylbenzidine substrate (Thermo Scientific). Mouse IFN-α (PBL Assay Science) was used as a positive control. Levels of human IFN-α in serum were measured using HEK-Blue IFN-α/β cells with QUANTI-Blue (InvivoGen) according to the manufacturer's protocol, with purified human IFN-α (Biolegend) as a positive control.

Quantitative RT-PCR.

Total aortic RNA was extracted from aortas using QIAzol Lysis Reagent (Qiagen), and cDNA was prepared from RNA using ReverTra Ace qPCR-RT Master Mix (TOYOBO). Quantitative real-time RT-PCR was performed in duplicate using Sensi FAST SYBR No-Rox Mix (Bioline) and quantified on the Roter-Gene Q 2plex system (Qiagen) using the ΔΔCt method with β-actin as a reference gene. Single cell RNA was extracted from

sorted aortic cells and reverse transcriptased using Single Cell-to-CT qRT-PCR kit (Ambion). Quantitative real-time RT-PCR was performed using indicated Taqman primers (Applied Biosystems; *Tbp*, Mm00446971_m1; *β-actin*, Mm02619580_g1; *Ido-1*, Mm00492590_m1; *Ifn-β1*, Mm00439546_s1) and quantified on ViiA7 (Applied Biosystems) using the ΔΔCt method with *Tbp* as a reference gene.

Antibody-Mediated In Vivo Blockade.

For depletion of PDCA-1-expressing cells, mice were injected *i.v.* with 250 μg of isotype antibody (Rat IgG2b, BioXcell), in-house-purified BST2 antibody (clone: 927) in PBS twice at 36 hours intervals.

5. Conflict of interest

Tibor Keler is an employee and shareholder of Celldex Therapeutics. All researchers declare no competing financial interests related to this work, except Tibor Keler.

Bibliography

1. West, M.A. *et al.* Enhanced dendritic cell antigen capture via toll-like receptor-induced actin remodeling. *Science* **305**, 1153-1157 (2004).

2. Granucci, F. *et al.* Early events in dendritic cell maturation induced by LPS. *Microbes Infect* **1**, 1079-1084 (1999).

3. Gil-Torregrosa, B.C. *et al.* Control of cross-presentation during dendritic cell maturation. *Eur J Immunol* **34**, 398-407 (2004).

4. Reis e Sousa, C. Dendritic cells in a mature age. *Nature reviews. Immunology* **6**, 476-483 (2006).

5. Vargas, P. *et al.* Innate control of actin nucleation determines two distinct migration behaviours in dendritic cells. *Nat Cell Biol* **18**, 43-53 (2016).

6. Merad, M., Sathe, P., Helft, J., Miller, J. & Mortha, A. The dendritic cell lineage: ontogeny and function of dendritic cells and their subsets in the steady state and the inflamed setting. *Annu Rev Immunol* **31**, 563-604 (2013).

7. Cresswell, P., Ackerman, A.L., Giodini, A., Peaper, D.R. & Wearsch, P.A. Mechanisms of MHC class I-restricted antigen processing and cross-presentation. *Immunological reviews* **207**, 145-157 (2005).

8. Bedoui, S. *et al.* Cross-presentation of viral and self antigens by skin-derived CD103+ dendritic cells. *Nat Immunol* **10**, 488-495 (2009).

9. Belz, G.T. *et al.* Distinct migrating and nonmigrating dendritic cell populations are involved in MHC class I-restricted antigen presentation after lung infection with virus. *Proceedings of the National Academy of Sciences of the United States of America* **101**, 8670-8675 (2004).

10. den Haan, J.M., Lehar, S.M. & Bevan, M.J. CD8(+) but not CD8(-) dendritic cells cross-prime cytotoxic T cells in vivo. *The Journal of experimental medicine* **192**, 1685-1696 (2000).

11. Savina, A. *et al.* The small GTPase Rac2 controls phagosomal alkalinization and antigen crosspresentation selectively in CD8(+) dendritic cells. *Immunity* **30**, 544-555 (2009).

12. Bougneres, L. *et al.* A role for lipid bodies in the cross-presentation of phagocytosed antigens by MHC class I in dendritic cells. *Immunity* **31**, 232-244 (2009).

13. Cheong, C. *et al.* Microbial stimulation fully differentiates monocytes to DC-SIGN/CD209(+) dendritic cells for immune T cell areas. *Cell* **143**, 416-429 (2010).

14. Forster, R. *et al.* CCR7 coordinates the primary immune response by establishing functional microenvironments in secondary lymphoid organs. *Cell* **99**, 23-33 (1999).

15. Ohl, L. *et al.* CCR7 governs skin dendritic cell migration under inflammatory and steady-state conditions. *Immunity* **21**, 279-288 (2004).

16. MartIn-Fontecha, A. *et al.* Regulation of dendritic cell migration to the draining lymph node: impact on T lymphocyte traffic and priming. *The Journal of experimental medicine* **198**, 615-621 (2003).

17. Robbiani, D.F. *et al.* The leukotriene C(4) transporter MRP1 regulates CCL19 (MIP-3beta, ELC)-dependent mobilization of dendritic cells to lymph nodes. *Cell* **103**, 757-768 (2000).

18. Saeki, H., Moore, A.M., Brown, M.J. & Hwang, S.T. Cutting edge: secondary lymphoid-tissue chemokine (SLC) and CC chemokine receptor 7 (CCR7) participate in the emigration pathway of mature dendritic cells from the skin to regional lymph nodes. *J Immunol* **162**, 2472-2475 (1999).

19. Britschgi, M.R., Favre, S. & Luther, S.A. CCL21 is sufficient to mediate DC migration, maturation and function in the absence of CCL19. *Eur J Immunol* **40**, 1266-1271 (2010).

20. Ngo, V.N., Tang, H.L. & Cyster, J.G. Epstein-Barr virus-induced molecule 1 ligand chemokine is expressed by dendritic cells in lymphoid tissues and strongly attracts naive T cells and activated B cells. *The Journal of experimental medicine* **188**, 181-191 (1998).

21. Bajenoff, M. *et al.* Stromal cell networks regulate lymphocyte entry, migration, and territoriality in lymph nodes. *Immunity* **25**, 989-1001 (2006).

22. Schumann, K. *et al.* Immobilized chemokine fields and soluble chemokine gradients cooperatively shape migration patterns of dendritic cells. *Immunity* **32**, 703-713 (2010).

23. Johnson, L.A. *et al.* An inflammation-induced mechanism for leukocyte transmigration across lymphatic vessel endothelium. *The Journal of experimental medicine* **203**, 2763-2777 (2006).

24. Xu, H. *et al.* The role of ICAM-1 molecule in the migration of Langerhans cells in the skin and regional lymph node. *Eur J Immunol* **31**, 3085-3093 (2001).

25. Lammermann, T. *et al.* Rapid leukocyte migration by integrin-independent flowing and squeezing. *Nature* **453**, 51-55 (2008).

26. Gatto, D. *et al.* The chemotactic receptor EBI2 regulates the homeostasis, localization and immunological function of splenic dendritic cells. *Nat Immunol* **14**, 446-453 (2013).

27. Iwasaki, A. & Kelsall, B.L. Localization of distinct Peyer's patch dendritic cell subsets and their recruitment by chemokines macrophage inflammatory protein (MIP)-3alpha, MIP-3beta, and secondary lymphoid organ chemokine. *The Journal of experimental medicine* **191**, 1381-1394 (2000).

28. Alvarez, D., Vollmann, E.H. & von Andrian, U.H. Mechanisms and consequences of dendritic cell migration. *Immunity* **29**, 325-342 (2008).

29. Lei, Y. *et al.* Aire-dependent production of XCL1 mediates medullary accumulation of thymic dendritic cells and contributes to regulatory T cell development. *The Journal of experimental medicine* **208**, 383-394 (2011).

30. Edelson, B.T. *et al.* CD8alpha(+) dendritic cells are an obligate cellular entry point for productive infection by Listeria monocytogenes. *Immunity* **35**, 236-248 (2011).

31. Vremec, D. *et al.* The surface phenotype of dendritic cells purified from mouse thymus and spleen: investigation of the CD8 expression by a subpopulation of dendritic cells. *The Journal of experimental medicine* **176**, 47-58 (1992).

32. Bursch, L.S. *et al.* Identification of a novel population of Langerin+ dendritic cells. *The Journal of experimental medicine* **204**, 3147-3156 (2007).

33. del Rio, M.L., Rodriguez-Barbosa, J.I., Kremmer, E. & Forster, R. CD103- and CD103+ bronchial lymph node dendritic cells are specialized in presenting and cross-presenting innocuous antigen to CD4+ and CD8+ T cells. *J Immunol* **178**, 6861-6866 (2007).

34. Helft, J., Ginhoux, F., Bogunovic, M. & Merad, M. Origin and functional heterogeneity of non-lymphoid tissue dendritic cells in mice. *Immunological reviews* **234**, 55-75 (2010).

35. Edelson, B.T. *et al.* Peripheral CD103+ dendritic cells form a unified subset developmentally related to CD8alpha+ conventional dendritic cells. *J. Exp. Med.* **207**, 823-836 (2010).

36. Shortman, K. & Heath, W.R. The CD8+ dendritic cell subset. *Immunological reviews* **234**, 18-31 (2010).

37. Waskow, C. *et al.* The receptor tyrosine kinase Flt3 is required for dendritic cell development in peripheral lymphoid tissues. *Nat. Immunol.* **9**, 676-683 (2008).

38. Ginhoux, F. *et al.* The origin and development of nonlymphoid tissue CD103+ DCs. *J. Exp. Med.* **206**, 3115-3130 (2009).

39. Schreibelt, G. *et al.* The C-type lectin receptor CLEC9A mediates antigen uptake and (cross-)presentation by human blood BDCA3+ myeloid dendritic cells. *Blood* **119**, 2284-2292 (2012).

40. Shrimpton, R.E. *et al.* CD205 (DEC-205): a recognition receptor for apoptotic and necrotic self. *Mol Immunol* **46**, 1229-1239 (2009).

41. Lewis, K.L. *et al.* Notch2 receptor signaling controls functional differentiation of dendritic cells in the spleen and intestine. *Immunity* **35**, 780-791 (2011).

42. Jaitin, D.A. *et al.* Massively parallel single-cell RNA-seq for marker-free decomposition of tissues into cell types. *Science* **343**, 776-779 (2014).

43. Dudziak, D. *et al.* Differential antigen processing by dendritic cell subsets in vivo. *Science* **315**, 107-111 (2007).

44. Mildner, A., Yona, S. & Jung, S. A close encounter of the third kind: monocyte-derived cells. *Adv Immunol* **120**, 69-103 (2013).

45. Rivollier, A., He, J., Kole, A., Valatas, V. & Kelsall, B.L. Inflammation switches the differentiation program of Ly6Chi monocytes from antiinflammatory macrophages to inflammatory dendritic cells in the colon. *The Journal of experimental medicine* **209**, 139-155 (2012).

46. Plantinga, M. *et al.* Conventional and monocyte-derived CD11b(+) dendritic cells initiate and maintain T helper 2 cell-mediated immunity to house dust mite allergen. *Immunity* **38**, 322-335 (2013).

47. Tamoutounour, S. *et al.* Origins and functional specialization of macrophages and of conventional and monocyte-derived dendritic cells in mouse skin. *Immunity* **39**, 925-938 (2013).

48. Langlet, C. *et al.* CD64 expression distinguishes monocyte-derived and conventional dendritic cells and reveals their distinct role during intramuscular immunization. *J Immunol* **188**, 1751-1760 (2012).

49. Satpathy, A.T. *et al.* Zbtb46 expression distinguishes classical dendritic cells and their committed progenitors from other immune lineages. *The Journal of experimental medicine* **209**, 1135-1152 (2012).

50. Yun, T.J. *et al.* Indoleamine 2,3-Dioxygenase-Expressing Aortic Plasmacytoid Dendritic Cells Protect against Atherosclerosis by Induction of Regulatory T Cells. *Cell Metab* **23**, 852-866 (2016).

51. Siegal, F.P. *et al.* The nature of the principal type 1 interferon-producing cells in human blood. *Science* **284**, 1835-1837 (1999).

52. Asselin-Paturel, C. *et al.* Mouse type I IFN-producing cells are immature APCs with plasmacytoid morphology. *Nat Immunol* **2**, 1144-1150 (2001).

53. Reizis, B., Bunin, A., Ghosh, H.S., Lewis, K.L. & Sisirak, V. Plasmacytoid dendritic cells: recent progress and open questions. *Annu. Rev. Immunol.* **29**, 163-183 (2011).

54. Kingston, D. *et al.* The concerted action of GM-CSF and Flt3-ligand on in vivo dendritic cell homeostasis. *Blood* **114**, 835-843 (2009).

55. Robbins, S.H. *et al.* Novel insights into the relationships between dendritic cell subsets in human and mouse revealed by genome-wide expression profiling. *Genome Biol* **9**, R17 (2008).

56. Sapoznikov, A. *et al.* Organ-dependent in vivo priming of naive CD4+, but not CD8+, T cells by plasmacytoid dendritic cells. *The Journal of experimental medicine* **204**, 1923-1933 (2007).

57. Nakano, H., Yanagita, M. & Gunn, M.D. CD11c(+)B220(+)Gr-1(+) cells in mouse lymph nodes and spleen display characteristics of plasmacytoid dendritic cells. *The Journal of experimental medicine* **194**, 1171-1178 (2001).

58. Cisse, B. *et al.* Transcription factor E2-2 is an essential and specific regulator of plasmacytoid dendritic cell development. *Cell* **135**, 37-48 (2008).

59. Ghosh, H.S., Cisse, B., Bunin, A., Lewis, K.L. & Reizis, B. Continuous expression of the transcription factor e2-2 maintains the cell fate of mature plasmacytoid dendritic cells. *Immunity* **33**, 905-916 (2010).

60. Bar-On, L. *et al.* CX3CR1+ CD8alpha+ dendritic cells are a steady-state population related to plasmacytoid dendritic cells. *Proceedings of the National Academy of Sciences of the United States of America* **107**, 14745-14750 (2010).

61. Birnberg, T. *et al.* Lack of conventional dendritic cells is compatible with normal development and T cell homeostasis, but causes myeloid proliferative syndrome. *Immunity* **29**, 986-997 (2008).

62. Jung, S. *et al.* In vivo depletion of CD11c+ dendritic cells abrogates priming of CD8+ T cells by exogenous cell-associated antigens. *Immunity* **17**, 211-220 (2002).

63. Reis e Sousa, C. Toll-like receptors and dendritic cells: for whom the bug tolls. *Semin Immunol* **16**, 27-34 (2004).

64. Akira, S. & Takeda, K. Toll-like receptor signalling. *Nature reviews. Immunology* **4**, 499-511 (2004).

65. Kim, T.S. & Braciale, T.J. Respiratory dendritic cell subsets differ in their capacity to support the induction of virus-specific cytotoxic CD8+ T cell responses. *PLoS One* **4**, e4204 (2009).

66. GeurtsvanKessel, C.H. *et al.* Clearance of influenza virus from the lung depends on migratory langerin+CD11b- but not plasmacytoid dendritic cells. *The Journal of experimental medicine* **205**, 1621-1634 (2008).

67. Brewig, N. *et al.* Priming of CD8+ and CD4+ T cells in experimental leishmaniasis is initiated by different dendritic cell subtypes. *J Immunol* **182**, 774-783 (2009).

68. Maldonado-Lopez, R. *et al.* CD8alpha+ and CD8alpha- subclasses of dendritic cells direct the development of distinct T helper cells in vivo. *The Journal of experimental medicine* **189**, 587-592 (1999).

69. Farrand, K.J. *et al.* Langerin+ CD8alpha+ dendritic cells are critical for cross-priming and IL-12 production in response to systemic antigens. *J Immunol* **183**, 7732-7742 (2009).

70. Mashayekhi, M. *et al.* CD8alpha(+) dendritic cells are the critical source of interleukin-12 that controls acute infection by Toxoplasma gondii tachyzoites. *Immunity* **35**, 249-259 (2011).

71. Mattei, F., Schiavoni, G., Belardelli, F. & Tough, D.F. IL-15 is expressed by dendritic cells in response to type I IFN, double-stranded RNA, or lipopolysaccharide and promotes dendritic cell activation. *J Immunol* **167**, 1179-1187 (2001).

72. Persson, E.K. *et al.* IRF4 transcription-factor-dependent CD103(+)CD11b(+) dendritic cells drive mucosal T helper 17 cell differentiation. *Immunity* **38**, 958-969 (2013).

73. Schlitzer, A. *et al.* IRF4 transcription factor-dependent CD11b+ dendritic cells in human and mouse control mucosal IL-17 cytokine responses. *Immunity* **38**, 970-983 (2013).

74. Sporri, R. & Reis e Sousa, C. Inflammatory mediators are insufficient for full dendritic cell activation and promote expansion of CD4+ T cell populations lacking helper function. *Nat Immunol* **6**, 163-170 (2005).

75. Hawiger, D. *et al.* Dendritic cells induce peripheral T cell unresponsiveness under steady state conditions in vivo. *J. Exp. Med.* **194**, 769-779 (2001).

76. Probst, H.C., Lagnel, J., Kollias, G. & van den Broek, M. Inducible transgenic mice reveal resting dendritic cells as potent inducers of CD8+ T cell tolerance. *Immunity* **18**, 713-720 (2003).

77. Miga, A.J. *et al.* Dendritic cell longevity and T cell persistence is controlled by CD154-CD40 interactions. *Eur J Immunol* **31**, 959-965 (2001).

78. Cella, M. *et al.* Ligation of CD40 on dendritic cells triggers production of high levels of interleukin-12 and enhances T cell stimulatory capacity: T-T help via APC activation. *The Journal of experimental medicine* **184**, 747-752 (1996).

79. Saito, Y., Boddupalli, C.S., Borsotti, C. & Manz, M.G. Dendritic cell homeostasis is maintained by nonhematopoietic and T-cell-produced Flt3-ligand in steady state and during immune responses. *Eur J Immunol* **43**, 1651-1658 (2013).

80. Fogg, D.K. *et al.* A clonogenic bone marrow progenitor specific for macrophages and dendritic cells. *Science* **311**, 83-87 (2006).

81. Naik, S.H. *et al.* Intrasplenic steady-state dendritic cell precursors that are distinct from monocytes. *Nat. Immunol.* **7**, 663-671 (2006).

82. Onai, N. *et al.* Identification of clonogenic common Flt3+M-CSFR+ plasmacytoid and conventional dendritic cell progenitors in mouse bone marrow. *Nat. Immunol.* **8**, 1207-1216 (2007).

83. Diao, J. *et al.* In situ replication of immediate dendritic cell (DC) precursors contributes to conventional DC homeostasis in lymphoid tissue. *J. Immunol.* **176**, 7196-7206 (2006).

84. Liu, K. *et al.* In vivo analysis of dendritic cell development and homeostasis. *Science* **324**, 392-397 (2009).

85. Varol, C. *et al.* Intestinal lamina propria dendritic cell subsets have different origin and functions. *Immunity* **31**, 502-512 (2009).

86. Bogunovic, M. *et al.* Origin of the lamina propria dendritic cell network. *Immunity* **31**, 513-525 (2009).

87. Mildner, A. & Jung, S. Development and function of dendritic cell subsets. *Immunity* **40**, 642-656 (2014).

88. Shigematsu, H. *et al.* Plasmacytoid dendritic cells activate lymphoid-specific genetic programs irrespective of their cellular origin. *Immunity* **21**, 43-53 (2004).

89. Corcoran, L. *et al.* The lymphoid past of mouse plasmacytoid cells and thymic dendritic cells. *J Immunol* **170**, 4926-4932 (2003).

90. Pelayo, R. *et al.* Derivation of 2 categories of plasmacytoid dendritic cells in murine bone marrow. *Blood* **105**, 4407-4415 (2005).

91. Yang, G.X. *et al.* Plasmacytoid dendritic cells of different origins have distinct characteristics and function: studies of lymphoid progenitors versus myeloid progenitors. *J Immunol* **175**, 7281-7287 (2005).

92. Naik, S.H. *et al.* Development of plasmacytoid and conventional dendritic cell subtypes from single precursor cells derived in vitro and in vivo. *Nat. Immunol.* **8**, 1217-1226 (2007).

93. Schmid, M.A., Kingston, D., Boddupalli, S. & Manz, M.G. Instructive cytokine signals in dendritic cell lineage commitment. *Immunological reviews* **234**, 32-44 (2010).

94. Eidenschenk, C. *et al.* Flt3 permits survival during infection by rendering dendritic cells competent to activate NK cells. *Proceedings of the National Academy of Sciences of the United States of America* **107**, 9759-9764 (2010).

95. Sathaliyawala, T. *et al.* Mammalian target of rapamycin controls dendritic cell development downstream of Flt3 ligand signaling. *Immunity* **33**, 597-606 (2010).

96. Feldman, M. & Fitzgerald-Bocarsly, P. Sequential enrichment and immunocytochemical visualization of human interferon-alpha-producing cells. *J Interferon Res* **10**, 435-446 (1990).

97. Starr, S.E. *et al.* Morphological and functional differences between HLA-DR+ peripheral blood dendritic cells and HLA-DR+ IFN-alpha producing cells. *Adv Exp Med Biol* **329**, 173-178 (1993).

98. Muller-Hermelink, H.K., Stein, H., Steinmann, G. & Lennert, K. Malignant lymphoma of plasmacytoid T-cells. Morphologic and immunologic studies characterizing a special type of T-cell. *Am J Surg Pathol* **7**, 849-862 (1983).

99. Facchetti, F. *et al.* Plasmacytoid T cells. Immunohistochemical evidence for their monocyte/macrophage origin. *Am J Pathol* **133**, 15-21 (1988).

100. Facchetti, F. *et al.* Leukemia-associated lymph node infiltrates of plasmacytoid monocytes (so-called plasmacytoid T-cells). Evidence for two distinct histological and immunophenotypical patterns. *Am J Surg Pathol* **14**, 101-112 (1990).

101. Grouard, G. *et al.* The enigmatic plasmacytoid T cells develop into dendritic cells with interleukin (IL)-3 and CD40-ligand. *The Journal of experimental medicine* **185**, 1101-1111 (1997).

102. Cella, M. *et al.* Plasmacytoid monocytes migrate to inflamed lymph nodes and produce large amounts of type I interferon. *Nat. Med.* **5**, 919-923 (1999).

103. Liu, Y.J. IPC: professional type 1 interferon-producing cells and plasmacytoid dendritic cell precursors. *Annu Rev Immunol* **23**, 275-306 (2005).

104. Swiecki, M. & Colonna, M. The multifaceted biology of plasmacytoid dendritic cells. *Nat. Rev. Immunol.* **15**, 471-485 (2015).

105. Asselin-Paturel, C., Brizard, G., Pin, J.J., Briere, F. & Trinchieri, G. Mouse strain differences in plasmacytoid dendritic cell frequency and function revealed by a novel monoclonal antibody. *J. Immunol.* **171**, 6466-6477 (2003).

106. Krug, A. *et al.* TLR9-dependent recognition of MCMV by IPC and DC generates coordinated cytokine responses that activate antiviral NK cell function. *Immunity* **21**, 107-119 (2004).

107. Dalod, M. *et al.* Interferon alpha/beta and interleukin 12 responses to viral infections: pathways regulating dendritic cell cytokine expression in vivo. *The Journal of experimental medicine* **195**, 517-528 (2002).

108. Swiecki, M. & Colonna, M. Unraveling the functions of plasmacytoid dendritic cells during viral infections, autoimmunity, and tolerance. *Immunol. Rev.* **234**, 142-162 (2010).

109. Wolf, A.I. *et al.* Plasmacytoid dendritic cells are dispensable during primary influenza virus infection. *J Immunol* **182**, 871-879 (2009).

110. Kumagai, Y. *et al.* Alveolar macrophages are the primary interferon-alpha producer in pulmonary infection with RNA viruses. *Immunity* **27**, 240-252 (2007).

111. Cervantes-Barragan, L. *et al.* Control of coronavirus infection through plasmacytoid dendritic-cell-derived type I interferon. *Blood* **109**, 1131-1137 (2007).

112. Cervantes-Barragan, L. *et al.* Plasmacytoid dendritic cells control T-cell response to chronic viral infection. *Proceedings of the National Academy of Sciences of the United States of America* **109**, 3012-3017 (2012).

113. Ciancanelli, M.J. *et al.* Infectious disease. Life-threatening influenza and impaired interferon amplification in human IRF7 deficiency. *Science* **348**, 448-453 (2015).

114. Davidson, S., Crotta, S., McCabe, T.M. & Wack, A. Pathogenic potential of interferon alphabeta in acute influenza infection. *Nat Commun* **5**, 3864 (2014).

115. Frenz, T. *et al.* Independent of plasmacytoid dendritic cell (pDC) infection, pDC triggered by virus-infected cells mount enhanced type I IFN responses of different

composition as opposed to pDC stimulated with free virus. *J Immunol* **193**, 2496-2503 (2014).

116. Feng, Z. *et al.* Human pDCs preferentially sense enveloped hepatitis A virions. *The Journal of clinical investigation* **125**, 169-176 (2015).

117. Dreux, M. *et al.* Short-range exosomal transfer of viral RNA from infected cells to plasmacytoid dendritic cells triggers innate immunity. *Cell Host Microbe* **12**, 558-570 (2012).

118. Barrat, F.J. *et al.* Nucleic acids of mammalian origin can act as endogenous ligands for Toll-like receptors and may promote systemic lupus erythematosus. *The Journal of experimental medicine* **202**, 1131-1139 (2005).

119. Honda, K. *et al.* Spatiotemporal regulation of MyD88-IRF-7 signalling for robust type-I interferon induction. *Nature* **434**, 1035-1040 (2005).

120. Guiducci, C. *et al.* Properties regulating the nature of the plasmacytoid dendritic cell response to Toll-like receptor 9 activation. *The Journal of experimental medicine* **203**, 1999-2008 (2006).

121. Sasai, M., Linehan, M.M. & Iwasaki, A. Bifurcation of Toll-like receptor 9 signaling by adaptor protein 3. *Science* **329**, 1530-1534 (2010).

122. Blasius, A.L. *et al.* Slc15a4, AP-3, and Hermansky-Pudlak syndrome proteins are required for Toll-like receptor signaling in plasmacytoid dendritic cells. *Proceedings of the National Academy of Sciences of the United States of America* **107**, 19973-19978 (2010).

123. Henault, J. *et al.* Noncanonical autophagy is required for type I interferon secretion in response to DNA-immune complexes. *Immunity* **37**, 986-997 (2012).

124. Lee, H.K., Lund, J.M., Ramanathan, B., Mizushima, N. & Iwasaki, A. Autophagy-dependent viral recognition by plasmacytoid dendritic cells. *Science* **315**, 1398-1401 (2007).

125. Guiducci, C. *et al.* PI3K is critical for the nuclear translocation of IRF-7 and type I IFN production by human plasmacytoid predendritic cells in response to TLR activation. *The Journal of experimental medicine* **205**, 315-322 (2008).

126. Cao, W. *et al.* Toll-like receptor-mediated induction of type I interferon in plasmacytoid dendritic cells requires the rapamycin-sensitive PI(3)K-mTOR-p70S6K pathway. *Nat Immunol* **9**, 1157-1164 (2008).

127. Villadangos, J.A. & Young, L. Antigen-presentation properties of plasmacytoid dendritic cells. *Immunity* **29**, 352-361 (2008).

128. Mouries, J. *et al.* Plasmacytoid dendritic cells efficiently cross-prime naive T cells in vivo after TLR activation. *Blood* **112**, 3713-3722 (2008).

129. Young, L.J. *et al.* Differential MHC class II synthesis and ubiquitination confers distinct antigen-presenting properties on conventional and plasmacytoid dendritic cells. *Nat Immunol* **9**, 1244-1252 (2008).

130. Hadeiba, H. *et al.* Plasmacytoid dendritic cells transport peripheral antigens to the thymus to promote central tolerance. *Immunity* **36**, 438-450 (2012).

131. Hadeiba, H. *et al.* CCR9 expression defines tolerogenic plasmacytoid dendritic cells able to suppress acute graft-versus-host disease. *Nat. Immunol.* **9**, 1253-1260 (2008).

132. Blasius, A.L. *et al.* Bone marrow stromal cell antigen 2 is a specific marker of type I IFN-producing cells in the naive mouse, but a promiscuous cell surface antigen following IFN stimulation. *J. Immunol.* **177**, 3260-3265 (2006).

133. Zhang, J. *et al.* Characterization of Siglec-H as a novel endocytic receptor expressed on murine plasmacytoid dendritic cell precursors. *Blood* **107**, 3600-3608 (2006).

134. Watarai, H. *et al.* PDC-TREM, a plasmacytoid dendritic cell-specific receptor, is responsible for augmented production of type I interferon. *Proc. Natl. Acad. Sci. USA* **105**, 2993-2998 (2008).

135. Tai, L.H. *et al.* Positive regulation of plasmacytoid dendritic cell function via Ly49Q recognition of class I MHC. *The Journal of experimental medicine* **205**, 3187-3199 (2008).

136. Mitsuhashi, Y. *et al.* Regulation of plasmacytoid dendritic cell responses by PIR-B. *Blood* **120**, 3256-3259 (2012).

137. Chiang, E.Y., Johnston, R.J. & Grogan, J.L. EBI2 is a negative regulator of type I interferons in plasmacytoid and myeloid dendritic cells. *PLoS One* **8**, e83457 (2013).

138. Blasius, A.L., Cella, M., Maldonado, J., Takai, T. & Colonna, M. Siglec-H is an IPC-specific receptor that modulates type I IFN secretion through DAP12. *Blood* **107**, 2474-2476 (2006).

139. Bunin, A. *et al.* Protein Tyrosine Phosphatase PTPRS Is an Inhibitory Receptor on Human and Murine Plasmacytoid Dendritic Cells. *Immunity* **43**, 277-288 (2015).

140. Cao, W. *et al.* Regulation of TLR7/9 responses in plasmacytoid dendritic cells by BST2 and ILT7 receptor interaction. *The Journal of experimental medicine* **206**, 1603-1614 (2009).

141. Subramanian, M. & Tabas, I. Dendritic cells in atherosclerosis. *Semin. Immunopathol.* **36**, 93-102 (2014).

142. Belz, G.T. & Nutt, S.L. Transcriptional programming of the dendritic cell network. *Nature reviews. Immunology* **12**, 101-113 (2012).

143. Burgdorf, S., Scholz, C., Kautz, A., Tampe, R. & Kurts, C. Spatial and mechanistic separation of cross-presentation and endogenous antigen presentation. *Nat Immunol* **9**, 558-566 (2008).

144. Copin, R., De Baetselier, P., Carlier, Y., Letesson, J.J. & Muraille, E. MyD88-dependent activation of B220-CD11b+LY-6C+ dendritic cells during Brucella melitensis infection. *J Immunol* **178**, 5182-5191 (2007).

145. Yilmaz, A. *et al.* Emergence of dendritic cells in rupture-prone regions of vulnerable carotid plaques. *Atherosclerosis* **176**, 101-110 (2004).

146. Paulson, K.E. *et al.* Resident intimal dendritic cells accumulate lipid and contribute to the initiation of atherosclerosis. *Circ. Res.* **106**, 383-390 (2010).

147. Koltsova, E.K. & Ley, K. How dendritic cells shape atherosclerosis. *Trends Immunol.* **32**, 540-547 (2011).

148. Choi, J.H. *et al.* Flt3 signaling-dependent dendritic cells protect against atherosclerosis. *Immunity* **35**, 819-831 (2011).

149. Buono, C. *et al.* B7-1/B7-2 costimulation regulates plaque antigen-specific T-cell responses and atherogenesis in low-density lipoprotein receptor-deficient mice. *Circulation* **109**, 2009-2015 (2004).

150. Angeli, V. *et al.* Dyslipidemia associated with atherosclerotic disease systemically alters dendritic cell mobilization. *Immunity* **21**, 561-574 (2004).

151. Packard, R.R. *et al.* CD11c(+) dendritic cells maintain antigen processing, presentation capabilities, and CD4(+) T-cell priming efficacy under hypercholesterolemic conditions associated with atherosclerosis. *Circ Res* **103**, 965-973 (2008).

152. Trogan, E. *et al.* Gene expression changes in foam cells and the role of chemokine receptor CCR7 during atherosclerosis regression in ApoE-deficient mice. *Proceedings of the National Academy of Sciences of the United States of America* **103**, 3781-3786 (2006).

153. Puhr, S., Lee, J., Zvezdova, E., Zhou, Y.J. & Liu, K. Dendritic cell development-History, advances, and open questions. *Semin Immunol* **27**, 388-396 (2015).

154. Josefowicz, S.Z., Lu, L.F. & Rudensky, A.Y. Regulatory T cells: mechanisms of differentiation and function. *Annu. Rev. Immunol.* **30**, 531-564 (2012).

155. Ait-Oufella, H. *et al.* Natural regulatory T cells control the development of atherosclerosis in mice. *Nature medicine* **12**, 178-180 (2006).

156. Salomon, B. *et al.* B7/CD28 costimulation is essential for the homeostasis of the CD4+CD25+ immunoregulatory T cells that control autoimmune diabetes. *Immunity* **12**, 431-440 (2000).

157. Subramanian, M., Thorp, E., Hansson, G.K. & Tabas, I. Treg-mediated suppression of atherosclerosis requires MYD88 signaling in DCs. *The Journal of clinical investigation* **123**, 179-188 (2013).

158. Coombes, J.L. *et al.* A functionally specialized population of mucosal CD103+ DCs induces Foxp3+ regulatory T cells via a TGF-beta and retinoic acid-dependent mechanism. *The Journal of experimental medicine* **204**, 1757-1764 (2007).

159. Beaty, S.R., Rose, C.E., Jr. & Sung, S.S. Diverse and potent chemokine production by lung CD11bhigh dendritic cells in homeostasis and in allergic lung inflammation. *J Immunol* **178**, 1882-1895 (2007).

160. Weber, C. *et al.* CCL17-expressing dendritic cells drive atherosclerosis by restraining regulatory T cell homeostasis in mice. *J. Clin. Invest.* **121**, 2898-2910 (2011).

161. Cybulsky, M.I., Cheong, C. & Robbins, C.S. Macrophages and Dendritic Cells: Partners in Atherogenesis. *Circ Res* **118**, 637-652 (2016).

162. Niessner, A. *et al.* Pathogen-sensing plasmacytoid dendritic cells stimulate cytotoxic T-cell function in the atherosclerotic plaque through interferon-alpha. *Circulation* **114**, 2482-2489 (2006).

163. Doring, Y. *et al.* Auto-antigenic protein-DNA complexes stimulate plasmacytoid dendritic cells to promote atherosclerosis. *Circulation* **125**, 1673-1683 (2012).

164. Macritchie, N. *et al.* Plasmacytoid dendritic cells play a key role in promoting atherosclerosis in apolipoprotein E-deficient mice. *Arteriosclerosis, thrombosis, and vascular biology* **32**, 2569-2579 (2012).

165. Sage, A.P. *et al.* MHC Class II-restricted antigen presentation by plasmacytoid dendritic cells drives proatherogenic T cell immunity. *Circulation* **130**, 1363-1373 (2014).

166. Daissormont, I.T. *et al.* Plasmacytoid dendritic cells protect against atherosclerosis by tuning T-cell proliferation and activity. *Circulation research* **109**, 1387-1395 (2011).

167. Reizis, B., Colonna, M., Trinchieri, G., Barrat, F. & Gilliet, M. Plasmacytoid dendritic cells: one-trick ponies or workhorses of the immune system? *Nature reviews. Immunology* **11**, 558-565 (2011).

168. Choi, J.H. *et al.* Identification of antigen-presenting dendritic cells in mouse aorta and cardiac valves. *J. Exp. Med.* **206**, 497-505 (2009).

169. Zhu, S.N., Chen, M., Jongstra-Bilen, J. & Cybulsky, M.I. GM-CSF regulates intimal cell proliferation in nascent atherosclerotic lesions. *J. Exp. Med.* **206**, 2141-2149 (2009).

170. Ochando, J.C. *et al.* Alloantigen-presenting plasmacytoid dendritic cells mediate tolerance to vascularized grafts. *Nature immunology* **7**, 652-662 (2006).

171. Jakubzick, C. *et al.* Minimal differentiation of classical monocytes as they survey steady-state tissues and transport antigen to lymph nodes. *Immunity* **39**, 599-610 (2013).

172. Gautier, E.L. *et al.* Gene-expression profiles and transcriptional regulatory pathways that underlie the identity and diversity of mouse tissue macrophages. *Nature immunology* **13**, 1118-1128 (2012).

173. Dorner, B.G. *et al.* Selective expression of the chemokine receptor XCR1 on cross-presenting dendritic cells determines cooperation with CD8+ T cells. *Immunity* **31**, 823-833 (2009).

174. Colonna, M., Trinchieri, G. & Liu, Y.J. Plasmacytoid dendritic cells in immunity. *Nature immunology* **5**, 1219-1226 (2004).

175. Dzionek, A. *et al.* BDCA-2, BDCA-3, and BDCA-4: three markers for distinct subsets of dendritic cells in human peripheral blood. *J. Immunol.* **165**, 6037-6046 (2000).

176. Defays, A. *et al.* BAD-LAMP is a novel biomarker of nonactivated human plasmacytoid dendritic cells. *Blood* **118**, 609-617 (2011).

177. Heng, T.S., Painter, M.W. & Immunological Genome Project, C. The Immunological Genome Project: networks of gene expression in immune cells. *Nature immunology* **9**, 1091-1094 (2008).

178. Liu, P. *et al.* CX3CR1 deficiency impairs dendritic cell accumulation in arterial intima and reduces atherosclerotic burden. *Arteriosclerosis, thrombosis, and vascular biology* **28**, 243-250 (2008).

179. Swiecki, M., Gilfillan, S., Vermi, W., Wang, Y. & Colonna, M. Plasmacytoid dendritic cell ablation impacts early interferon responses and antiviral NK and CD8(+) T cell accrual. *Immunity* **33**, 955-966 (2010).

180. Maganto-Garcia, E., Tarrio, M.L., Grabie, N., Bu, D.X. & Lichtman, A.H. Dynamic changes in regulatory T cells are linked to levels of diet-induced hypercholesterolemia. *Circulation* **124**, 185-195 (2011).

181. Foks, A.C., Lichtman, A.H. & Kuiper, J. Treating atherosclerosis with regulatory T cells. *Arteriosclerosis, thrombosis, and vascular biology* **35**, 280-287 (2015).

182. Pallotta, M.T. *et al.* Indoleamine 2,3-dioxygenase is a signaling protein in long-term tolerance by dendritic cells. *Nature immunology* **12**, 870-878 (2011).

183. Kim, J.M., Rasmussen, J.P. & Rudensky, A.Y. Regulatory T cells prevent catastrophic autoimmunity throughout the lifespan of mice. *Nature immunology* **8**, 191-197 (2007).

184. Fu, W. *et al.* A multiply redundant genetic switch 'locks in' the transcriptional signature of regulatory T cells. *Nature immunology* **13**, 972-980 (2012).

185. Goubier, A. *et al.* Plasmacytoid dendritic cells mediate oral tolerance. *Immunity* **29**, 464-475 (2008).

186. Klingenberg, R. *et al.* Depletion of FOXP3+ regulatory T cells promotes hypercholesterolemia and atherosclerosis. *The Journal of clinical investigation* **123**, 1323-1334 (2013).

187. Bettelli, E. *et al.* Reciprocal developmental pathways for the generation of pathogenic effector TH17 and regulatory T cells. *Nature* **441**, 235-238 (2006).

188. Duan, M. *et al.* Distinct macrophage subpopulations characterize acute infection and chronic inflammatory lung disease. *J Immunol* **189**, 946-955 (2012).

189. Malissen, B., Tamoutounour, S. & Henri, S. The origins and functions of dendritic cells and macrophages in the skin. *Nature reviews. Immunology* **14**, 417-428 (2014).

190. Bradford, B.M., Sester, D.P., Hume, D.A. & Mabbott, N.A. Defining the anatomical localisation of subsets of the murine mononuclear phagocyte system using integrin alpha X (Itgax, CD11c) and colony stimulating factor 1 receptor (Csf1r, CD115) expression fails to discriminate dendritic cells from macrophages. *Immunobiology* **216**, 1228-1237 (2011).

191. Banchereau, J. & Pascual, V. Type I interferon in systemic lupus erythematosus and other autoimmune diseases. *Immunity* **25**, 383-392 (2006).

192. Savarese, E. *et al.* U1 small nuclear ribonucleoprotein immune complexes induce type I interferon in plasmacytoid dendritic cells through TLR7. *Blood* **107**, 3229-3234 (2006).

193. Gilliet, M., Cao, W. & Liu, Y.J. Plasmacytoid dendritic cells: sensing nucleic acids in viral infection and autoimmune diseases. *Nat. Rev. Immunol.* **8**, 594-606 (2008).

194. Ishibashi, S. *et al.* Hypercholesterolemia in low density lipoprotein receptor knockout mice and its reversal by adenovirus-mediated gene delivery. *J. Clin. Invest.* **92**, 883-893 (1993).

195. Matthews, W., Jordan, C.T., Wiegand, G.W., Pardoll, D. & Lemischka, I.R. A receptor tyrosine kinase specific to hematopoietic stem and progenitor cell-enriched populations. *Cell* **65**, 1143-1152 (1991).

196. Cheong, C. & Choi, J.H. Dendritic cells and regulatory T cells in atherosclerosis. *Mol. Cells* **34**, 341-347 (2012).

197. Stary, H.C. *et al.* A definition of advanced types of atherosclerotic lesions and a histological classification of atherosclerosis. A report from the Committee on Vascular Lesions of the Council on Arteriosclerosis, American Heart Association. *Arterioscler Thromb Vasc Biol* **15**, 1512-1531 (1995).